AUTOMATIC IMPULSE RESPONSE FOR EXPERIMENTAL MODAL ANALYSIS ON RUNNING HARMONICS CONDITION

A. JANNIFAR

FACULTY OF ENGINEERING
UNIVERSITY OF MALAYA
KUALA LUMPUR

2018

AUTOMATIC IMPULSE RESPONSE FOR EXPERIMENTAL MODAL ANALYSIS ON RUNNING HARMONICS CONDITION

A. JANNIFAR

THESIS SUBMITTED IN FULFILMENT OF THE REQUIREMENT FOR THE DEGREE OF DOCTOR OF PHILOSOPHY

FACULTY OF ENGINEERING
UNIVERSITY OF MALAYA
KUALA LUMPUR

2018

UNIVERSITY OF MALAYA

ORIGINAL LITERARY WORK DECLARATION

Name of Candidate: A. Jannifar

Matric No: KHA050017

Name of Degree: DOCTOR OF PHILOSOPHY

Title of Project Paper/Research Report/Dissertation/Thesis ("this Work"):

AUTOMATIC IMPULSE RESPONSE FOR EXPERIMENTAL MODAL ANALYSIS ON RUNNING HARMONICS CONDITION

Field of Study:

MACHINE STRUCTURAL DYNAMIC

I do solemnly and sincerely declare that:

(1) I am the sole author/writer of this Work;
(2) This Work is original;
(3) Any use of any work in which copyright exists was done by way of fair dealing and for permitted purposes and any excerpt or extract from, or reference to or reproduction of any copyright work has been disclosed expressly and sufficiently and the title of the Work and its authorship have been acknowledged in this Work;
(4) I do not have any actual knowledge nor do I ought reasonably to know that the making of this work constitutes an infringement of any copyright work;
(5) I hereby assign all and every rights in the copyright to this Work to the University of Malaya ("UM"), who henceforth shall be owner of the copyright in this Work and that any reproduction or use in any form or by any means whatsoever is prohibited without the written consent of UM having been first had and obtained;
(6) I am fully aware that if in the course of making this Work I have infringed any copyright whether intentionally or otherwise, I may be subject to legal action or any other action as may be determined by UM.

Candidate's Signature Date: 20 February 2018

Subscribed and solemnly declared before,

Witness's Signature Date: 21 February 2018

Name:

Designation:

AUTOMATIC IMPULSE RESPONSE FOR EXPERIMENTAL MODAL ANALYSIS ON RUNNING HARMONICS CONDITION

ABSTRACT

A machine that undergoes resonance will demonstrate high vibration level and often leads to mechanical problems such as a worn rotating element, looseness and crack propagation. However, within the scope of Condition Based Maintenance (CBM), the vibration analysis technique typically employed within the troubleshooting protocols unable to resolutely diagnose resonance as the root of such problems since the conclusions are made based on the anomalies of signal captured representing the faults. Thus, a measurement system that can resolve the resonance frequency of machines is indispensable. Experimental Modal Analysis (EMA) is a well-known technique used to extract the dynamic characteristics (resonance related parameters) of structure under non-operational condition. Nevertheless, the cost of shutdown of operating machines is significantly high especially in power generation industries. Therefore, the need to conduct EMA in operational condition has motivated the present research. In operating condition, harmonic excitation signal produced by the running cyclic machine may contaminate the input and output signals. Therefore, this disturbance must be filtered to attain clean output response signal that is purely from the input force. In this study, a time based block-averaging algorithm was proposed to eliminate the harmonic contribution along with the use of an innovative automatic impact device to control the periodicity of the data triggering, signifying data flow at predefined block size. A formula was proposed to synchronize the impact and harmonic frequencies, thus ensuring successful elimination of the later. A decimal part of 0.5 within the impact frequency (representing 180 degrees phase difference between incoming blocks) demonstrated much efficient combination in removing the

harmonic frequency in comparison to other values. In contrast, a triggering frequency magnitude that contained only a natural part produced insignificant elimination progress. Experiment conducted on a Fault Simulation Rig (FSR) showed that the dynamic characteristics of the structure of under the proposed operational EMA revealed close agreement with the classical EMA run under non-operational mode. The 1st and 2nd natural frequencies of non-operational condition, (10.9 *Hz* and 18.4 *Hz*) were slightly shifted to lower frequency (9.9 *Hz* and 17.6 *Hz*) under operational condition. Moreover, modal damping of the first two modes changed from 5.25% and 2.88% to 5.32% and 3.21%, respectively. Mode shapes for both non-operational and operational conditions remained highly similar, with pitching and heaving as the dominant mode shapes. The proposed method executed when the machine is running at superimposed frequency of the structure (i.e. 10 *Hz*) required 9623 *impacts* to enable block averaging to reach threshold coherence of more than 0.75. It was indicated that the differences of resonance frequencies and modal damping between both static and operational conditions was associated to the boundary condition of the machine structure that was not rigidly supported. The proposed EMA system applied under operational condition by utilizing a periodic control input force and time based block averaging algorithm can serve as added feature within the current machine maintenance protocols to ensure reliable diagnostic which will overcome unscheduled shutdown.

Keywords: automatic impact device, time based block-averaging, harmonic signal elimination, EMA under operational condition

TINDAK BALAS IMPAK AUTOMATIK UNTUK EKSPERIMEN ANALISIS MODAL DI BAWAH KEADAAN SUMBANGAN HARMONIK

ABSTRAK

Sebuah mesin yang mengalami resonans akan menunjukkan tahap getaran tinggi dan sering membawa kepada masalah mekanikal seperti elemen berputar yang haus, kelonggaran dan sebaran retakan. Bagaimanapun, dalam penyelenggaraan berasaskan kondisi (CBM), teknik analisis getaran yang digunakan dalam protokol penyelesaian masalah getaran tidak dapat untuk mendiagnosis resonans dengan tegas sebagai punca masalah itu memandangkan kesimpulan dibuat berdasarkan anamoli isyarat yang direkodkan yang mewakili kesalahan. Oleh itu, sistem pengukuran yang boleh menyelesaikan frekuensi salunan mesin adalah amat diperlukan. Eksperimen Analisis Modal (EMA) adalah teknik terkenal yang digunakan untuk mengekstrak ciri-ciri dinamik (parameter yang berkaitan resonans) struktur di bawah keadaan tidak beroperasi. Bagaimanapun, kos pemberhentian operasi mesin adalah lebih tinggi terutamanya dalam industri penjanaan kuasa. Oleh itu, keperluan untuk menjalankan EMA dalam keadaan operasi telah mendorong penyelidikan ini. Dalam keadaan operasi, isyarat pengujaan harmonik yang dihasilkan oleh mesin kitaran yang beroperasi boleh mencemarkan isyarat masuk dan keluar. Oleh itu, gangguan ini perlu ditapis untuk mencapai isyarat tindak balas keluar yang bersih berdasarkan kuasa input sematamata. Kajian ini, algoritma blok-pemurataan berdasarkan masa dicadangkan untuk menghapuskan sumbangan harmonik bersama-sama dengan penggunaan alat impak automatik berinovatif untuk mengawal jangka masa bagi data yang dilepaskan, yang menandakan aliran data pada saiz blok yang telah ditetapkan. Satu formula telah dicadangkan untuk menyegerakkan frekuensi impak dan harmonik, dengan itu memastikan kejayaan penghapusan elemen yang terkemudian.

Bagian perpuluhan 0.5 dalam frekuensi impak (mewakili 1800 fasa yang berbeza antara blok-blok yang masuk) menunjukkan kombinasi yang lebih berkesan dalam menghapuskan frekuensi harmonik berbanding dengan nilai-nilai lain. Sebaliknya, magnitud frekuansi cetusan yang mengandungi hanya bahagian semulajadi menghasilkan kemajuan penghapusan tidak signifikan. Eksperimen yang dijalankan pada Pelantar Simulasi (FSR) menunjukkan bahawa ciri-ciri dinamik struktur di bawah EMA operasi yang dicadangkan menghasilkan nilai yang hampir sama dengan EMA konvensional yang dilakukan di bawah mod bukan operasi. Frekuensi tabii pertama dan kedua dalam keadaan bukan operasi, (10.9 Hz dan 18.4 H) telah sedikit beralih kepada frekuensi yang lebih rendah (9.9 Hz dan 17.6 Hz) di bawah keadaan operasi. Selain itu, redaman modal bagi dua mod pertama berubah daripada 5.25% dan 2.88% kepada 5.32% dan 3.21%, masing-masing. Bentuk mod untuk keadaan bukan operasi dan operasi kekal sangat berdekatan, dengan mod getaran secara lerurus dan kilasan, sebagai bentuk mod dominan. Perlaksanaan kaedah yang dicadangkan apabila mesin sedang berjalan pada frekuensi lapisi struktur (iaitu 10 Hz) memerlukan 9623 impak untuk membolehkan pemurataan blok mencapai ambang kepaduan lebih daripada 0.75. Pemerhatian menunjukkan bahawa perbezaan frekuensi resonan dan modal redaman antara kedua-dua kondisi statik dan operasi dikaitkan dengan keadaan sempadan struktur mesin yang tidak disokong secara tegar. Sistem EMA yang dicadangkan digunakan di bawah keadaan operasi dengan menggunakan kawalan berkala daya input dan algoritma pemurataan blok berasaskan masa boleh berfungsi sebagai ciri tambahan dalam protokol penyelenggaraan mesin untuk memastikan diagnostik yang dipercayai yang akan mengatasi penutupan tidak berjadual.

Kata Kunci: alat impak automatik, blok-pemurataan berdasarkan masa, penghapusan sumbangan harmonic, EMA di bawah keadaan operasi

ACKNOWLEDGEMENTS

All acclaim is because of Allah S.W.T and to the grand prophet Muhammad S.A.W. the best model character for humanity.

I am very thankful to Assoc. Prof. Ir. Dr. Mohd Faizul Mohd Sabri as appointed caretaker supervisor, Assoc. Prof. Dr. Rahizar Ramli as my supervisor, and Prof. Dr. Abdul Ghaffar Abdul Rahman as the earliest supervisor. I might want to take this chance to express my thankfulness that Dr. Mohd Nashrul Mohd Zubir has given significant exhortation, bolster, motivation and important recommendations, all consolation and basic remarks at a final point important over the end of this exploration. I am also thankful to Prof. Ir. Dr. Sulaiman Wadi, Assoc. Prof. Dr. Kazi MD. Salim Newaz and Dr. Raja Ariffin Bin Raja Ghazilla for their encouragement during last difficult stage of my study period. I also exceptionally thankful to partners and closest companions, Prof. Dr. Indra Mahlia, Dr. Iskandar, Mr. Norhafizan bin Ahmad and Mr. Mukhtar Mohd Yunus and all individuals in the Department of Mechanical Engineering, University of Malaya. I would say thank to the Lhokseumawe State of Polytechnic, Lhokseumawe, Indonesia for financial support and permitting a leave of study during extended time frame.

Much gratitude goes to the dearest parents and youngest sister: Fachruddin, Mulyani, and Faciasetiana, in memorial of tsunami disaster in Lhoknga, Indonesia on December 26th, 2004. I am also thankful to my sister and brothers: Dinni Agustina, A. Junnifar, and A. Mulyagusdin, relatives and every one of the individuals who participated and communicated all the best for me. It was so nice to my wife: Yurisa Hikmah, my children: Meulu Alina, Rausanfikr Ali and Khawarizmi Ali, who have given an enormous patience to keep my spirit on the track.

TABLE OF CONTENTS

LIST OF FIGURES

LIST OF TABLES

LIST OF SYMBOLS AND ABBREVIATIONS

List of Symbols

Symbol		Quantity
A	:	Amplitude of the acceleration signal, Initial condition
A_g	:	Amplitude of FSR fluctuation, magnitude of amplitude reduction after 50 blocks under simulation
A_{Ri}	:	Amplitude of vibration of the rig by the solenoid stand motion
a_e	:	Independent variable, exponential coefficient for windowing of signal
a_s	:	Magnitude of amplitude reduction after 50 blocks
a_{sl}	:	Slope for linear equation
b	:	Offset of a linear equation
e	:	Amplitude of Suppressed harmonic, resultant harmonic amplitude,
F_o	:	Impulse force
F_p	:	Processed force input signal
F_r	:	Raw force input signal
$F(\omega)$	:	Load as input in frequency domain
f	:	Frequency
f_{FSH}	:	Frequency of Simulated fluctuating harmonic excitation
f_{FST}	:	Frequency of pulse generated by virtual signal generator
f_{SH}	:	Frequency of steady state harmonics excitation
f_{ST}	:	Frequency of nominal triggering
$f(t)$	:	Driving force signal
$f(x_{ca})$	:	Output value

$H(\omega)$: Transfer function

h : Amplitude of incoming harmonic signal

k : Stiffness

l_{fg} : Gap between the solenoid and force sensor

l_{ig} : Initial gap between solenoid and force sensor, initial gap

ω : Angular frequency

ω_o : |Frequency of running harmonic

ω_b : Frequency of table oscillation

ω_d : Damped natural frequency

ω_n : Undamped natural frequency, natural frequency

R_{BT} : Block rate where the data is transferred upon receiving the trigger signal

r : Frequency Ratio of table excitation frequency to the mass natural frequency, frequency ratio

r_{DCY} : Duty cycle of square wave signal

r_{dec} : Decimal component of f_{SH}/f_{ST}

r_{HTT} : Ratio of harmonic excitation frequency to triggering frequency

r_{nat} : Natural component of f_{SH}/f_{ST}

S_{ff} : Power spectral density of driving force signal or input signal

ζ : Damping ratio

S_{ff} : PSD of driving force signal

S_{On} : Number of samples of TTL high timespan

S_{xf} : Cross-spectral density between two signal, response of the structure to the driving force signal $x(t)$ and driving force signal, $f(t)$

S_{xx} : PSD of response signal

t : Time

t_1 : Time of impulse end

T_{On} : Timespan of the TTL high in one period

T_{Off} : Timespan of the TTL low in one period

T_{AD} : Entire PC signal processing timespan

T_{Sout} : Period of output sampling rate which is limited by an selected DAQ specification

T_{Sole} : Period of solenoid based on the designed frequency

θ : Phase angle , initial condition

U_{MH} : Difference between maximum and minimum value of the running frequency from a real electric motor

U_{SH} : Random coefficient of simulated harmonic excitation frequency

U_{ST} : Periodical shift in the pulse, random coefficient of simulated triggering frequency.

V : Voltage

X_p : Processed output response signal

Xr : Raw output response signal

$X(\omega)$: Response signal in frequency domain

x : Sample number in sequential order

x_s : Linear line with a particular gradient

$\overline{x}_{ca}$: Mean value of the input force sample

x_{ca} : Independent variable for calibration slope

x_s : Constant of linear line

$x(t)$: Signal of response of the structure to the driving force

y_{EIW} : Constant of exponential input force window

y_{ST} : Constant of saw tooth signal

Y : Amplitude of table motion

List of Abbreviations

Symbol		Meaning
AI	:	Analog Input
AO	:	Analog Output
BS	:	Block Size
BR	:	Block Rate
CBM	:	Condition Based Maintenance
CPU	:	Central Processing Unit
DAQ	:	Data Acquisition
DC	:	Direct Current
DDV	:	Dynamic Design Modification
EMA	:	Experimental Modal Analysis
FFT	:	Fast Fourier Transform
FIFO	:	First In First Out
FRF	:	Frequency Response Function
FSR	:	Fault Simulation Rig
IA	:	Initial Amplitude
ICE	:	Internal Combustion Engine
ICP	:	Integrated Circuit Piezoelectric
ISTA	:	Impact Synchronous Time Averaging
LCR	:	Inductance Capacitance and Resistance
MAX	:	Measurement and Automation Explorer
MEMS	:	Micro Electro-Mechanical Systems
MDOF	:	Multi Degrees of Freedom
NI	:	National Instrument
GUI	:	Graphical User Interface
OMA	:	Operational Modal Analysis
PC	:	Personal Computer
PSD	:	Power Spectral Density
SR	:	Sampling Rate

SDOF	:	Single Degree of Freedom
TF	:	Transfer Function
TSA	:	Time Synchronous Averaging
USB	:	Universal Serial Bus
VI	:	Virtual Instrumentation

LIST OF APPENDICES

CHAPTER 1: INTRODUCTION

1.1 Background

It is well-acknowledge that rotating and reciprocating machines have been at the forefront of technological advancement in reshaping the civilization. Element of repetitive motion has always play a pivotal role in modern scientific discoveries, particularly on proofing theories via experimental endeavor which require incorporation of cyclic machines to perform critical tasks such as delivering fluids, performing combustion, compression and expansion as well as operating different manufacturing sequences (turning, milling, drilling etc.). Within the scope of industrial revolution, the dependency of cyclic machineries to execute wide spectrum of physical tasks is irrefutable. Over the course of 200 years, rotating machines have been employed in all mass production factories and facilities which substantiate their role as extremely important component to improve the productivity and performance within competitive production environment. Unfortunately, over the years, engineers and scientists have discovered that systems which consist of a combination of structures and rotating and cyclic machines were subjected to different level of vibrations depending on the speed of reciprocating element. These vibrations play a dominant role in shortening the life of parts and structures linked to the rotating machines. Often, these vibrations were translated into misalignment, irregular sound and friction, crack propagation, loosening of fasteners, all which lead to mechanical failures.

The above drawbacks have motivated engineers and scientists to formulate mitigation strategies to reduce the vibration. On this note, relentless efforts have been dedicated on resolving the dynamic parameters of the structures, particularly the resonance frequencies with an aim to shift the cyclic machine operation further away

from these points. This practice is well-known as Experimental Modal Analysis (EMA). Manufacturer of rotating machines typically highlight the allowable operational speed to ensure prolonged used and avoiding premature failure of the parts and components linked to the machine. However in normal industrial practices, these cyclic machines are mounted on much larger and complex systems which inadvertently modulate the dynamic parameters of the systems. Further, vibration transmission from other sources also implicates the performance of the overall facility. Often resolving the modal characteristics of the complete assembly is not common during operation due to the need to shut down the overall system which incurs production loss. Therefore engineers have resorted to perform routine periodic maintenance to replace any worn and damage parts. The maintenance of the machines plays a critical role in ensuring continuous operation in the production line. However, achieving an all-time peak performance of the production facilities is an intractable work for production managers.

In light of the need to continuously monitor the structural health subjected to vibration, the predictive maintenance or Condition Based Maintenance (CBM) was introduced which prioritize on measuring vital physical parameters such as level of vibration, sound, temperature and pressure, stress and strain, humidifies etc. The approach uses different sensors and signal processing unit to characterize the operational behavior of the components within the system. Detected anomalies on the signals captured will be correlated to various mechanical problems on the system such as misalignment, creep, corrosion, crack and torsion which can lead to system failure. The capacity of early detection of machine component faults to avoid the breakdown is a significant point of CBM.

Within the scope of CBM, vibration analysis is one of the most popular tools in performing monitoring and maintenance tasks of structures subjected to cyclic forces (Riemann, Perini, Cavalca, de Castro, & Rinderknecht, 2013; Ristivojevic, Mitrovic, & Lazovic, 2010; Taghizadeh-Alisaraei, Ghobadian, Tavakoli-Hashjin, & Mohtasebi, 2012). The sensor (typically accelerometer) is used to sensitively measure vibration signals which can later be analyzed to identify faulty condition such as crack propagation, misalignment and loose connection. Nowadays, rapid development of virtual instrumentation system which includes state of the art sensors and actuators, Data Acquisition (DAQ) and interfaces devices and advanced signal processing technique has made vibration analysis more convenient and economical. For instance, small chipped gear teeth inside rotating machine could be identified by vibration analysis much faster than other approaches.

In vibration analysis, considerable vibration levels of rotating machines can conduct issues of misalignment, excessive wear, imbalance, oil whirl in bearings, chipped gear teeth and crack propagation to name a few. Studies have indicated that most problems associated to excessive vibration levels can be identified by using vibration analysis (Z. G. Tian & Liao, 2011; Van Horenbeek, Van Ostaeyen, Duflou, & Pintelon, 2013; Zio & Compare, 2013). However, the origin of this excessive vibration which leads to the above problems may be traced all the way from the operating condition of the cyclic machines which include the influence by resonance.

In CBM based vibration analysis, most detection of mechanical fault and the corresponding decision are based on signal anomalies in time and frequency domains. However, the process mainly bypasses the root of the problems which may involve resonance element penetrating into the system, thus causing uncontrolled and severe vibration which lead to the above mechanical fault. Excluding resonance

within the vibration analysis of structures leads to inaccurate decision on the root cause of mechanical fault which will incur capital and time costs. Refurbishment and repair works would force a complete shutdown of the system and it is critical for the root cause to be firmly resolved. Otherwise recurrence of the problems within the short span on restoration of operation would be detrimental to the production and revenues. illustrates a typical spectrum within vibration analysis which indicates the condition of the running speed coinciding with the resonance frequency on Frequency Response Function (FRF) measurement.

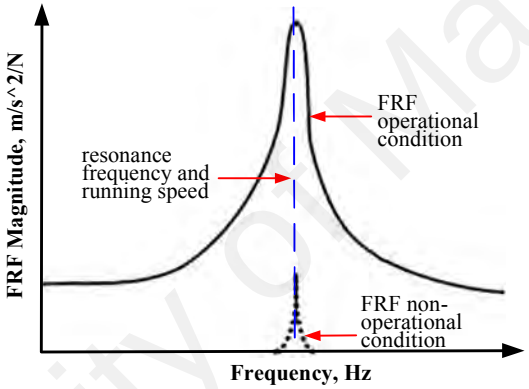

Figure 1.1: A running speed signal covers a natural frequency signal

Several studies have shown that inaccurate diagnosis on the root cause of excessive vibration level may potentially manifest by adopting the CBM protocols (Ameri, Grappasonni, Coppotelli, & Ewins, 2013; Dion, Tawfiq, & Chevallier, 2012; Hanson et al., 2007). Indeed, conventional vibration analysis has limitation to identify the presence of resonance problem under operational condition of rotating machines. Furthermore, it is not able to detect the presence of resonance on the integrated structure when the running speed of the cyclic machine overlaps with the structure resonance frequency.

Unidentified resonance problem during vibration analysis culminate into the breakdown in rotating machine. As such, vibration level increases tremendously,

giving rise to the cyclic stress on the machine component and culminates into total failure such as fracture and crack (Cheung, Wong, & Cheng, 2013; Eissa & Amer, 2004). Therefore, undiscovered resonance problems embarks significant issues that cause serious implications on the overall machine condition.

As highlighted previously rotating machine is not designed to consider a different end user designed platforms where the rotating machine is mounted. Instead, the platform to support the rotating machine (called a build-up structure) has unique dynamic characteristics that are different from the build-in rotating machine alone. Therefore, if the natural frequency of the newly compounded structure coincides with running speed of the rotating machine, a significant dynamic instability will manifest. This is essentially attributed to the change in the dynamic characteristics by introducing additional build-in rotating machine boundary condition over the platform.

Different techniques have been developed to resolve the dynamic characteristic of the integrated structure. In particular, EMA is a well-known method to determine three dynamic characteristics: natural frequencies, modal damping and mode shapes. The concept relies on generating force input into the system and tracing the output response in time domain via motion tracking sensor. These force input and response output signal will be computed in frequency domain to attain the modal parameters of the system. However, in a realistic condition monitoring environment, EMA is conducted during non-operational condition, rendering it unsuitable to be incorporated CBM platform. Conducting EMA under operational condition in the presence of harmonic excitation frequency produces a response output signal that would eventually result in misleading FRF, which is the product of force input/response output raw signals from the measurements. Further, mode shape of

the system under resonance could not be completely resolved using the normal EMA practiced under operational condition.

Due to the above impediments, researchers have sought an alternative modal analysis approach to confidently attain the dynamic characteristics with running harmonic from cyclic machines. Thus, Operational Modal Analysis (OMA) was introduced to meet the above requirement. The concept relies on measuring only the output response from the structure which is combined with complex statistical computation to remove the harmonic effect, leading to the attainment of disturbance free modal parameters. However due to due sophisticated identification method through rigorous stochastic process adopted, the results are subjected different level of uncertainty depending on the running condition, which further complicates identification of modal parameters. On the other hand, the much straightforward force input/response output analysis based EMA produces highly reliable dynamic responses which makes it a much popular option in conducting modal analysis, even at a cost of disabling the source of harmonic from cyclic devices within the integrated system.

The above limitation of EMA has motivated the present work to explore an innovative approach in isolating the harmonic signal contribution within the response output signal measurement, leading to a much purified response originating from the force input signal to yield much reliable modal identification. On this note, the existing Time Synchronous Averaging (TSA) technique typically used to eliminate disturbance in vibration measurement would be adopted as the basis in filtering the running harmonic from output response. However, while TSA aims at preserving the harmonic, the present challenge is to suppress this component in order to obtain an ideal response output vs force input product represented by FRF. Thus, modification

of the existing EMA protocol is essential to achieve the above objective. In essence if the force input which also serve as trigger for force input and response output data flow can be made in periodic mode, a strategy can be formulated to conduct the impact such that the harmonic will be canceled with increasing number of knockings. To achieve this configuration the hardware need to be modified by incorporating automatic impact device onto the EMA system which serves as a new approach in delivering the input force onto the structure.

1.2 Problem Statement

As the conventional EMA is not feasible to be performed under operational condition, there are three problems statements formulated.

1. How to achieve periodical impact on a structure to enable automatic PC-controlled impact device to preserve a force impact as well as manual human operator action during EMA under non-operational condition.
2. How to apply time synchronous averaging as effective as possible to enable the highest rate for the harmonic elimination progress during EMA under operational condition.
3. How to combine automatic PC-controlled impact device, an enhanced time synchronous averaging technique and EMA under non-operational algorithm in one integrated virtual instrumentation system, to enable validated EMA under operational condition

1.3 Research Aim and Objective

This study aims to develop an innovative approach to obtain modal parameters of a structure under operational condition based on a EMA platform. To achieve this goal, three specific objectives are outlined as follows.

1. To develop an automatic solenoid driven impact device to be used in providing periodic input force onto the structure.
2. To develop a methodology for eliminating harmonic excitation disturbance in acquired signals using a combination of time synchronous impact and averaging approaches.
3. To perform comparative modal parameters assessment on the proposed EMA under operational condition with the classical EMA.

1.4 Proposed Method

The outline of the proposed method to meet the objective is given as follows:

1. Objective 1

Classically EMA protocol involves delivering the required impact force which serves as input onto the structure. On this note, Integrated Circuit Piezoelectric (ICP) impact hammer is used to manually excite the structure by which the output response will be captured using wide variety of displacement sensor such as accelerometer, proximity, laser etc. This impact will also serve as triggering switch to instruct data flow at specific block size representing a pre-designed number of sampling. The non-periodic nature of the impact is not suitable for the present approach where the impact sequence need to be precisely controlled in order to perform harmonic elimination via signal processing strategy. In order to achieve periodic mode of impact, an electromagnetically driven solenoid system will be developed. A virtual

instrumentation software (Dasylab) will be used to provide the control signal which will flow to a dedicated circuit and further energize the solenoid, prompting the movement of the solenoid plunger. In order to attain the impact force for every stroke, a force sensor will be incorporated on the structure where the solenoid end-effector will establish impact at specific time. The signal will then flow to the next stage for further processing. In this chapter, issues of generating the periodic signal from the software and its mobility through different interfaces modules will be addressed. Further the complete system performance will be compared with the conventional manual impact apparatus to ascertain and verify the reliability to deliver quality impact on the structure.

2. Objective 2

In classical EMA, force input/response output signal generated from the impact will flow in specific block size which is determined by the preset number of sampling. Users typically performed several knockings on the structures by which the signal contained in each incoming block will be averaged. In this way, disturbance and non-synchronized signal will be eliminated, enabling much smoother modal analysis. However the above sequences are performed at the shutdown condition of the structure to avoid complication on modal parameters calculated from generated FRF should the structure is subjected to external harmonic excitation from running cyclic device. Thus in order to address this problem the knockings should be performed at specific interval such that the data averaging process for each sequential block would cancel the harmonic component of the signal. To idea revolves executing each knocking task at different phase of the running harmonic generated by the cyclic device. The excitation frequency can be determined in prior using tachometer or any equivalent instruments. In this way the harmonic

component inside each data block will be at different phase from each other, enabling the harmonic signal to be significantly reduced with increasing number of averaging blocks. While TSA works based on synchronizing the phase in each averaging block, the present work attempt to desynchronize the phase via the combination of controlled periodic impact and time based averaging techniques. Using Dasylab as Virtual Instrumentation (VI) software tool, a simulation environment will be constructed to investigate the effectiveness of the above concept. Further, a mathematical expression will be formulated to link between the data triggering impact and harmonic excitation as a new strategy to eliminate the harmonic signal. Both computers generated and real experimental data will be used during the simulation to attain much reliable results. Different operating conditions will be explored to investigate the capability of the proposed concept to alleviate the harmonic effect. This software will be tied to the automatic impact device to form a new apparatus to conduct EMA under operational condition in the next stage

3. Objective 3

It is well acknowledged that EMA serves as the most reliable modal analysis technique within the scope of dynamic characterization. This stems from the systematic process to obtain the modal parameters which involves force input/response output signal generation, synchronous time averaging of the signals, FRF generation and attainment of dynamic properties of the system. However a strict condition must be adhered to achieve high quality results (i.e. the structure must be in stationary condition prior to data taking process). This is primarily needed in order to ensure all the output responses are the results of the impact force exerted onto the structure by the ICP impact hammer, and thus further analysis will be based on these so-called 'clean' signals. In this light, conducting EMA under operational condition

serve as a new challenge for engineers particularly those who involved in condition monitoring arena. The harmonic originating from the cyclic device will penetrate into the data processing path, leading to incorrect model parameters particularly the damping constant and mode shape. The structural and components health need to be monitored and inspected and any mechanical faults should be correctly diagnosed to reduce downtime cost and unproductively. The ability to conduct EMA under operational condition improves the diagnostic process such that the modal parameters can be confidently attained while the source of mechanical faults can be reliably identified; either originally comes from the resonance, installation, aging, or human errors. The incorporation of resonance element within the diagnostic criteria will be an added value within the field of CBM, which currently devoid of resonance as the potential cause of mechanical fault. In the present work the complete hardware and software developed within the first two objectives will be linked to form a complete instrument in order to conduct EMA both in running and static condition. The results obtain via this approach will be compared with the conventional manually driven impact hammer based EMA as reference. Different conditions will be investigated, particularly on the most critical scenario where the running harmonic coincide or close to the resonance of the structure. The ability to isolate the harmonic contribution from the resulting modal parameters will be verified by comparing the coherence, FRF and mode shape results to the classical EMA approach.

1.5 Scope the Study

This study focused on an innovative improvement of the EMA technique to measure dynamic characteristic of rotating machines structure under operational condition. The work was divided into three major sections: developing an automated impact system to deliver controlled and adaptable periodic impact on the structure,

development of software as well as formulating a strategy to conduct harmonic elimination using modified apparatus and averaging technique, conducting comparative assessment on the developed system with the classical EMA to validate the performance. In this study, some limitations are identified as follows.

1. Due to industry restriction, the proposed EMA under operational technique was carried out in a laboratories scale structure, named Fault Simulation Rig (FSR). Nevertheless within modal analysis research perspective, this practice is widely accepted to demonstrate and simulates mechanical faults as long as the established measurement tools are used as reference for validation.
2. First two modes were selected to compare the dynamic characteristics by EMA under non-operation and operational condition. The first two modes were expected to be sufficient to validate the proposed method.
3. One axis accelerometer was used during measurement. One axis accelerometer was sufficient to produce comparable mode shape at validation stage between EMA under operational and non-operational condition.

Under the present scope of study, the proposed EMA under operational condition will serve as additional feature to the existing EMA protocols since the core concept of dynamic identification remains the same. Modification was only performed at the initial measurement and time based averaging stages while processing of filtered data will be similar to as the classical EMA. This feature will support the existing vibration analysis for enriching predictive CBM technique on structure in running condition

1.6 Organization of Thesis

The thesis comprises of five chapters covering all works to address the research question and objectives. CHAPTER 1: described background of this study. A particular problem in vibration analysis of rotating machines was explained, and a new technique was proposed to solve it. CHAPTER 2: summarized several related works conducted in past research to shed light on the novelty and gap of the recent work. CHAPTER 3: described the process of developing automatic impact device to deliver much controlled periodic input force onto the structure. CHAPTER 4: discussed on formulating a strategy to perform harmonic elimination as well as developing a specific software interface modules to enable data communication between the hardware and software. CHAPTER 5: focused on executing the concept on real experimental test rig. Rigorous comparative assessment was performed relative to the classical EMA technique to gauge its effectiveness in isolating the harmonic and producing reliable results. The conclusions and suggestions of this study were outlined in CHAPTER 6:.

Results of calibration, equipment, software as well as the list of experiments and simulation that were conducted to fulfill the objectives in the research were elaborated in Appendix A to Appendix OO. Specifically the information of the name of experiment, structure used, input force sensor and output response sensors, Dasylab file names, etc. were tabulated in Appendix A to Appendix E. Appendix G contained the Table of Calibration of Force Sensor which showed the result of back to back calibration between Force sensor and ICP impact hammer. Within Appendix H to Appendix U, the overall worksheet used to conduct EMA under operational condition was devided into several sections representing the executed tasks. Appendix V to Appendix GG presented the Graphical User Interface (GUI) layout of

EMA under operational condition to ease interaction between operator and the proposed system. The integrated layout contains buttons to complete different tasks such as: raw signal acquisition, force input and response output windowing and averaging, elimination progress, solenoid monitoring and FRF results. Appendix JJ to Appendix OO showed the specification of instruments that were employed for the present work.

CHAPTER 2: LITERATURE REVIEW

2.1 Development of Input Force and Response Output Devices for EMA

Within the scope of vibration analysis, it is well-known that the dynamic characteristic of integrated structure is measured via EMA. The typical measuring instruments required for EMA include ICP impact hammer and accelerometer, which provide the force input and response output signals combined with analysis software to determine the essential modal parameters (i.e. natural frequency, damping ratio and mode shape). While this procedure has been well-established and successful, there are some issues with regard to the implementation of the measuring tool that have been highlighted by previous researches. Schwarz and Richardson (1999) in particular mentioned about the lack of consistency in impact hammer application which is unable to achieve a periodical input force onto the tested structure. Moreover, the nature of the impact hammer application, which mostly relies on operator skill and experience, leads to problems typically associated to double knocks. These impediments have compromised the reliability of the signals generated, which would be later processed to obtain the FRF. Another major setback on the current practice is the need to shut down all the cyclic devices mounted on the structure to eliminate the effect of harmonic excitation during the data acquisition procedure. While this condition can be met under laboratory based experiments, a practical issue may arise in conducting similar procedure on the actual structure where shutting down of the machineries would translates into substantial amount of loses in the production. Thus, a new system that can address the above drawbacks is highly sought. On this note, the present work is directed on developing an automatic impact device to replace the conventional ICP impact hammer that is normally used in EMA under non-operational condition. The new system would comprise a

combination of electromagnetically driven solenoid, a force sensor, electrical relay circuit and controlling software. It is worth to mention that the ability to switch into fully automated configuration would not only address the pertinent issues related to human error but also pave promising avenues on exploring the capability of the new system to address the limitation of the classical EMA in terms of moving towards conducting modal analysis under operational conditions.

Some works have been conducted to adapt the classical EMA procedure onto different complexities of measuring conditions, which require adjustment and employment of different types of input force sensor and output response sensors. Capoluongo et al. (2007) replaced the typical accelerometer by Fiber Bragg Grating (FBG) as response output sensor for performing modal analysis test to detect structural damage. Similar approach was implemented by Cumunel, Delepine-Lesoille, and Argoul (2012) with the use of long-gage fiber optic sensor to estimate the dynamic characteristic of a beam in identifying structural damage. Farshidi, Trieu, Park, and Freiheit (2010) used a combination of air excitation and microphone array as input for resolving dynamic characteristic of delicate structure that is susceptible to damage or contamination.

Solenoid, as an electromechanical device has been used extensively in system transformation from manual to automatic operation to improve reliability and efficiency. By replacing the end-effector connected to the Ferro-magnetic plunger, different tasks can be achieved in much consistent way. For instance, a new device to produce vacuum output and valve control has been documented and patented (Rogers & Wang, 1987), (Miki & Yamamoto, 1999). Solenoid has been adopted for many applications (Debonnel, Yu, & Peterson, 2005; Islam, McMullin, & Tsui, 2011; Jaffey & Khoe, 1974; Rashedin & Meydan, 2006). Luk, Liu, Jiang, and Tong (2009)

suggested the use of solenoid to inspect the binding integrity of wall tiles. J. Tian et al. (2016) and Shang, Tian, Li, Wang, and Cai (2015) have used electromagnetic actuator to deliver high input force, large stroke and fast response motion on their novel compliant mechanism for precision positioning and machining applications. In industry, solenoid is incorporated in wide range of devices such as brakes, copiers, pump, interposers, coin changers and disk drive. A valve controlled mechanism connected to a camshaft in Internal Combustion Engine (ICE) has been studied by Zhao and Seethaler (2010). Solenoid has emerged as among the cheapest actuator in the market with mass production and wide spectrum of performance and accessibility ("Principle of Operation, Why use solenoids?," 2017).

Within the scope of vibration, the use of solenoid valve to inject air pressure has been documented in non-contact EMA study by Farshidi et al. (2010). A new solenoid driven vibro-impact device with high impact forces was developed by Nguyen and Woo (2008) to enhance the penetration rates of the impact. Design and control of mechanical system such as solenoid has been well articulated in the literature (Gevers, 2005; Q. Li & Wu, 2004; Q. Li, Zhang, & Chen, 2001). Similar to the previous control architecture, the solenoid driving motion in this study is governed by ON-OFF pulse timing. In addition, the present actuator serves as a stand-alone device without direct connection to the tested structure in order to avoid excessive vibration transmission caused by the inertia force of the solenoid plunger.

In this work, efforts were given to develop an automatic impact system consisting of electromechanically actuated solenoid and force sensor to replace an ICP impact hammer in classical EMA. To the best of our knowledge, this concept has not been articulated in-depth within the EMA practice. This design aims to address the problems related to non-periodic input force in the EMA as well as generation of

undesirable double-knock on the tested structure, which would compromise modal analysis. Further, a periodical impact attained through this design can be potentially exploited to eliminate harmonic excitation signal, which could extent the classical EMA application beyond the non-operational condition. Within the development stage, issues of pulse generation and its transmissibility to the solenoid, end-effector motion trajectory, force-sensing capability, solenoid supporting structure and its isolation, as well as the gap between the end-effector and the sensing pad were addressed systematically. Validation was performed by comparing the results with signals generated via conventional ICP impact hammer based classical EMA.

2.2 Suppression of Harmonic Excitation Signal in EMA

Within the scope of mechanical system and signal processing, harmonic excitation disturbance and its elimination has received specific attention among the researchers (Assaad, Eltabach, & Antoni, 2014; Mark, 2015; Sharma & Parey, 2017; Szczepanik, 1989; Yao, Di, & Han, 2012). A significant portion of the works has been dedicated on solving gear related problems (Combet & Gelman, 2007; Mark, 2015; Sharma & Parey, 2017). Mark (2015) presented a novel time-synchronous method to suppress harmonic contribution from mating gear and the gear pair. Yao et al. (2012) proposed an adaptive notch filter to eliminate the harmonics originating from nonlinearity of the mechanical system, leaving only the output acceleration in response to the sinusoidal input.

It is well-acknowledged that for EMA, harmonic excitation signal, naturally comes from rotating or cyclic machineries such as electric motor and piston penetrates into the output as well as force input signals, thus compromising FRF evaluation. This condition leads to unreliable prediction of modal parameters (i.e. resonance frequencies, mode shapes and damping ratio). This problem has long

hindered EMA to be conducted under operational condition. Thus, within scientific community, EMA is performed under complete shut-down of rotating components mounted on the integrated structure (Choi, Li, Samali, & Crews, 2007; Jalali & Parvizi, 2012; Song & Jhung, 1999).

Despite the above limitation, EMA has been highly preferred in resolving modal parameters over wide range of structures primarily due to the reliability of the results (Lee & Kim, 2001; Song & Jhung, 1999). Further, although the birth of micro/nano technologies has revolutionized EMA in terms of the apparatus involved, the requirement of generating force input/output responses remains as the core feature in understanding the dynamic characteristic of structures (Xiong & Oyadiji, 2017). Salim, Aljibori, Salim, Khir, and Kherbeet (2015) in his review described in detail different techniques developed to harvest vibration energy based on Micro Electro-Mechanical Systems (MEMS) architecture. In this context, the transducers mounted on the structure serve to generate electrical power as well as to sense the corresponding force, which can be used to determine the modal parameters via force input/output signals. Jalali and Parvizi (2012) used EMA to obtain the modal properties of liquid containing conduit structures and high- lighted the sensitivity of dynamic parameters in response to the change in liquid volume. Y. Li, Chen, Zhang, and Zhou (2017) used impact hammer based EMA to resolve the dynamic model of high speed motorized spindles under free and working state conditions. Similarly, Choi et al. (2007) employed an impact hammer to generate and input force which was then coupled with accelerometer signals to correlate the change in modal parameter with structural damage at specific location in timber beam

The post-processing of signals under EMA route involves elimination of the disturbance generated during data acquisition process. In this context, TSA is

employed to obtain noise free signals, which is realized via implementing different averaging algorithms (Combet & Gelman, 2007; Mark, 2015). This approach has proven to be successful in removing the disturbance overlapping the actual FRF.

In the recent years, attempts to adopt signal averaging technique in EMA to suppress harmonic excitation have been highlighted (Rahman, Ong, & Ismail, 2011). Major problem stems from the nature of the structural behavior by which the existing averaging technique is performed without running harmonic. Thus, the algorithm does not take into account the harmonic signal which leads to difficulty in achieving signal elimination. It is worth to mention that, while averaging technique to reduce the presence of noise that covers the running speed is well-established within the context of CBM, the EMA perceives harmonic excitation signal as disturbance that needs to be eliminated to ensure reliable FRF result.

Based on the literature, harmonic signal elimination is predominantly adopted in OMA which focuses only on analyzing the response of the structure in the absence of the force input (Combet & Gelman, 2007; Mark, 2015). On this note, TSA is used as tool to preserve the frequency of interest and eliminating non-synchronized frequencies and noises. This method is not compatible with the EMA technique which is based on non-operational modal analysis. Recently, Rahman et al. (2011) reported the use of TSA in EMA platform to eliminate the harmonic excitation.

In essence, TSA separates running speed signal from other incoming signal disturbances such as noise, random transient and irrelevant harmonic excitation. Upon receiving triggering signal, output signals that come in blocks will be averaged sequentially and this process will suppress any asynchronous signal as the number of block increases (Shang et al., 2015). From this concept, it is evident that synchronization between the triggering and block averaging is crucial to eliminate

noise from the running speed. Also, in different perspective, the manipulation of these two parameters may hold the key to suppress the harmonic excitation amplitude of the tested structure. (Rahman et al., 2011) adopted the above idea in their EMA under operational condition which they later named as ISTA. On this note, it is worth to highlight that the mechanism of harmonic signal suppression was not elaborated in detail. The coherence which is one of the underpinning criteria for verifying disturbance free force input/output signals was not presented. Further, as the impact or triggering frequency generated by ICP impact hammer was random, the reduction of the harmonic amplitude is predominately dependent on the number of averaging, rather than a consistent signal reduction in every averaging sequence.

Hitherto, it is worth to mention that the idea of harmonic elimination in EMA under operational condition is still in question. Therefore, in this study an attempt would be made to exploit the underlying characteristic of TSA with an aim to suppress the harmonic excitation up to the minimum level. It is anticipated that a suitable selection of the triggering force input and harmonic signal frequencies serves as the underlying key to perform effective elimination. This would lead to a parameter that governs the elimination process as well as the criteria to ensure successful elimination of the harmonics. Further, a periodical impact is expected to yield much favorable outcome in comparison to random triggering impact.

2.3 Acquiring Modal Parameters under Operational Condition Using EMA

It is well-known that EMA is traditionally conducted under complete shut-down of the rotating machineries within the tested structure (Beyen & Kutanis, 2011). The main reason is due to the interference of the harmonics originating from the cyclic motion which will penetrate into the FRF, resulting into misleading interpretation of modal parameters (Magalhães, Cunha, Caetano, & Brincker, 2010). Thus, within the

scope of modal analysis, EMA is construed as non-operational vibration analysis since the presence of the running speed signal compromises the reliability of post-processing signals.

Over the years, researches have come forward with alternative approach to conduct modal analysis under operational condition by which OMA was later developed to address the above problem (Ebrahimi, Esfahanian, & Ziaei-Rad, 2013; Mao et al., 2014; Mendrok & Kurowski, 2013; Mohanty & Rixen, 2004). Brincker and Kirkegaard (2010) highlighted that OMA has been developed since sixties, yet due to the complexities and limitations of its applications, the method was less common than EMA. In principle, the ability of OMA to be realized is predominantly attributed to the processing of solely the output signal, unlike EMA which uses both force input and output signals to generate FRF (Agneni, Coppotelli, & Grappasonni, 2012; C. Devriendt, De Sitter, Vanlanduit, & Guillaume, 2009; Modak, Rawal, & Kundra, 2010). This technique uses the response of the structure where the source of excitation could be in the form of random or harmonics to generate the FRF. OMA has been successfully implemented in civil engineering structure such as bridge, building, platforms and towers as highlighted by Batel (2002). The advantage of OMA in comparison with EMA lies on its ability to take into account the changes in boundary conditions that manifest on structure under operational mode en route to resolving the dynamic characteristics (Christof Devriendt, 2010; B. Li et al., 2013; Mohanty & Rixen, 2004). Nevertheless, its application in problems related to mechanical engineering has not been widely accepted due to the presence of harmonic excitation especially at high amplitude. He added that OMA has been adopted to resolve problems in rotating machinery and gears.

Without external excitation as input, OMA strongly relies on sophisticated identification method through rigorous stochastic process to remove the dynamic effect from the output response. Further, due to the statistical approach adopted, the results are subjected to certain level of uncertainty depending on the running condition, which further complicates identification of modal parameters. Moreover, since the measurements are performed at ambient vibration level, which is typically lower than serviceable level of the structure, a much accurate damping ratio, which is known to be amplitude-dependent, would be difficult to be determined. The challenges above make EMA remains the highly sought technique when it comes to performing modal analysis, even at a cost of shutting down the rotating devices within the integrated system.

It is evident that in realizing EMA under operational condition, the interference of the harmonics within FRF and coherence calculation needs to be addressed. On this note, eliminating the harmonic component embedded within the incoming output signal would yield much purified output response generated solely by the impact hammer input. Thus, by looking at the signal processing path, a strategy can be formulated to isolate and remove the unwanted disturbance prior to the formation of FRF. Researchers have invested immense efforts to eliminate the harmonic disturbance under EMA and OMA schemes(Agneni et al., 2012; Brincker & Kirkegaard, 2010; C. Devriendt et al., 2009; C. Devriendt & Guillaume, 2008). On this note, problems associated to the effectiveness and compatibility of the elimination approach to be incorporated within the classical modal analysis remain to be the persisting challenges and this paves an avenue for continuous improvement to achieve a highly robust system.

EMA has experience significant evolution in terms of the apparatus employed in generating the force input/output signals. The advancement in sensor and actuator fields has paved avenues for different techniques to be adopted aiming to address different limitations in accomplishing the measurements to resolve the modal parameters. Farshidi et al. (2010) employed a microphone array to measure the output acceleration of cantilever beam subjected to non-contact force input by air-impulse. Jamil and Yusoff (2016) introduced a combination of electromagnetic and laser based measurements to attain the modal parameters for milling tool under operational condition. Trebuňa and Hagara (2014) used a high speed camera to obtain the displacement of a plate which was later correlated to the input by impact hammer to generate the modal parameters. Cakir, Uysal, and Acar (2016) used the conventional impact hammer/accelerometer pair to obtain the modal parameters of a new masonry arches composite material.

Recently an attempt has been made by (Rahman et al., 2011) to utilize the well-established TSA, typically used for noise reduction in signal processing to suppress harmonic excitation under EMA technique. In their work, a series of knocking were generated manually under the running condition of electric motor mounted on the FSR. Each knock serves as a triggering signal to enable the response output to be captured and stored in pre-determined block size with specific number of samples per block. They highlighted that by selecting and averaging specific signal blocks triggered by the impact hammer knocking, harmonic elimination is possible based on the generated FRF results, which showed attenuated peak of harmonic frequency. In this note, it is worthy to highlight that a rigorous post-processing is essentially required in terms of performing meticulous selection of the blocks that lead to the suppression of the harmonic. Further, the mechanism for harmonic elimination was

not fully elaborated due to the random selection of the signal blocks, which prevent the process to be translated into appropriate analytical expression. Moreover, the integration of the coherence results into the analysis which would shed light on the effectiveness of the proposed harmonic elimination technique and this parameter was not presented within the previous studies (Rahman et al., 2011).

TSA technique has been known to be used in both eliminating the noise and isolating the harmonics (Braun, 2011; McFadden, 1989). A novel time synchronous approach was developed by Mark (2015) to suppress harmonic contribution from mating gear and the gear pair. A designed criterion was introduced to equate the number of contiguous revolutions of the gears of interest to a natural multiple of number of teeth on the mating gear to isolate the transmission error originating from the non-tooth meshing. Several studies have focused on comparing the dynamic characteristics between EMA and OMA within a particular structure (De Vivo, Brutti, & Leofanti, 2013; Ebrahimi et al., 2013; Najafi, Schmidt Paulsen, Belloni, Bedon, & Mann, 2014; Xu & Zhu, 2013). These studies were mostly conducted to justify the reliability of OMA to yield similar modal parameters in accordance to EMA results.

In the present work, we attempt to the address the persisting limitation and challenges on realizing EMA under operational condition en route to achieve highly reliable analysis in compliance to the results obtained under classical EMA. The novel aspect of this work lies on the suppression of the harmonics right from the output response prior to the construction of FRF, which lead to much reliable analysis to match the results from EMA. By using the newly developed automatic impact-knocking device, a periodical knockings are generated consistently, giving much reliable input to the system for further processing. The use of specific design

criteria for the impact knocking and block averaging will ensure successful elimination, which is articulated through the output response. Further, in order to demonstrate the effectiveness of the new approach, the investigation will be conducted at the resonance condition of the tested structure. The quality of the output will be rigorously analyzed in terms of the coherence property, which is the critical evaluation parameter that will determine the success of harmonic elimination from the input-output perspective. This study would serve as foundation to extend the applicability of the EMA on resolving dynamics characteristics under harmonic disturbance where OMA was normally adopted.

Window function in EMA has an essential role to ensure both incoming input force and output response signal is able to proceed properly by the Fast Fourier Transform (FFT) module. Windows function for EMA has been discussed by HP a long time ago (Packard, 1997). A recent study about advanced window function to enhance EMA has been also conducted by Chao, Cheet, Yee, Rahman, and Ismail (2016). However in this research, to keep the result of the EMA under the operational condition is comparable to the EMA under a non-operational condition, the original setting for the conventional EMA is preserved as same as in proposed EMA.

EMA has evolved in theory, methodology, and application since introduced in the last century by a documentation (Backus, 1960). In this study, EMA under-operational condition has implicated to transform Reliability Centered Maintenance (RCM) as the latest variant of CBM to be an integrated maintenance technique that involves the resonance related problem identification to be adopted in the industry. So far, utilization CBM in maintenance activity has been excluded conventional EMA (Jardine, Lin, & Banjevic, 2006; J. Lee et al., 2014; Sikorska, Hodkiewicz, &

Ma, 2011). Real-case application of EMA and has been documented. Many real cases industrial application of RCM, in an industry has been documented (De Carlo & Arleo, 2013; Maletič, Maletič, Al-Najjar, & Gomišček, 2014; Rastegari & Bengtsson, 2014; Tsarouhas, 2013; Yang, Kang, Zhao, Li, & Li, 2014). In addition, EMA result has studied to be an essential part for Dynamic Design Verification (DDV) on a structure that supports rotating machinery due to resonance related problem by Noroozi et al. (2016) and Abdul Rahman, Noroozi, Dupac, Al-Attas, and Vinney (2013). Also, Dossing (1984) reported DVD of a prototype rapid transit train using modal analysis. Some critical reviews have been initiated to reflect timeline of EMA. Studies in EMA has been critically reviewed in recent years by Ramli et al. (2017). Panza (2015) reviewed experimental techniques for NVH analysis on a commercial vehicle. Kumar, Reddy, and Rao (2013) reviewed the application of EMA testing in the civil engineering field, on beam structure.

CHAPTER 3: DEVELOPMENT OF AN AUTOMATIC IMPACT DEVICE FOR PERFORMING EMA UNDER OPERATIONAL CONDITION

3.1 Introduction

An automatic impact device system, which consists of a combination of computer controlled linear solenoid and force sensor was developed to replace an ICP impact hammer in classical EMA procedure. A dedicated electrical circuit was constructed to transform an artificial signal generated by virtual instrumentation software into an analog output for driving and controlling the solenoid motion. Under the present configuration, the solenoid was positioned vertically above the force sensor that was mounted on a tested structure. The gap between the solenoid end-effector and the force-sensing pad was adjusted to obtain the optimum characteristics of the generated force input signal. This includes attaining the maximum amplitude from the impact along with the establishment of single impulse profile onto the tested structure under different operating conditions. For the validation purpose, the acquired force input signal along with the natural frequency of the structure was systematically compared with the results generated under the classical EMA procedure. The present results have demonstrated that the new system is capable to match the performance of the currently used impact hammer system in terms of providing reliable input force and modal parameter at static condition of the structure. Further, due to its capability to provide periodical impact onto the structure, the introduced system can also be extended to conduct EMA under operational condition which paves a new paradigm for vibration analysis of structures with running harmonics.

3.2 Driving Solenoid

The nature of classical EMA requires a well-trained operator to perform series of knocking on a structure using specially designed piezoelectric hammer prior to analysis. Often this task is regarded as time-intensive and physically demanding segment of EMA. The instrument is tied to a single operator, which poses a restriction on the modularity and ability of the system to serve as operator friendly scheme. Further, there is a criterion that requires the hammer to be knocked in perpendicular direction to the surface and any double knocks or rattling should be avoided. Focusing on the motion of the hammer tip there is a path that should be followed when the ICP impact hammer is replaced by a combination of solenoid and force sensor.

One of the persisting challenges in realizing fully automated devices is managing the synchronization between different interconnected hardware instruments and control signals. In this section, solenoid control process is divided into three distinctive parts. The first task is generating the desired signal via the software (Dasylab). A hardware-interfacing module would then be established to channel the generated signal for controlling the solenoid actuator. The final component is reconfiguration of the signal to attain impulse mode input on the structure.

3.2.1 Generating Square Wave

In order to exert an impact force to the structure which serves as input in EMA, a square wave signal was considered as the basis of driving signal for the solenoid actuator. To achieve this task, virtual instrumentation software from Dasylab was used to artificially generate the required signal (Figure 3.1) which would trigger the solenoid plunger motion. Figure 3.1(a) shows the worksheet developed to generate

and transmit the signal to DAQ device for driving the solenoid. The worksheet consists of a module *G1* that generates square wave signal from Dasylab library by which the signal characteristics can be adjusted according to the designed input parameters in module *Modula G1*.

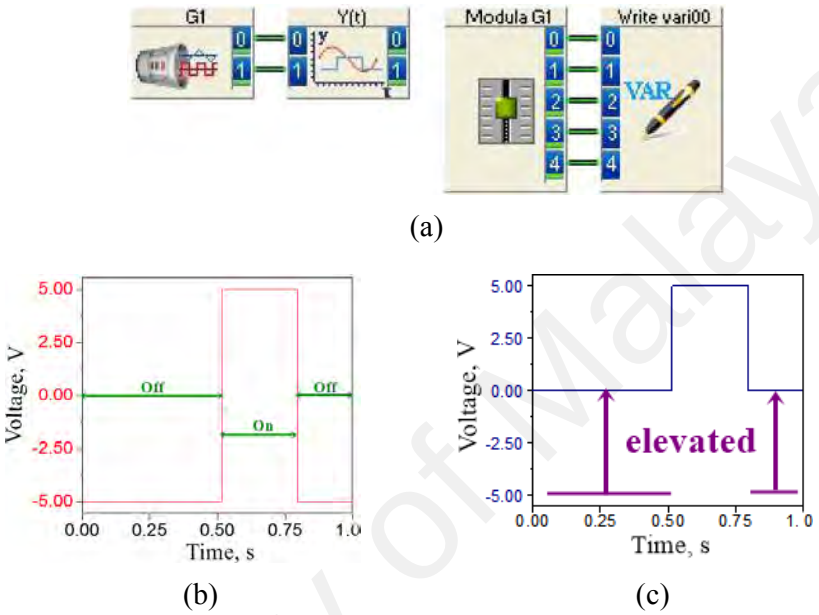

Figure 3.1: Generation of square wave signal. (a) Worksheet for signal generation (b) Original signal and (c) Elevated signal.

This module performs the mathematical operation to shift and modulate the signal to match the requirement for energizing the solenoid. The values for the parameter are saved into the module Write vari00.

The characteristics of the square wave signal generated by the signal generator module within the software are presented in Figure 3.1(b). The signal consists of two timespan, 'On' and 'Off' along with the magnitude, also well-known as TTL high and TTL low, respectively. It is worth mentioning that the signal generated by the software built-in library requires slight modification in order to ease communication with the DAQ hardware, which works on 'On' and 'Off' signals, correspond to 0 and 5 V magnitudes specifically, the signal was modulated to a new form as given in

Figure 3.1(c). This can be conveniently accomplished by assigning and modifying the parameters within the modules used to generate the signal. On this note, the duty cycle, r_{off} that specifies the proportion of the 'On' to the 'Off' signals in one period is given by Equation (3.1). Where, T_{on} and T_{off} denotes the timespan of 'On' and 'Off' signal, respectively.

$$r_{DCY} = \frac{T_{On}}{T_{Off}} \tag{3.1}$$

3.2.2 Hardware Interfacing between Signal Generator and Actuator

The artificial signal generated by the software would travel through two major interfacing hardware, namely DAQ and relay circuit to activate the solenoid plunger motion. In essence, DAQ device, model NI USB-6008 was employed to enable two-way communication between the software and hardware using Measurement and Automation (MAX) driver interface. In the present case, the generated square wave signal by Dasylab was converted into analog signal at 150 samples/s and was further transmitted into the DAQ analog output channel by a Universal Serial Bus (USB) cable. The signal flow is shown schematically in Figure 3.2 along with the actual image of the device.

The signal leaving the DAQ analog channel will enter a relay circuit that serves to energize the solenoid and execute the motion. In the present work, a multipurpose 24 V DC solenoid was used to deliver the desired knocking on the structure. The inductance and resistance was measured using high precision Inductance Capacitance Resistance (LCR) meter from PINTEK LCR-900. Full specification of the solenoid is presented in Table 3.1.

It is worth to highlight that the output voltage from the DAQ was insufficient to drive the solenoid. Hence, a 24 V DC input was supplied to the circuit to achieve the

task. Under this configuration, the signal from the DAQ was used as a switch to control the duration of the solenoid in energized or idle mode. Figure 3.3 shows the relay circuit diagram alongside the physical connection of the actual components.

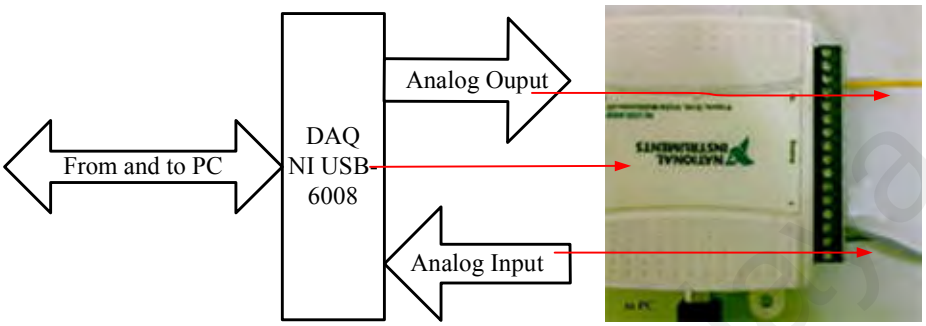

Figure 3.2: Hardware interface for signal communication between Personal Computer (PC) based controller and output device

Table 3.1: Specification of the solenoid

Parameter	**Value**
Dimension (L x W x D), mm	35 x 25 x 20
Weight, g	97
Inductance, mH	46.20
Resistance, kΩ	0.21
Full stroke, mm	10

In order to gain control over the solenoid activation signal, data communication between the software and hardware interfaces need to be synchronized. NI USB-6008 consists of 12 bits analog and digital input/output channels. In the present work, an analog output channel with output rate of 150 Hz was used to transmit pulse signals from the software into the relay circuit. In order to match the hardware capability, the sampling for the signal generated by software was made identical to the hardware specification (i.e. 150 samples/s), which provides a sampling period of (1/150) s. The 'Off' (0 V) and 'On' (5 V) segments of the square wave signal were determined by multiplying the sampling period with the number of samples. A block system was used to represent the number of samples that moved to the analog

channel in the hardware. The block size was determined by the number of samples inside each block. A block period was configured to accommodate a specific number of samples within the block size.

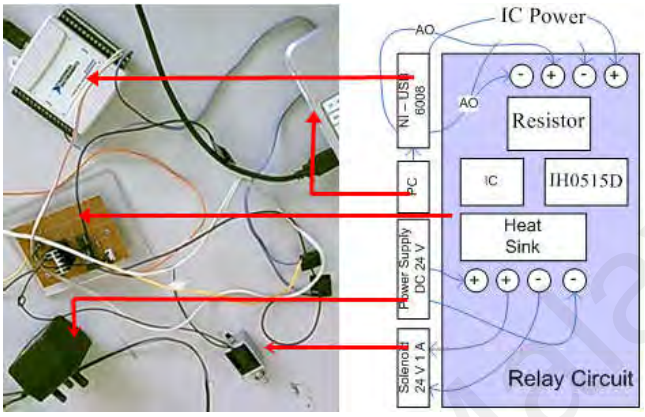

Figure 3.3: Relay circuit diagram for solenoid control

The minimum block period was governed by the hardware output rate, meaning that inaccurate data would be transmitted if the block period was set less than 1/150 s. By selecting one sample per block (block size) with block period of (1/150) s, each sample ('On' or 'Off' state) was transmitted to the DAQ output channel and then to the relay circuit. Hence, the duration of 'On' and 'Off' of the solenoid can be directly configured by assigning the number of sample for 'On' and 'Off' signals. This is important in order to avoid information lost due to periodical mismatch between the solenoid activation frequency and the sampling rate. Further, this is also to ensure that each block provides precise information on the time when 'On' and 'Off' signals occur. Consequently, the duty cycle, r_{DCY} in Equation (3.1) can be expressed in terms of the above sampling parameters via the following Equation (3.2):

$$r_{DCY} = \frac{S_{On} T_{Sout}}{T_{sole}} \tag{3.2}$$

Where, S_{On} is the number of sample for time 'On' chosen manually, T_{Sout} is the period of output sampling rate which is limited by the NI USB-6008 specification and T_{Sole} is solenoid period based on the designed frequency.

Using similar worksheet as in Figure 3.1(a), the exact timing for both 'On' and 'Off' portions of the signal can be assigned by configuring the block size within the time-based set-up of the software to control signal information in each sampling. The synchronization between the transmitted signal and the DAQ will ensure precise activation of the solenoid. An Analog Output (AO) module named *AO-Sole* was appended on the existing signal generator worksheet as shown in Figure 3.4(a) to enable direct interfacing between the software and the hardware via the DAQ.

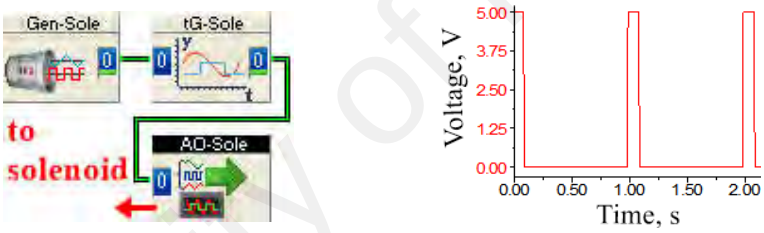

(a) (b)

Figure 3.4: Signal generation and transmission for solenoid control. (a) Worksheet with interfacing module (i.e. *AO-Sole*) and (b) Generated square wave signal

Figure 3.4(b) shows a typical square wave signal generated from the minimum duty cycle for the current configuration is 0.0067 which is equivalent to 1 'On' and 149 'Off' samples. In realizing reliable control of the solenoid, it is critical to consider the hardware specification along the signal path. Thus, the limitation of the DAQ was accounted to avoid signal mismatch between related devices.

3.2.3 Simulating the Effect of Impact Time Interval

In order to achieve the desired response from the impact of the solenoid end-effector, the contact time between the solenoid end-effector and the force sensor pad

should be minimized. On this note, the solenoid has to be controlled to achieve an impulse mode of input from the impact. The effect of the impact timespan can be observed by analyzing the response of Single Degree of Freedom (SDOF) system under impulse forcing function. The output displacement of the system under square wave forcing signal is decomposed into two specific components. For timespan of $0 < t < t_1$, equivalent to the time 'On' of the pulse, the corresponding output response is given by Equation (3.3)

$$x(t) = \frac{F_o}{k} - \frac{F_o}{k\sqrt{1-\zeta^2}} e^{-\zeta\omega_n t} \cos(\omega_d t - \theta), \quad for\ 0 \le t \le t_1 \tag{3.3}$$

Where, k is the stiffness, F_0 is the impulse force, ζ is the damping ratio, ω_n is the undamped natural frequency, ω_d is the damped natural frequency and θ is the phase angle. Meanwhile the response after the withdrawal of the impact is provided by Equation (3.4),

$$x(t) = \frac{F_0 e^{-\zeta\omega_n t}}{k\sqrt{1-\zeta^2}} \left\{ e^{-\zeta\omega_n t_1} Cos\left[\omega_d(t-t_1) - \theta\right] - cos(\omega_d t - \theta) \right\}, \quad for\ t > t_1 \tag{3.4}$$

It is worthy to mention that the SDOF approach would predominantly replicate the effect of impulse forcing input on Multi Degree of Freedom (MDOF) system. This is due to the alignment of the multi degree coordinate transformation towards the original coordinate by which the mode contribution will have similar effect as SDOF system.

A program attached in Appendix F was written in Matlab platform to solve Equation (3.3) and (3.4) in order to simulate the response from different impulse time. In actual impact sequence, the contact time between the hammer tip and the

surface of a structure is determined by the softness on the hammer cap. However, within the new driving impact configuration, the solenoid end-effector contact time on the structure can be controlled by specifying the number of sample, S_{On} . Figure 3.5 shows the response of damped SDOF at different impulse time. The input data for the response were given as follows: maximum frequency 30 Hz, stiffness 50 N/m, damping ratio 0.05%, input force 5 units and phase 0 rad. Contact timespan was set at 0.05, 0.1, 0.5 and 1 s respectively. It was evident from the figure that, as the contact time increases, the output signal deteriorated which adversely implicate the FRF, leading to the false interpretation in modal analysis.

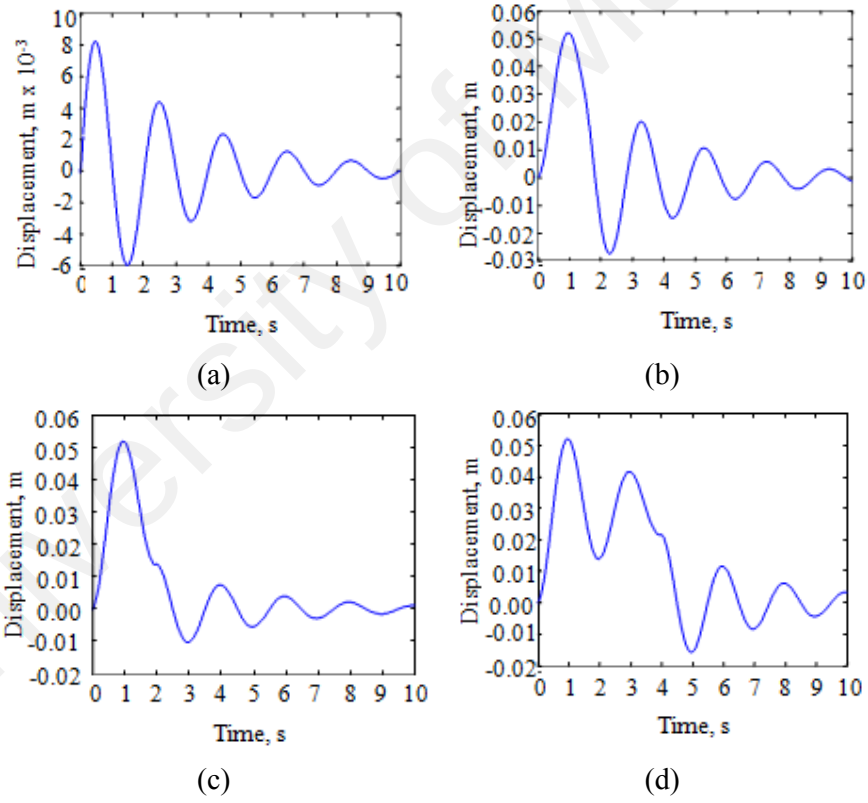

Figure 3.5: Output response of damped SDOF system at different impact time. (a) 0.05 s (b) 0.1 s, (c) 0.5 s and (d) 1 s

The result highlighted the importance of exerting impulse knocking on the structure when performing EMA in order to attain reliable data for further analysis.

3.2.4 Transmissibility of Generated Signal

Further verification on the controlling signal was conducted to ensure the conformity of the solenoid in response to the driving input signal. An experimental set-up was constructed to perform the above task as shown in Figure 3.6.

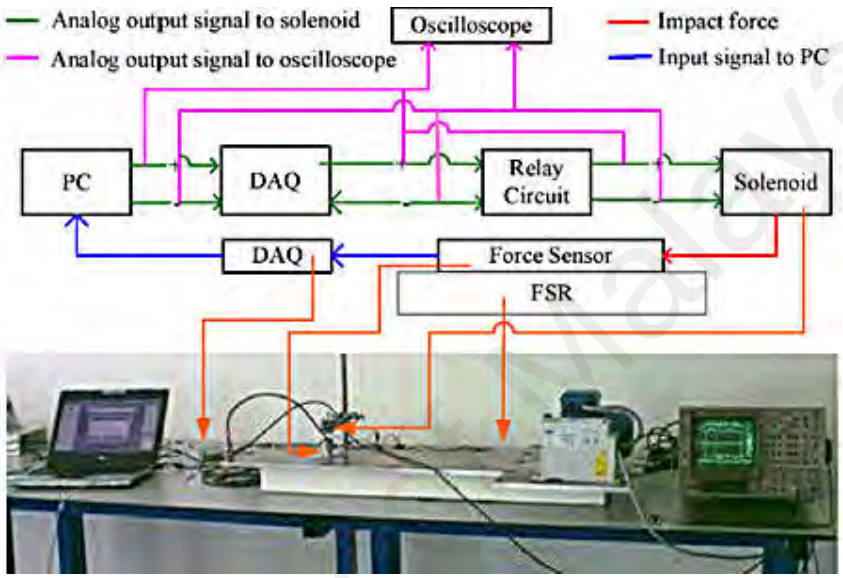

(a)

(b)

Figure 3.6: Signal transmissibility verification to control the solenoid. (a) Hardware configuration and (b) Worksheet

The rig consists of a solenoid held on a separate stand and a force sensor, model PCB 208C01 (Appendix KK) which was mounted on the FSR together with motor and inverter. The aim was to gain consistent output from the force sensor in accordance to the controlling signal. An oscilloscope was employed to monitor the generated signal as it flows to different part of the hardware until reaching the relay circuit and

further serves as a trigger for energizing the solenoid. The block diagram in Figure 3.6 elaborates the process of signal transmissibility verification. The force signal from the contact between the solenoid end-effector and the force sensor was transmitted back to Dasylab through NI 9234 (Appendix LL) sound and vibration DAQ, to be further analyzed. This approach also serves to identify and isolate potential problems occurring in between hardware which can be systematically rectified. The list of DAQs and sensors used for the present work is presented in Table 3.2 along with the corresponding functions.

Table 3.2: List of DAQ and sensors used for solenoid control as well as force and acceleration measurements of the tested structure

Device	Model	Function
Force Sensor	PCB 208C01	Converting impact force into electrical signal
Accelerometer	WR 786C	Converting vibration into electrical signal
DAQ	NI USB-6008	Transmitting analog signal into the relay circuit to control the solenoid
DAQ	NI 9234	Receiving electrical signal from force sensor and accelerometer to be converted into measurable quantity

An extension of the existing worksheet in Figure 3.4(a) was performed to include the necessary module for acquiring signals from the force sensor as shown in Figure 3.6 (b). In particular, an analog input module *Task DA00* was introduced to acquire signal from NI 9234 after the force sensor which was later displayed in module *YtChart00*. The input signal was eventually recorded and displayed in module *Rec-Sole* for comparative assessment.

Two separate test conditions were configured to evaluate the performance of solenoid in generating impulse input onto the structure. It is acknowledged that low duty cycle would closely replicate impulse signal to yield better output response that leads to much reliable FRF. Using the worksheet in Figure 3.6 (b), the output force signal with S_{On} equals to one and three, corresponds to duty cycle of 0.0067 and

0.0200, respectively were compared as shown in Figure 3.7. Both signals were generated frequency at 1 Hz.

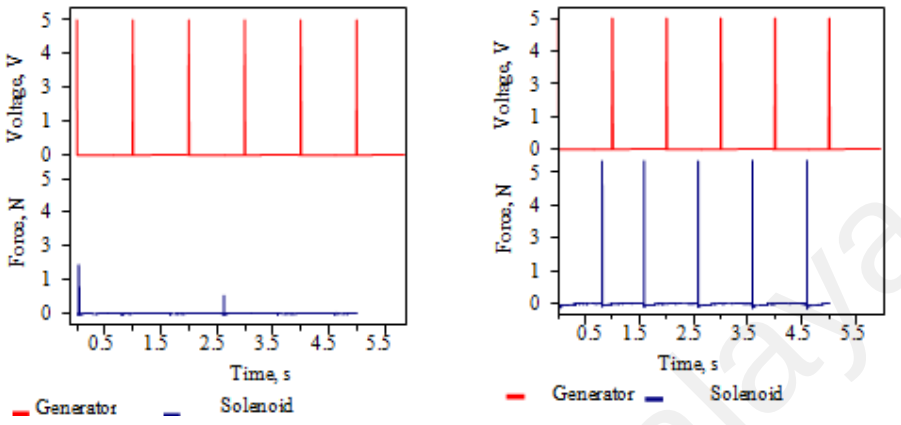

(a) (b)

Figure 3.7: Impact force generated for different number of samples. (a) 1 sample and (b) 3 samples. The red signal represents the generated signal from the software.

Figure 3.7 highlighted the effect of assigning different timespan of 'On' pulse signal on the output response based on the given hardware constraints. Specifically, choosing S_{On} equivalent to 1 sample resulted in low output force as shown in Figure 3.7(a). This can be explained by looking at the role of the impulse signal which served as a gate for the current with 24 V DC voltages to flow and energize the solenoid. The relatively high duty cycle for the impulse signal in Figure 3.7(b) signified more time for the current to flow and energize the solenoid, leading to consistent impact on the force sensor which can be seen from the magnitude. Further, the output force remained in impulse mode indicating that the structural response would yield high integrity FRF.

3.3 Substitution and Calibration of Force Sensor with ICP Impact Hammer

The ability to generate impulse force input with the combination of solenoid and force sensor as demonstrated in the previous section which would pave new dimension on conducting EMA on top of the conventional manual impact hammer

approach. In this section, further investigation was directed on evaluating the performance of the new impact device configuration relative to the existing ICP impact hammer method. In essence, series of signals generated by the proposed method would be compared for validating its conformity to conduct EMA.

For validating the reliability of the force sensor used in the current configuration, a 'back to back' calibration was conducted with a built-in force sensor from ICP impact hammer. The aim of the calibration was to ascertain the output data generated by the proposed approach relative to the conventional practice. The calibration was performed by knocking the ICP impact hamper directly to the force sensor as shown in Figure 3.8(a). This would allow both sensors to receive identical impact from a single physical source which would ease data analysis. The schematic of the sensors along with the communication hardware are presented in Figure 3.8(a).

A worksheet was developed to perform the above data acquisition as well as calibrating task as shown in Figure 3.8(b). Analog signal from force sensor and impact hammer flowed back to NI 9234 in module *Task DA00*. Module *Scalling01* was employed to perform zero offset on both incoming signals prior to knocking by using the first block of data once the worksheet was activated. Module *Scalling00* meanwhile contained correction factor for force sensor (i.e. channel 0) to match the impact hammer data. Module *Data Trigger00* served as triggering signal for module *Relay00* which allowed signals to be acquired as the impact generates voltage signal larger than 4V. Module *ComY/t* displayed the acquired signal while module *Statistic00* evaluated the maximum value of the signal. A reference signal for ICP impact hammer was also displayed on top of the original and compensated force sensor data. These signals flowed to Microsoft Excel worksheet shown in Appendix G, using module *DDE Output00*.

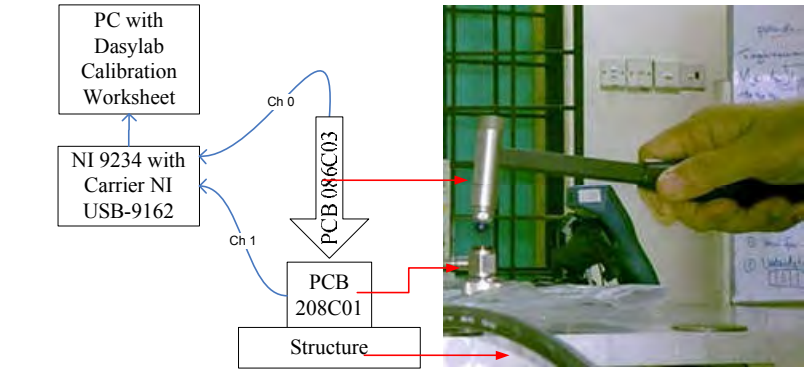

(a)

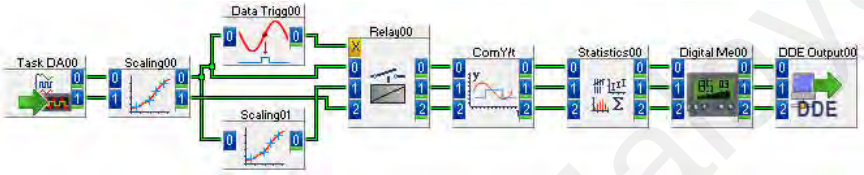

(b)

Figure 3.8: "Back to back" calibration between force sensor and ICP impact hammer. (a) Measurement setup (b) Worksheet for data acquisition

Figure 3.9(a) shows the result of force measurement from both the ICP impact hammer model PCB 086C03 as specified in Appendix MM, and the force sensors with respect to every consecutive knocking before and after the calibration. The data before the calibration were acquired by setting the correction factor to unity to provide uncompensated data for the force sensor. The range of force measurement was limited between 5N to 25N in proportion to the knocking intensity of the hammer against the force sensor. The results showed a slight deviation of the force sensor signal relative to impact hammer. In order to determine the correction factor for the force sensor the following equation was adopted based on linear interpolation concept ("DASYLab Help," 2007) as shown in equation (3.5).

$$f(x_{ca}) = a_{sl} x_{ca} + b \tag{3.5}$$

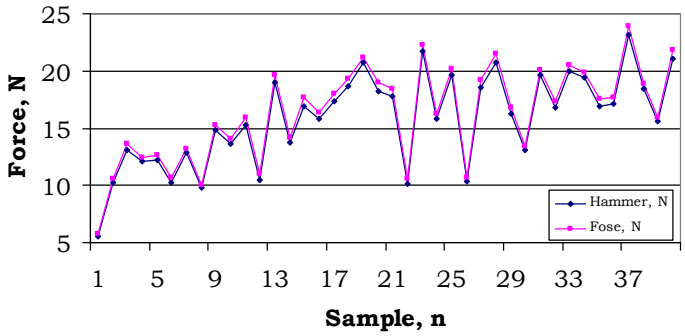

(a)

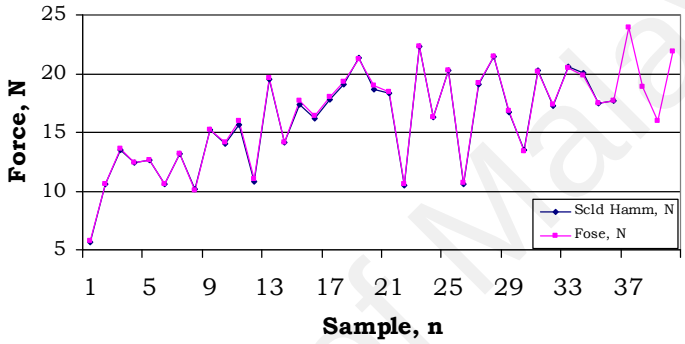

(b)

Figure 3.9: Calibration of force sensor data between force sensor and ICP impact hammer. a) Before and b) After calibration

Where, $f(x_{ca})$ is the output value, a_{sl} is the slope for linear equation, b specifies the offset of the linear equation and x_{ca} is the sample number in sequential order. With $f(x_{ca})$ as the mean value of the output sample and $\bar{x}_{ca}$ represents the mean value of the input sample, a_{sl} is evaluated by the following equation:

$$a_{sl} = \frac{\sum (x_{ca} - \bar{x}_{ca})(f(x_{ca}) - f(\bar{x}_{ca}))}{\sum (x_{ca} - \bar{x}_{ca})^2} \tag{3.6}$$

Using the above two equations the correction factor for the data generated by the force sensor was adjusted to 0.973 to match the response of ICP impact hammer. The results from force sensor after calibration were shown in Figure 3.9(b). The calibration exercise confirmed that the input signal difference was not attributed to the internal defect of the sensor which would give inconsistent reading for every

knocking. Further, the relatively small change in correction factor indicated the reliability of the force sensor to replace the conventional ICP impact hammer arrangement under the present proposed concept

3.4 Configuring Mobile Platform Apparatus for Driving Solenoid

The mobile platform for accommodating the solenoid should be taken into consideration for ensuring the viability of the proposed automated driving impact system. Sources of vibration originating from the apparatus as well as other components within the set-up need to be well-accounted. Rattling in the input as well as noise from the output signal is highly undesirable and should be minimized to gain reliable FRF. In addition, the path taken for the solenoid end-effector on the force sensor surface during the impact requires specific attention in order to produce single impulse effect as well as addressing the limitation of the conventional ICP impact hammer approach.

3.4.1 Supporting Structure of the Solenoid

By understanding the kinematics of ICP impact hammer on structures in typical EMA, it is evident that generation of a single contact point, unidirectional force and single impact are the critical criteria to be established between the hammer and structure during the knocking stage. These serve to reduce the irregularities in output force generation that mostly attribute to double knocking and multi-dimensional forces and contacts which complicate and compromise the analysis. With this in mind, the present solenoid was positioned in perpendicular to the test structure to attain the above requirement as shown in Figure 3.10(a).

(a) (b)

Figure 3.10: Configuration of solenoid and force sensor under the present scheme. (a) Solenoid assembly on mobile stand and (b) force sensor mounted on the tested structure.

The force sensor was positioned inline to the solenoid plunger axis. The solenoid plunger position assures that the impact force is distributed symmetrically on the force sensor base and ultimately to the integrated structure. Figure 3.10(b) shows the attachment of force sensor on a base fixed to the FSR tested structure.

An isolated solenoid driving architecture was required to minimize the inertial impact on the tested structure as well as to embed portability and modularity within the device. In order to incorporate these features, a laboratory retort stand was selected to support and position the solenoid as shown in Figure 3.10(a). The flexibility of the clamps and adjustable feature of the rods enabled extensible domain of the solenoid towards different parts of the structure to achieve more measuring points.

3.4.2 Installation of Solenoid Isolation Cap and Sensor Loop Insulator

One of the critical design specifications for the new driving impact system relates to the contact between the interacting surfaces of solenoid end-effector and test structure. It is well-known that, in classical EMA, the choice of the hammer caps is governed by the surface contact as well as the range of excitation frequency. This would translate into either softer or harder cap to align with spherical, pointed as well

as flat caps profiles (*P.C.B. Piezotronics, Impact Hammers Model: 086C03*, 2013). For the present work, a single impulse signal along with low excitation frequency was required. Isolation between two impact materials was employed to avoid double impact, leading to a selection of a much softer cap. A piece of rubber was installed on the solenoid end-effector to meet the above requirement. In addition, a plastic sheet was placed under the force sensor to avoid interference in current flow between the force sensor and the accelerometer mounted on the same metal structure (i.e. typically recognized as sensor loop) ("General operating guide for use with piezoelectric ICP Accelerometer," 2015; Scott, 2009) as illustrated in Figure 3.11.

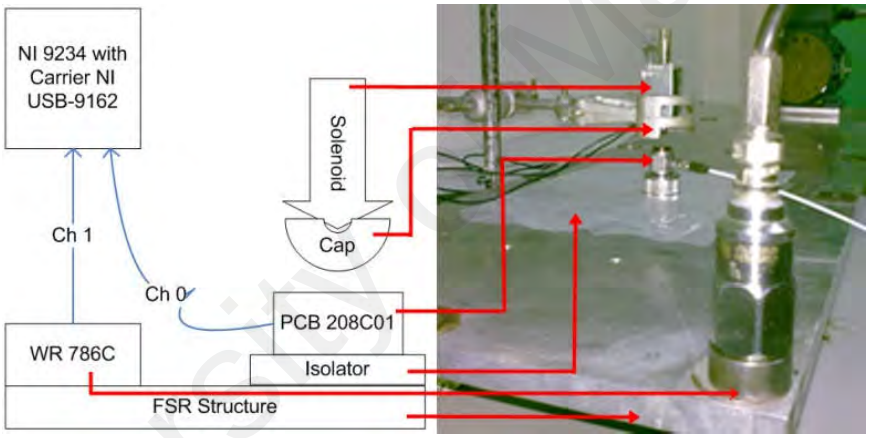

Figure 3.11: Placement of plastic sheet on force sensor to isolate interference signal from accelerometer.

3.4.3 Attachment of Damper on Solenoid Supporting Structure

Theoretically, after each cyclic loading the solenoid stand would react by its inertia. Hence, the solenoid stand acts as a source of vibration that transmits the force to the table supporting the solenoid stand as well as the FSR test platform. The FSR ultimately reacts in response to the table excitation. The theory of transmissibility between different vibrating structures has been thoroughly discussed both in analytical and experimental platforms (Inman, 2014).

In principle, the response of FSR caused by the solenoid stand during measurement can be simplified as a SDOF system represented by Equation (3.7).

$$x(t) = Ae^{-\zeta\omega_n t}\sin(\omega_d + \theta) + X_{ri}\,Cos(\omega_o t - \phi) \tag{3.7}$$

The first term of Equation (3.7) represents a transient part where A and θ are defined by initial condition while the second term signifies the steady state condition. As the plunger of the solenoid moves under pushing and pulling cycles, the supporting structure vibrates around its center of gravity by a pitching motion. This behavior can be modeled as the second term in the above expression, where, A_{ri} is the amplitude of vibration of the rig caused by the solenoid stand motion. The amplitude can be further described by Equation (3.8).

$$\frac{A_{ri}}{Y} = \left[\frac{1 + (2\zeta r)^2}{(1 - r^2)^2 + (2\zeta r)^2}\right]^{1/2} \tag{3.8}$$

Where Y, denotes the amplitude of table motion, ζ is the damping ratio, and r is the frequency ratio, equivalent to ω_b/ω_n. In the above equation, ω_b represents the frequency of table oscillation and ω_n signifies the natural frequency of the FSR.

It is evident from the above equation that a high damping ratio is required to suppress the force transmission from the solenoid stand to the table and FSR. High damping ratio can be achieved by incorporating a high damped material (Inman, 2014) on the structure of interest. On this note, an insole was installed under the stand base to absorb the oscillatory motion as shown in Figure 3.12. This material has been used as damping material for attenuation of the vibration in wide spectrum of researches (Leber & Evanski, 1986).

The insole was expected to reduce the amplitude of the stand vibration that penetrates into the structure. An experiment was performed to observe and measure the performance of the damper to reduce the vibration transmissibility.

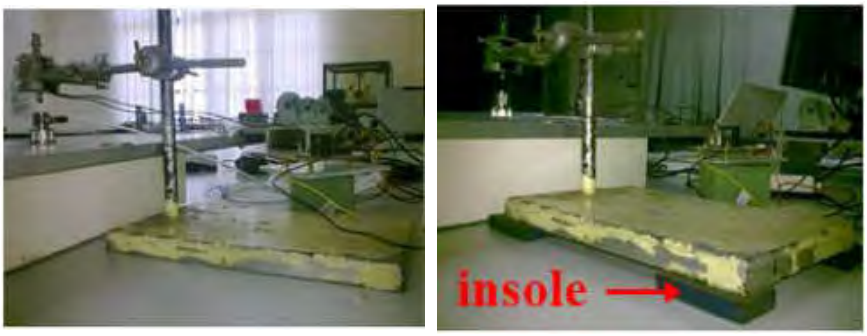

(a) (b)

Figure 3.12: Solenoid mobile stand under (a) undamped and (b) Damped configurations

An accelerometer model WR 786C specified in Appendix NN, was installed on the FSR as shown in Figure 3.13(a) to record the vibration signal from the knocking exercise. Within the experimental procedure, the solenoid plunger was made to undergo a single cyclic motion without engaging the test bed to activate the vibration of the support base. The transmitted vibration signal experienced by the FSR was monitored and recorded using an analog input module in Dasylab for further processing.

Figure 3.13(b) described the measured vibration data of FSR table subjected to inertial response from the base of the solenoid holder upon solenoid activation. As evident from Figure 3.13(b), the excitation from the solenoid base caused significant disturbance on FSR stationary condition based on highly fluctuated generated signal. In contrast, the use of insole as damper enabled large segment of the vibration intensity to be suppressed as highlighted in Figure 3.13(c). Attenuated inertial disturbance on the tested structure would ensure acceptable signal to noise ratio during operation which leads to much reliable FRF.

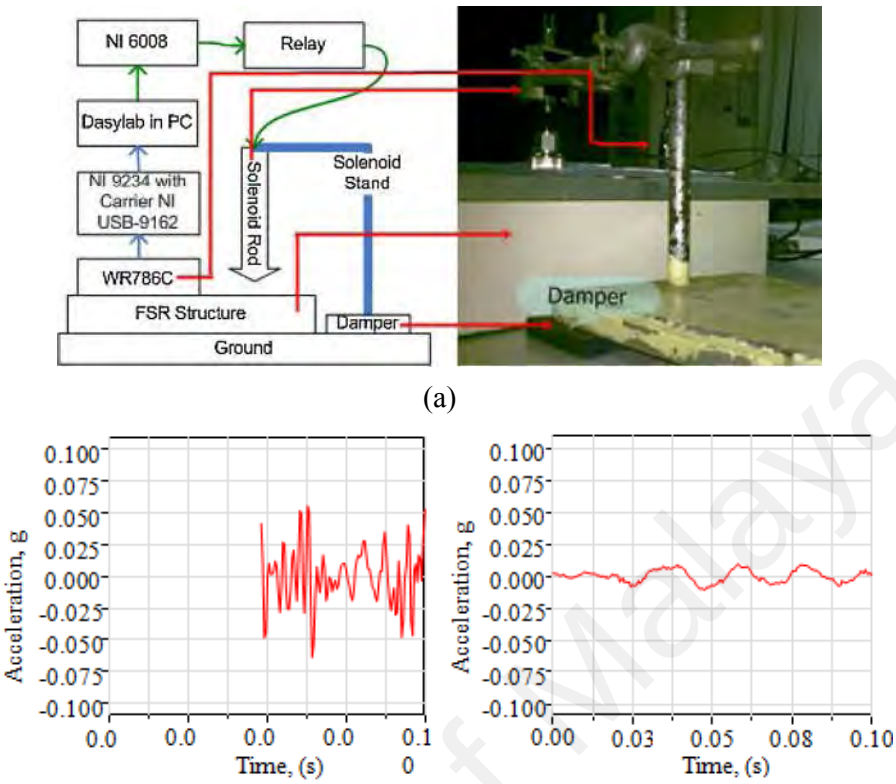

Figure 3.13: Process of measuring the effect of damping on the solenoid stand response. (a) Measurement setup, (b) Output response in undamped and (c) Damped configurations

3.4.4 Setting Solenoid Clearance under Non-Operational Condition

Another important aspect to be considered within the proposed impact system was to determine the optimum stroke of the solenoid plunger which would deliver the highest input without compromising its quality. As the solenoid was primarily held on a laboratory clamp which was also susceptible to vibration originating from the base, the distance between the solenoid end-effector and force sensor pad need to be adjusted to avoid double knock or lose of knock conditions as illustrated in Figure 3.14(a). In order to systematically adjust the solenoid position relative to the force sensor, two screws were mounted onto the solenoid casing by which the adjustment could be achieved by configuring the gap between the screw and the clamp surface.

A caliper was then used to measure the distance to provide better gap resolution within every adjustment.

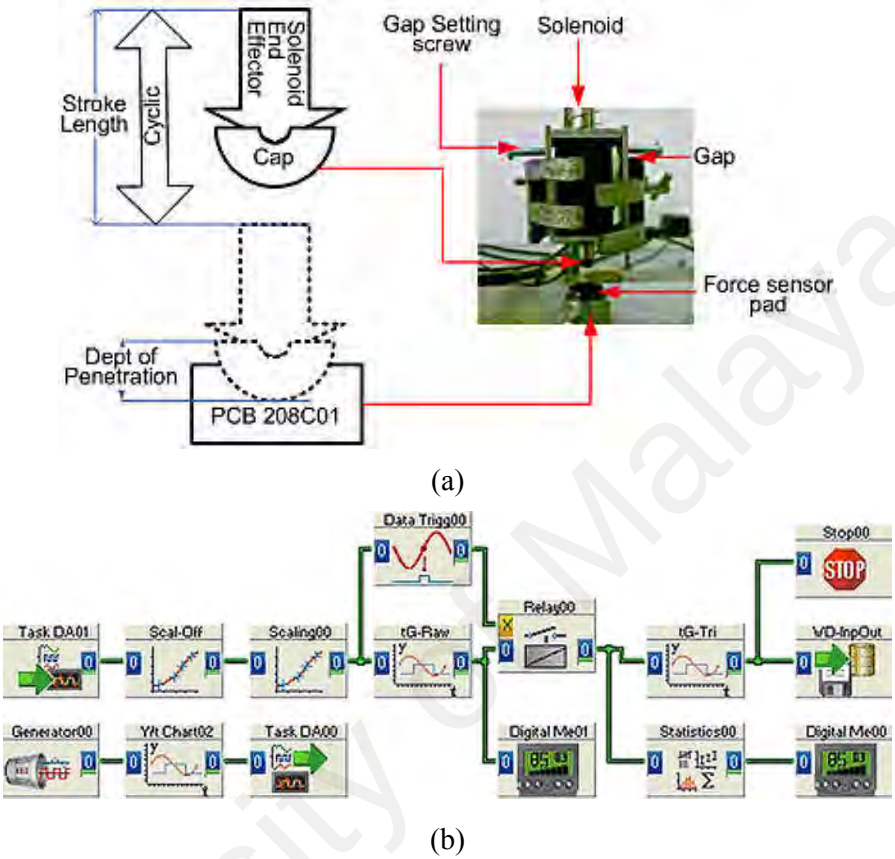

Figure 3.14: Hardware configuration, (a) and worksheet, (b) for measuring the effect of solenoid position on impact force generation

An experiment was conducted to measure the force input with reference to different gap settings. The knocking on the structure was accomplished via the newly developed automated solenoid driving system described previously. Two experimental conditions were investigated to attain the optimum gap for the solenoid, namely, with and without harmonic excitation. For the present exercise, the FSR was subjected to non-operating condition from rotating component mounted on the FSR.

A worksheet was developed to allow real time implementation of the automated impact driving system as shown in Figure 3.14(b). Module *Generator00* generated impulse signal which was displayed in module *Y/t Chart 02*. Module *Task DA00* then

channeled the control signal to the NI USB-6008 to activate the solenoid. The impact signal from the solenoid flowed to module *Task DA01* which was assigned to acquire signal from force sensor, PCB 208C01. Module *Scal-off* and *Scaling00* were used to set the offset adjustment and further recalibrate the input signal by using the first data block. The resultant offset signal was further displayed in module *tGRaw*. Module *Data Trigg00* prompted data acquisition as the plunger knocked on the force sensor while module *Relay00* allowed the data to pass through the next stage. The signals finally flowed through the module *WD-InpOut* and were saved in Dasylab Data Format (DDF) file. Module *Stop00* terminated the measurement after one cycle.

The setting for the data acquisition was given as follows: The sampling rate was set at 2048 Hz, block size was fixed at 4048 samples/block, triggering level, 3 N, pre-trigger samples, 50, impulse frequency, 1 Hz and duty cycle was 0.015. The gap was adjusted at 0, 1.6, 3.2 and 4.8 mm, respectively.

Using worksheet as shown in Figure 3.14(b) and the input data, the experiment was performed and the results were shown in Figure 3.15. It was understood that the quality of the force input was crucial to ensure reliable FRF. Low quality impact force would translate into misleading interpretation of the vibration characteristics. In the present case, a zero gap setting produced a double impact signal as shown in Figure 3.15(a), which would adversely affect the output response signals.

A plot of force generated at different solenoid gap as given in Figure 3.16 revealed an optimum gap setting that delivered disturbance free impact at maximum capacity. The above trend of impact can be linked to the solenoid characteristic under step response as shown in Figure 3.17.

A laser displacement sensor from ONO SOKKI model LD-1110M-020 was used to measure the displacement of the solenoid end effector with respect to time. The

figure underlined the importance of operating the solenoid within the period of its rise time, i.e. 24 ms to ensure that the end-effector followed a linear motion prior to reaching the force sensor pad as well as to avoid dynamic instability should the plunger was allowed to operate at its full stroke. For a given time 'On' of the input pulse signal, the segment where the impact force increased with respect to increase of the gap was attributed to the increase in potential energy of the plunger as the solenoid was energized.

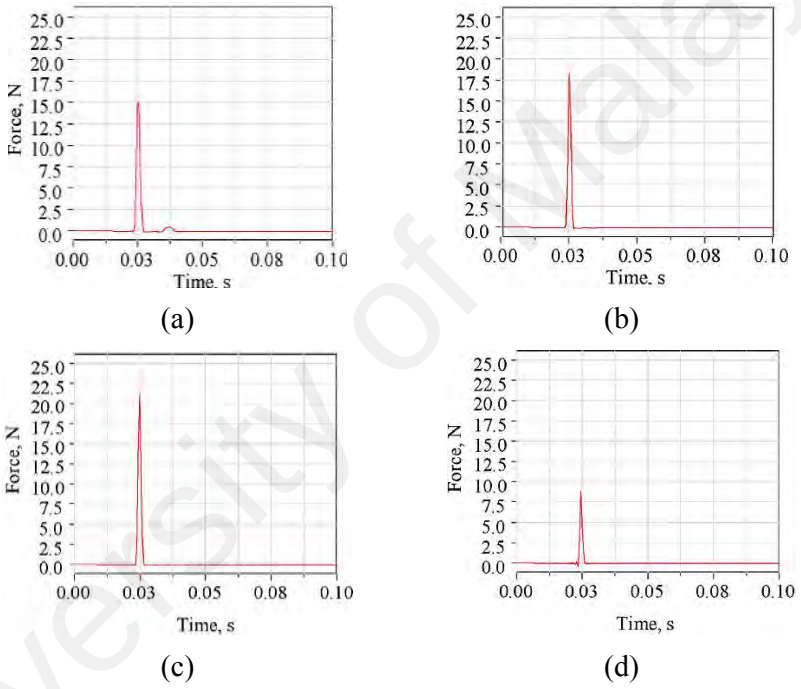

Figure 3.15: Force signal input measurement at different clearance between solenoid and clamp. (a) 0 mm (b) 1.6 mm, (c) 3.2 mm and (d) 4.8 mm

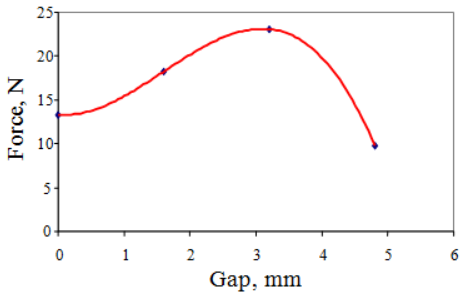

Figure 3.16: Graph of impact force versus gap clearance between the solenoid and clamp

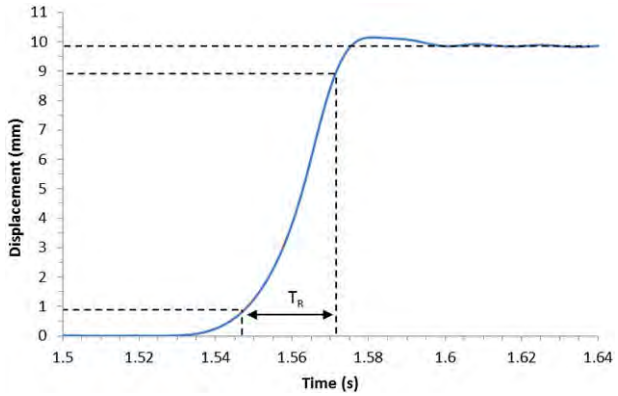

Figure 3.17: Step response of solenoid end-effector. TR represents rise time of the end effector motion

These impacts occurred before the completion of the entire high signal (3 samples/20ms), thus resulting in increasing trend of impact force. The plunger reached its peak corresponds to the moment when the current was disengaged from the solenoid (Off state of the signal). As the gap increased beyond the maximum force, the plunger experienced deceleration due to the opposing force exerted by the spring and this led to the reduction of the inertial impact on the force-sensing pad. Increase in the pulse duration given by the software would translate into sustained current onto the solenoid, more energy converted from electromagnetic to kinetic energy, longer trajectory of the plunger and higher the impact force. The results showed that setting the gap too close or too far to the force sensor would render negative effect both in the magnitude as well as in the knocking characteristic of the solenoid. Thus, it is imperative to properly assign an appropriate clearance to achieve optimum impact loading.

3.4.5 Setting Solenoid Clearance under Operational Condition

Further investigation was conducted to obtain the optimum gap for the solenoid under operational condition (i.e. FSR subjected to harmonic excitation by rotating motor). In this case, due the contribution from the fluctuating motion of FSR

originated by the running motor, the gap between solenoid end-effector and the force sensing-pad follows a harmonic characteristic as shown in equation (3.9):

$$l_{fg} = l_{ig} - (A_g \ Sin \ \omega_o \cdot t) \tag{3.9}$$

Where, l_{fl} represents the gap between the solenoid and force sensor, l_{ig} and A_g denoting the initial gap and FSR fluctuation amplitude and ω_o is the running speed.

The path of motion for solenoid plunger as well as the FSR was illustrated in Figure 3.18. It was anticipated that the harmonic excitation from the operating motor would reduce the performance of the solenoid in terms of generating the desired impact force. As shown in the figure, if the end-effector hit the force sensor pad during the negative amplitude of the harmonic, a second impact would potentially manifest right after the disengagement of the plunger and during the retraction motion due to the change in the oscillatory motion. This problem can be mitigated by increasing the clearance between the end-effector and the sensor pad to allow the solenoid to establish a contact only at the positive segment of the operational structure harmonic.

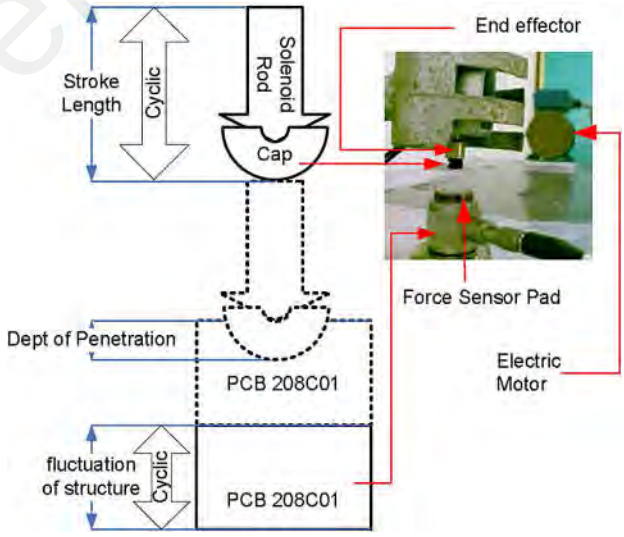

Figure 3.18: Solenoid end-effector motion on the force sensor under operational condition

Using similar worksheet as in Figure 3.14(b) along with the corresponding data acquisition setting, series of knockings were generated with different gaps and the results were presented in Figure 3.19. The operational speed of the motor was set at 20 Hz. An optimum gap obtained from the non-operational condition was selected as the basis of the current investigation. The result in Figure 3.19(a) showed that the optimum gap setting for nonoperational condition exhibited detrimental effect when employed under operational condition. As explained previously, this was highly attributed to the fluctuation in penetration depth of solenoid end-effector which led to double knockings. Thus, determination of the suitable gap in operational condition requires the user to obtain the optimum gap under non-operational condition, running the structure to obtain the harmonic amplitude and adjusting the plunger slightly away from the force sensor pad to allow impact to occur at the positive half of the harmonic and thus mitigating double impact. On this note, the gap has to be set higher to compensate the fluctuation in FSR at the expense of the impact strength as given in Figure 3.19 (b).

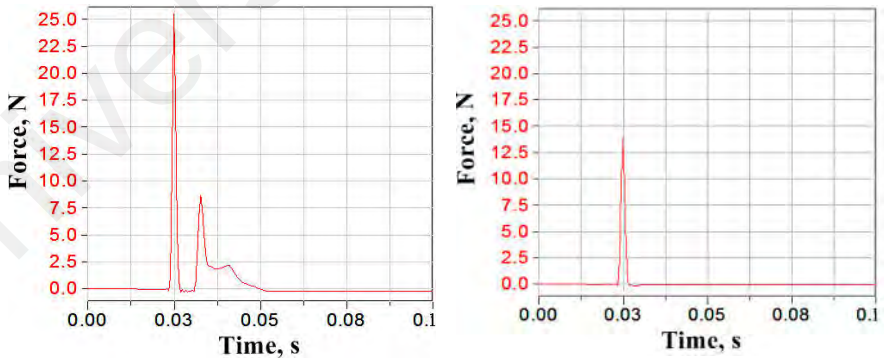

(a) (b)

Figure 3.19: Effect of operational condition on the input signal at different gap: (a) 3.2 mm and (b). 3.7 mm

The Figure showed that an impulse force can be effectively attained under operational condition which translates into reliable FRF with respect to input requirement in classical EMA.

3.5 Validation of Input Signal

In order to ascertain the quality of the signal generated through the proposed method, a comparative assessment with signals generated via classical EMA method was required. Since the classical EMA is conducted in non-operational mode the input signals is expected to match the results obtained using the newly developed automated impact device in terms of the signal characteristics. In addition, the results under operational mode will shed light on the possibility of extending EMA through signal elimination process for isolating the vibration signal from the harmonics.

Reference input signal was obtained by measuring force input generated by knocking the ICP impact hammer on the test structure as shown in Figure 3.20. The acquired signal was compared with signals generated using the solenoid based driving impact system under both non-operational and operational conditions. A similar worksheet as shown in Figure 3.14(b) was used to acquire the force signal under the present experiment. The acquisition required only one-block samples.

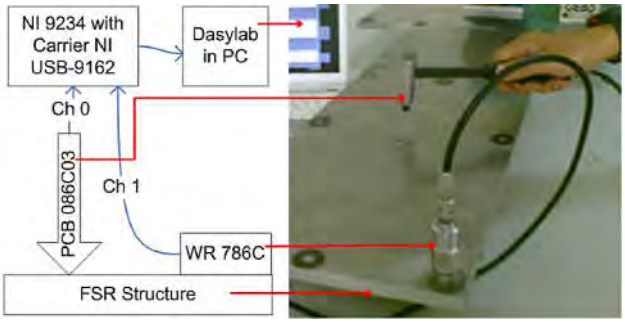

Figure 3.20: Hardware configuration for acquiring reference signals using classical EMA approach.

Pre-trigger sample was set as 1000 samples and the post-trigger was fixed at 3048 samples. Reference signal was compared with the signals acquired from a proposed system. The data acquisition parameter was set similar to the above solenoid based impact system (i.e. sampling rate = 2024 samples-s and block size of 4048 samples) to give a block period of 2s.

Using the worksheet and the designated input values, a single measurement was performed for each condition by which the results were given in Figure 3.21. The result showed that knocking using an ICP impact hammer produced an impact response with a peak recorded around 0.03s.

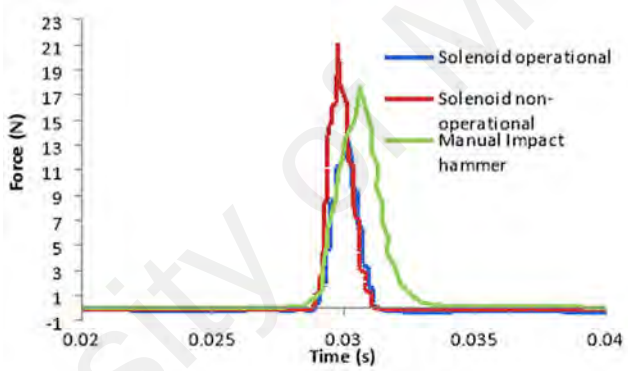

Figure 3.21: Comparison of force input signal generated under manual impact hammer

The signal decreased sharply after reaching the peak and disappears without producing secondary peak. The above result was further compared with impact force generated by the driving solenoid for non-operational and operational conditions. The results revealed close agreement of the input signals between the conventional ICP impact hammer and the newly developed solenoid based system. It was observed that a single peak was generated under all experimental conditions, which is a critical property for gaining highly reliable output response. Further, the time interval between the signal rise and fall was consistent for each of the approach, indicating

that the new solenoid based impact system can be used to replace the conventional ICP impact hammer system.

Further investigation was performed to compare the natural frequency obtained from each impact knocking approach. This endeavor also reflected the reliability of the force input signal, which has strong influence on the post-processing results. provides the FRF, as well as the corresponding real and imaginary plots between the ICP impact hammer and the solenoid based impact-knocking approaches.

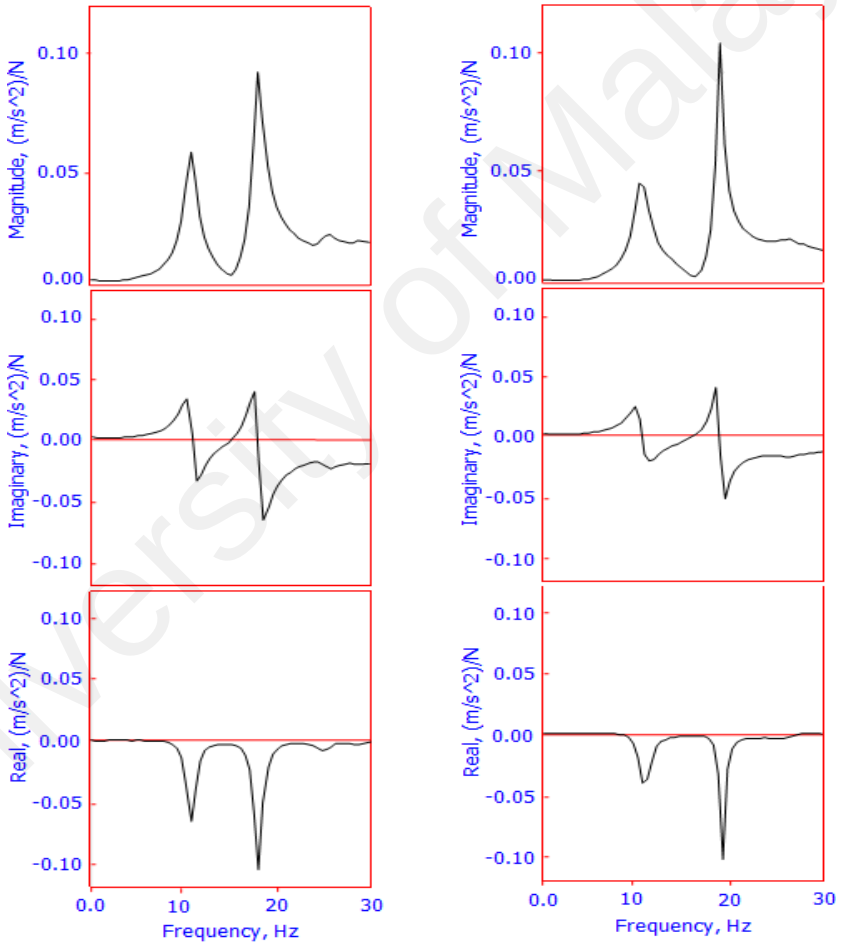

(a) (b)

Figure 3.22: Plot of FRF and the corresponding real and imaginary components obtained via (a) ICP impact hammer and (b) solenoid based automatic impact device

The results obtained by each technique had the average data from five consecutive knockings. It was evident that the present approach has the capability of capturing modal characteristics of the conventional impact hammer based EMA, judging by relatively similar natural frequency indicated by the zero crossing and peak for real and imaginary components, respectively. Both approaches unveiled two resonance frequencies at 11 and 18 Hz. This suggests that the new system can be adopted to conduct modal analysis, paving a new horizon on systematic modal identification with minimal human intervention. In addition, the ability to control the solenoid frequency would potentially solve the persisting obstacles of realizing harmonic elimination that deals with consistent knocking on the structure as highlighted by Rahman et al. (2011)

3.6 Summary

This chapter has focused on developing an automatic impact device for replacing ICP impact hammer in classical EMA. A combination of a force sensor and an electromechanical driven solenoid was used within the present hardware architecture to replicate the effect of ICP impact hammer. Virtual instrumentation software was adopted to enable direct manipulation of the solenoid through series of hardware communication devices. Different worksheets were established within the software to perform signal output to energize the solenoid as well as to acquire input from different sensors for further analysis. A systematic validation was performed for the results attained within the present approach with reference signal from well-established EMA. A square wave signal with specific duty cycle was generated within the instrumentation software to control the solenoid, which enabled a desirable input force to be exerted on the FSR integrated structure. Problem with the

vibration transmissibility of the solenoid stand was addressed with the appropriate damping. Series of experiments were conducted to obtain the optimum clearance between the solenoid and the force sensor to achieve high quality impact force at maximum amplitude. Comparative assessment between the signal generated via conventional ICP impact hammer method and the present approach has revealed a close agreement in terms of the ability to generate single impact force as well as attaining similar natural frequency. The results have led to a conclusion that the replacement of ICP impact hammer with automatic driving solenoid based impact system in EMA exercise is feasible. Further, the ability to control impact parameter particularly the frequency would pave promising avenue for performing EMA under operational mode, which is not feasible under classical scheme. Several experiments using hardware, software and specified file names involved to pairing up solenoid to force sensor tabulated in 0 to Appendix C, under classification, namely pairing up solenoid and force sensor.

CHAPTER 4: PERFORMING HARMONIC SIGNAL ELIMINATION IN EMA UNDER OPERATIONAL CONDITION

4.1 Introduction

This study focuses on introducing a criteria for conducting harmonic excitation signal elimination as well as investigating its effectiveness towards achieving complete isolation of harmonic disturbance in performing EMA under operational condition. By modulating the ratio between harmonic excitation and impact knocking frequencies, it was revealed that the harmonic signal was efficiently attenuated with sufficient number of averaging blocks. The results highlighted close agreement between simulation and experimental approaches with maximum deviation of 2%, under specific design criteria. It was determined that a non-periodic triggering frequency significantly affect the elimination performance in terms of trend and amplitude reduction. This work underlines the importance of controlling the triggering frequency to yield the desired design criteria for achieving rapid and highly efficient elimination of harmonic excitation signal. The results have proven that the proposed technique can be further adapted to isolate the harmonic in classical EMA conducted under operational condition.

4.2 Simulation of Harmonic Excitation Signal Elimination

4.2.1 Proposed Concept of Harmonic Elimination

Figure 4.1 illustrates the typical process for performing EMA along with the extracted raw data results. Due to the nature of the data acquisition process, EMA is executed under static condition of the structure, thus making it a highly reliable tool to resolve modal parameters of the structure since the force input and output response signal can be directly correlated to give unity coherence as shown in the results.

However similar EMA exercise under operational condition i.e. Figure 4.1(b) with running harmonic, ω_o would be detrimental en route to resolving the dynamic characteristic of the structure such as modal damping and mode shape since the coherence is tainted by the harmonic originating from the rotating structure. Due to this underlying issue, researchers have immediately switched to OMA to obtain the modal parameters under operational mode.

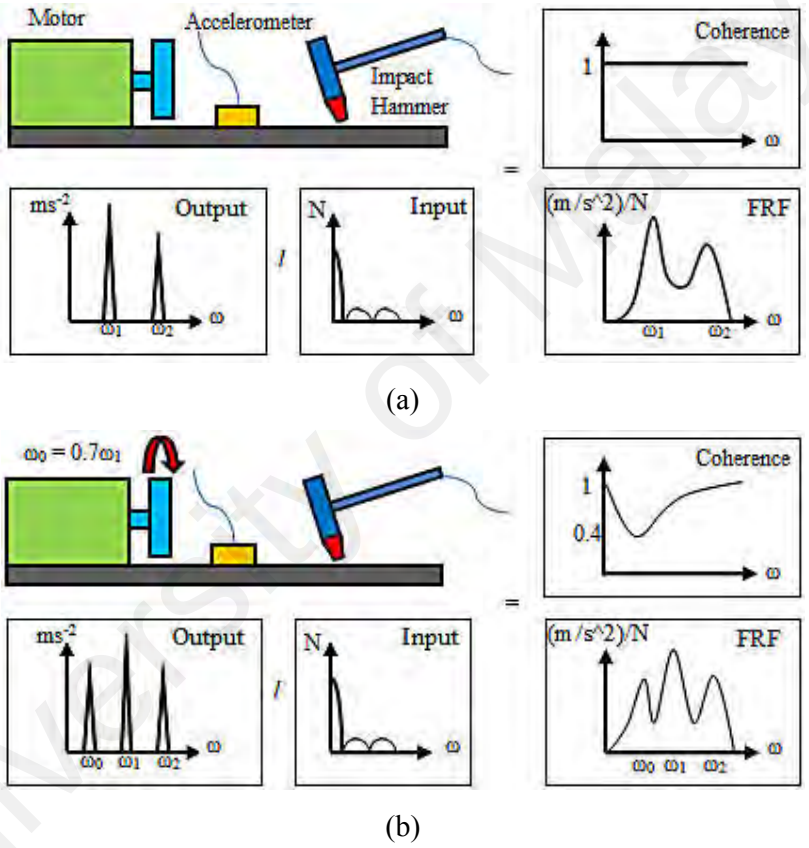

Figure 4.1: EMA execution in different structural condition (a) Typical EMA protocol executed in static condition (b) EMA conducted with harmonic excitation, ω_0

Figure 4.2 illustrates the protocol for obtaining FRF, an essential raw data for resolving the modal parameters of the structure EMA. The typical sequence for classical EMA starts by manual knocking of the impact hammer on the structure which excites the structure to yield transient signal. The output signal from the accelerometer will be combined via mathematical correlation with force input signal

generated by the built in force sensor within the impact hammer to give the desired FRF. In order to realize EMA under operational condition, a slight modification of the existing protocol requires an additional block to be appended to perform the averaging of each incoming signal generated by the accelerometer in response to each knocking sequence.

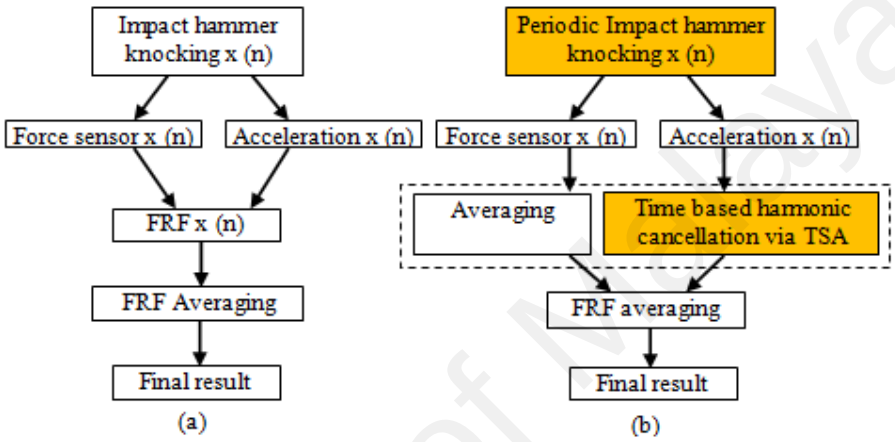

Figure 4.2: Protocol for extracting FRF in EMA (a) Typical EMA sequence under static condition and (b) Adopting consistent periodicity of impact hammer and TSA to suppress harmonic excitation signal in operational condition.

Further, another crucial criterion requires the knocking input to be in periodical form, in order for the amplitude of the harmonic to be consistently suppressed at each averaging sequence. While the harmonic is suppressed after sufficient number of averaging blocks, the transient signal which contains the resonance frequency of the system will be consistently preserved. The above concept can be realized by replacing the manually driven impact hammer with linear actuator working under electromechanical or piezo-resistive principles as shown in Figure 4.3. This will deliver the required periodic knocking which serve as triggering signal for data flow. The data analysis software will play an essential role to determine the block size of the response output signal upon each triggering to ensure consistent signal attenuation via TSA.

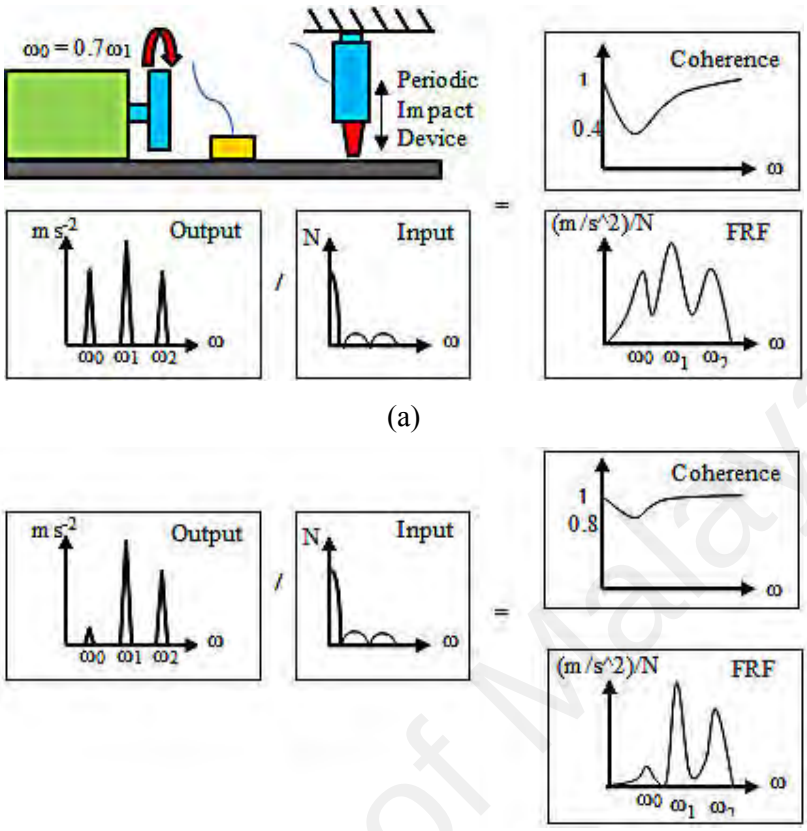

Figure 4.3: Implementation of periodic knocking on the structure via linear actuator along with expected results: (a) Initial stage (b) After sufficient number of averaging

It is worth to mention that while TSA has been widely adopted to preserve the harmonic signal of interest, the present concept uses the same principle to eliminate the harmonic to ensure much cleaner response output signals prior to further processing.

This research attempts to investigate the feasibility of eliminating the harmonic signal in operational structure via the above concept. Thus, the focal point of the present work is directed on realizing a criterion between the knocking and harmonic frequencies to achieve highly efficient harmonic elimination with minimal averaging. A simulation environment will be constructed to perform the elimination with real harmonic data from test structure. The harmonic elimination progress will be

monitored by extracting and tracing the amplitude of the running frequency for every averaging block.

4.2.2 Worksheet Development

In order to demonstrate the proposed signal elimination process, a simulation model was constructed with the use of Dasylab virtual instrumentation software. Within this computational platform, the amplitude, frequency and disturbance of the harmonics can be conveniently generated and adjusted. A moving averaging equation as represented by Equation. (4.1) was adopted for the purpose of averaging the harmonic signal. The averaging process works by sequentially overlapping each incoming signal block to the previous cumulative blocks and getting the average with the total number of blocks. The reciprocal period between each successive block represents the triggering frequency which is equivalent to the knocking of the impact hammer. In the above expression, *e* denotes the resultant harmonic amplitude; *h* is the incoming harmonic amplitude and subscript n symbolizes the number of progressive block.

Run	**Averaging**
1	$e_1 = h_{11}$
2	$e_2 = (h_{11} + h_{12})/2$
3	$e_3 = (h_{11} + h_{12} + h_{13})/3$
…	**…..**
n	$e_n = (h_{11} + h_{12} + h_{13} + ... + h_{1n})/n$

(4.1)

In reality, the motor frequency is not constant due to external factors. This fluctuation can be added into the steady state harmonics excitation frequency, f_{SH} via Equation (4.2). Where f_{FSH} is the simulated fluctuating harmonic excitation frequency, f_{SH} is the nominal harmonic excitation frequency, U_{MH} is the difference

between maximum and minimum value of the running frequency from a real electric motor and *rand()* is the function that generates random number.

$$f_{FSH} = f_{SH} - 0.5U_{MH} + rand(U_{MH}) \tag{4.2}$$

In this study, another parameter was introduced, namely, a ratio of harmonic excitation frequency to the triggering frequency, r_{HTT}, which is represented by Equation (4.3):

$$r_{HTT} = \frac{f_{FSH}}{f_{FST}} \tag{4.3}$$

Where, f_{FST} signifies the pulse frequency generated by virtual signal generator. f_{FST} can be described in similar fashion as in Equation (4.2) by combining nominal triggering frequency, f_{ST} and the fluctuation term, U_{ST} to provide periodical shift in the pulse. Figure 4.4 graphically illustrates the nominal frequency of f_{ST} and f_{SH} which fluctuate for a given U_{MH} and U_{ST}.

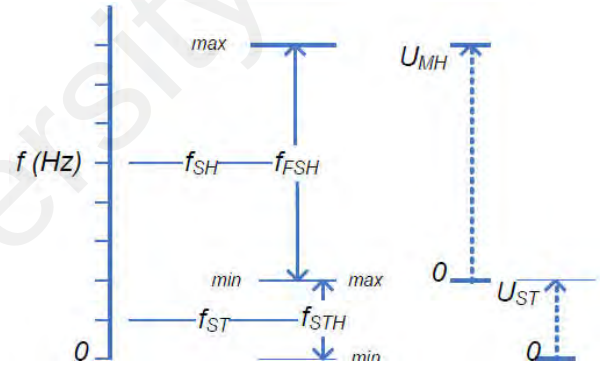

Figure 4.4: Representation of randomness in harmonic excitation and triggering frequencies

Based on Equation (4.3) it is evident that r_{HTT} that yields a natural number leads to synchronization of signals from each incoming block which causes failure of harmonic elimination. In contrast, r_{HTT} that produces a decimal point reflects a non-synchronization of the phase between two consecutive signal blocks. This also means that the rotor frequency is not a natural based multiplication factor of the triggering

frequency. The above condition can be well described in Figure 4.5, which demonstrates the overlapping of two successive blocks separated by triggering signals originating from the impact onto the tested structure.

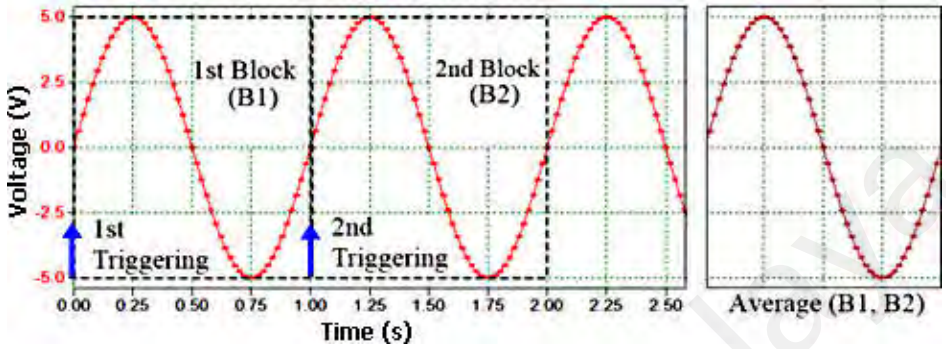

(a)

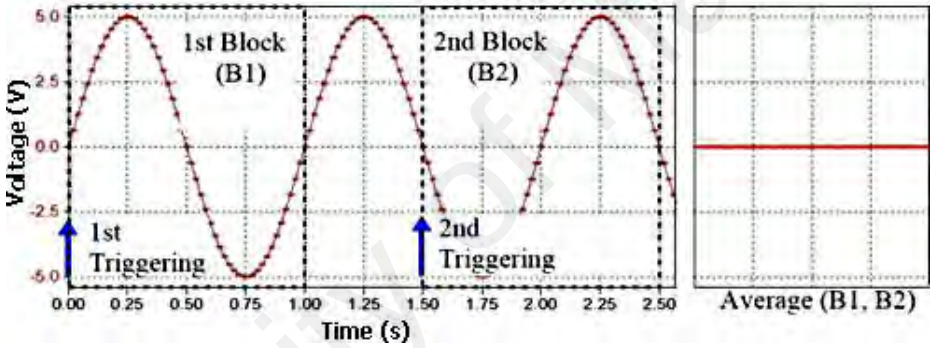

(b)

Figure 4.5: Averaging process of two consecutive blocks at different triggering frequencies. The harmonic frequency is set at 1 Hz and each block size contains 50 samples (a) 1 Hz (b) 0.67 Hz

As evident from the figure, a triggering signal that prompts response output signals data flow plays a decisive role in ensuring successful cancellation between two averaging block signals. A ratio that comprises a natural number signifies identical phase of response output signal for each triggering sequence as observed in Figure 4.5(a). In contrast, a careful selection of triggering signal frequency that yields fractional value of r_{HTT} would result in effective cancellation of the harmonicas illustrated in Figure 4.5(b). From the above explanation, r_{HTT} can be further separated into two parts as given in equation (4.4).

$$r_{HTT} = r_{nat} + r_{dec} \tag{4.4}$$

Where, r_{nat} signifies the natural component which of the ratio f_{SH}/f_{ST}, and r_{dec} is the decimal component, representing the combination of fluctuating component and phase shift obtained from designed criteria.

A virtual signal processing architecture as shown in Figure 4.6 was created in Dasylab platform to simulate the proposed harmonic signal elimination concept. The worksheet contains different modules, which represent signal generation components, a relay that determines the time between each triggering signal and the averaging module to perform the elimination procedure. Maximum and minimum deviations of the rotor speed were recorded and inserted into the worksheet as predefined values.

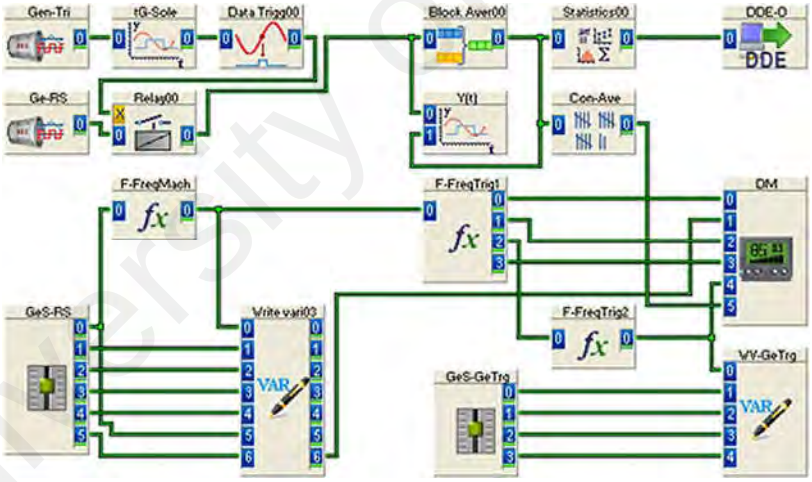

Figure 4.6: Worksheet for conducting signal averaging process

The function of each module within the above worksheet is briefly explained as follows: module *Gen-Tri* generates the triggering signal from the software and is displayed by using module *tG-Sole*. The signal flows into module *DataTrigg00* and module *Relay00* is used as a gate to allow harmonic signal generated by module *Ge-RS* to pass through the module. Signal from module *Relay00* then flows into module *Block Aver00* where the averaging is performed by Equation (4.1). The resultant

post-averaging signal would be compared with preprocessed signals inside module *Y/(t)*. Maximum values of signal leaving the module *Block Aver00* is further evaluated by module *Statistics00* and is finally recorded in Microsoft Excel file using module *DDE-O*. Module *Con-Ave* counts the number of block evaluated which is later displayed in module *DM*.

4.2.3 Accessing Real Data Input from Motor Speed

In order to simulate this randomness, the motor speed needs to be obtained via experiment to determine the maximum and minimum values that will be used as input to simulate the motor frequency. The hardware configuration for the measurement of the motor speed is shown in Figure 4.7(a) along with the corresponding worksheet, Figure 4.7(b). A deflector tape was positioned on the motor disk to reflect the infrared signal generated by the tachometer model Monarch PLT200.

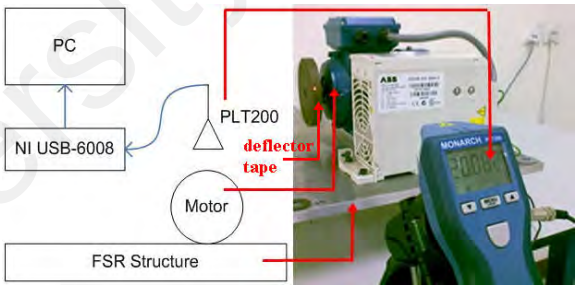

(a)

(b)

Figure 4.7: Measurement of motor speed (a) Hardware configuration (b)Worksheet

The reflected signal was then transmitted into the DAQ device model NI USB-6008. A triggering analysis module, AI-Tacho measures the period between two successive high signals and converts it into frequency of the motor. The response output was

displayed using module *DigitalMe00* and subsequently sent to Microsoft Excel file via module *DDEOuput00*. The input data for measuring the motor running speed are given as follows: The speed of the motor is set at 20 Hz by three phase inverter model ABB ACS150, tachometer sampling rate was fixed at 10000samples^{-s} and the block size was given as 1000 samples. Using worksheet as shown in Figure 4.7(b), the measurement was executed with the above input data to provide a fluctuated motor speed between the maximum and the minimum of 20.020 Hz and 19.980 Hz, respectively. The difference between these peaks then served as input parameter, U_{MH} for random function in Equation (4.2).

4.2.4 Amplitude Suppression by Periodic Averaging

The simulation of harmonic excitation signal elimination commences by scrutinizing the effect of disturbance free periodic signals on harmonic elimination via the proposed averaging concept. Using the simulation worksheet along with Equation (4.1) until Equation (4.4), relevant signals were generated, processed and displayed. For the current simulation, the random part of the Equation (4.2) was set to zero to provide only the disturbance free harmonic segment. Next, a sampling rate of 2048 samples/s and block size equal to 4096 samples/block were used for the averaging process. Using worksheet as shown in Figure 4.6 and data input in Table 4.1, a simulation was conducted and the results were shown in Figure 4.8. As expected, Figure 4.8(a) demonstrates that the resultant amplitude from the present averaging scheme with r_{HTT} as natural number remains unchanged after 25 averages. In contrast, by incorporating a decimal component, r_{dec} into the ratio, the amplitude signals in time domain was progressively suppressed after each consecutive averaging as shown in Figure 4.8(b), (c) and (d), respectively.

Table 4.1. Input data for simulation with periodical signals

Parameter	Set 1	Set 2
Impact frequency, f_{ST} (Hz)	0.4	0.396
Motor speed, f_{SH} (Hz)	20	20
Frequency ratio, r_{HTT}	50	50.5
Natural component, r_{nat}	50	50
Decimal component, r_{dec}	0	0.5
Rand. Coef. of Harmonics, U_{MH}	0	0
Rand. Coef. of Impulse U_{ST}	0	0

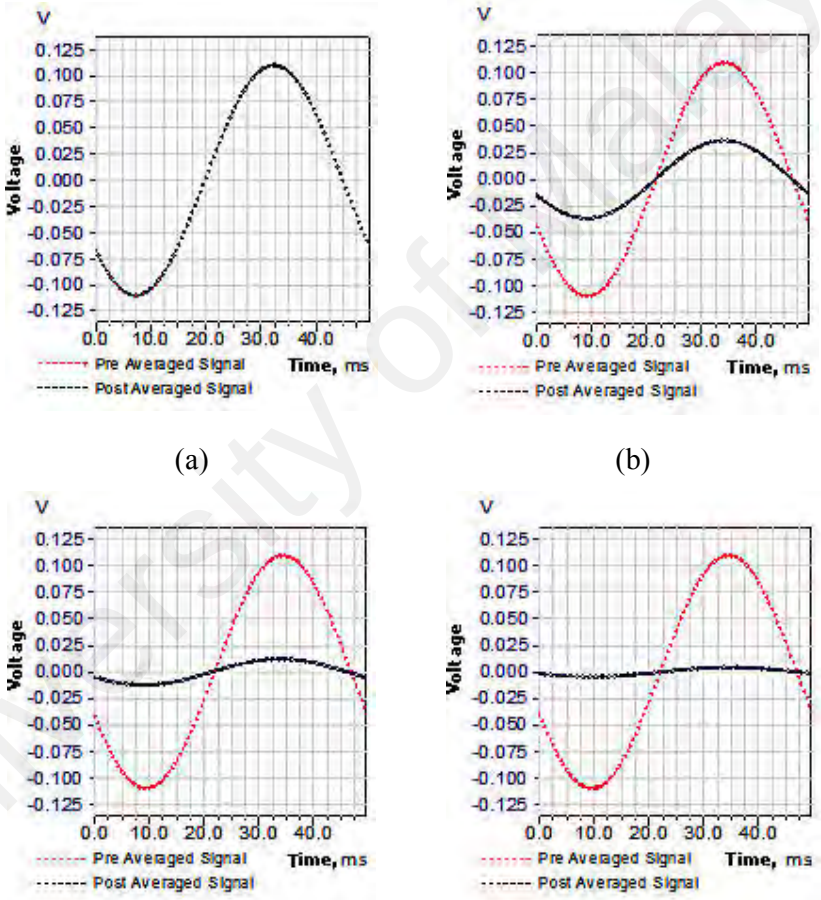

Figure 4.8: Progress of harmonic signal elimination for different data set: (a)Set 1, post average = 25 , (b) Set 2, post average = 3, (c) Set 2, post average = 9 and (d) Set 2, post average = 25 averages

The results indicate that a meticulous selection of phase difference between the triggering and harmonic signals is critical to achieve successful harmonic signal

elimination. Figure 4.9(a) further substantiates the pre-requisite condition to attenuate the harmonic signals.

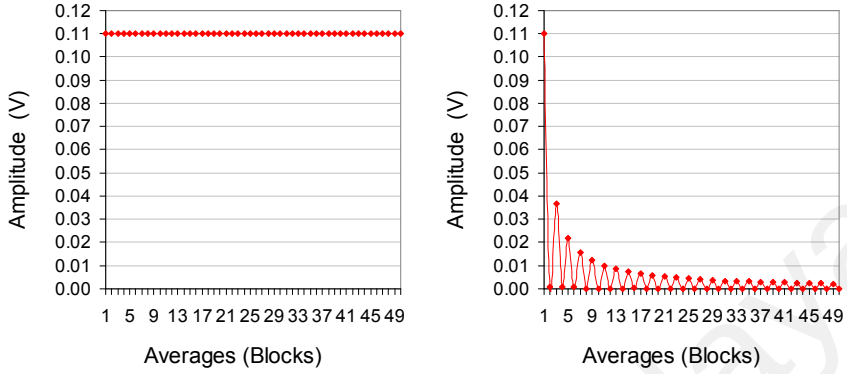

(a) (b)

Figure 4.9: Attenuation progress of the signal amplitude for (a) Set 1 and (b) Set 2 configurations

The figure shows that the amplitude of post-averaged signal remains constant after each successive block by keeping r_{HTT} as natural value. On the other hand, by adjusting r_{HTT} to contain a decimal part, the amplitude from the averaging signal changes tremendously as evident in Figure 4.9 (b), highlighting an exponential decay pattern with the increasing number of averaging blocks. While it is understood that electrical motor typically runs at preset operating condition, the results elucidate the importance of triggering frequency to modulate r_{HTT} thus enabling direct control on the harmonic excitation signal elimination.

4.2.5 Amplitude Suppression by Non-Periodic Averaging

Further investigation was conducted to observe the effect of non-periodic harmonic excitation signal under the present signal elimination protocols. It is worth to mention that application of non-periodic averaging is a common practice in EMA to eliminate noise prior to post-processing. However, no set of guidelines particularly on the periodicity of the input force exist with the use of conventional ICP impact

hammer. Further, this simulation attempts to prove the feasibility of using the existing averaging technique with additional control over the triggering signal which could pave an avenue towards achieving EMA under operational condition. Using U_{MH} as input for random function, a set of random values can be generated which will be added into Equation (4.2) to provide much realistic representation of the motor harmonic signal.

Using similar worksheet as in Figure 4.6, the simulation was conducted with predetermined input values as given in Table 4.1, with parameters U_{MH} and U_{ST} were fixed at 0.040 and 0.0015, respectively for both set of inputs. The results for the simulation are provided in Figure 4.10. The figure shows significantly different results of harmonic excitation amplitude reduction by two sets of r_{dec} values. By looking at Figure 4.10(a), the amplitude reduction progressed rather slowly with each consecutive averaging. The magnitude remained high at 0.07 even after 50 averages. In contrast, the amplitude shown in Figure 4.10(b) experienced a dramatic drop after just 5 averages and gradually reduced to below 0.01 after 50 averages. The results further consolidate the fact that r_{HTT} plays a dominant role on determining the rate of amplitude reduction in averaging process. It can be deduced that in order to obtain reduction in the harmonic signal amplitude, the phase difference between two consecutive block averaging signals should be within the range of ($0<\theta<2\pi$) which correspond to ($0<r_{\mathrm{dec}}<1$), with π gives the highest rate of amplitude decay. This explains a slow reduction of the amplitude in Figure 4.10(a), which is dominated by the contribution of the frequency randomness to yield a small value of r_{dec}.

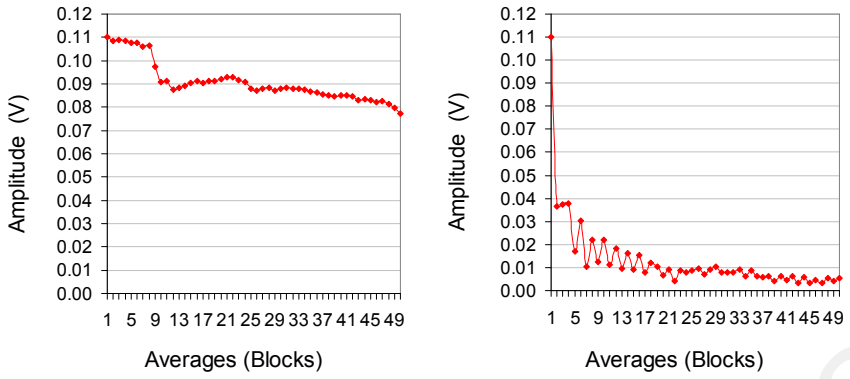

(a) (b)

Figure 4.10: Simulation results for harmonic signal elimination for (a) Set1and (b) Set 2 configurations

Likewise, the result in Figure 4.10(b) shows similar trend of amplitude decay as in Figure 4.9(b) due to the dominating effect r_{HTT}. Another important fact is that the randomness would enhance the amplitude reduction for r_{dec} that falls near 0 or 1 which is known to yield null amplitude reduction. In essence, a periodical triggering is paramount to realize harmonic reduction which explains why triggering from ICP impact device, which is highly non-periodic could not achieve consistent results.

4.3 Experimental Validation on Harmonic Excitation Signal Elimination

4.3.1 Harmonic Amplitude Suppression by Actual Harmonic Signal

Validation of the simulation results was conducted under experimental condition to ensure that the simulation work- sheet is reliable to predict any change in input parameters such as f_{FSH} and f_{FST}. In this section, a similar averaging process was performed with continuous real time measurement data from the actual FSR structure containing motor under operational condition. The flexibility in conducting simulation allows wide spectrum of input parameters to be investigated without engaging into time intensive hardware adjustment.

A hardware system for validation was configured as shown in Figure 4.11. The configuration consists of an accelerometer model WR 786C, tachometer model Monarch PLT200, as well as DAQs model NI 9234 and NI USB-6008.

A slight modification of the worksheet in Figure 4.6 was performed considering the current real time averaging mode. This was to include relevant modules for acquiring real time signals from the structure and rotating machine for further processing.

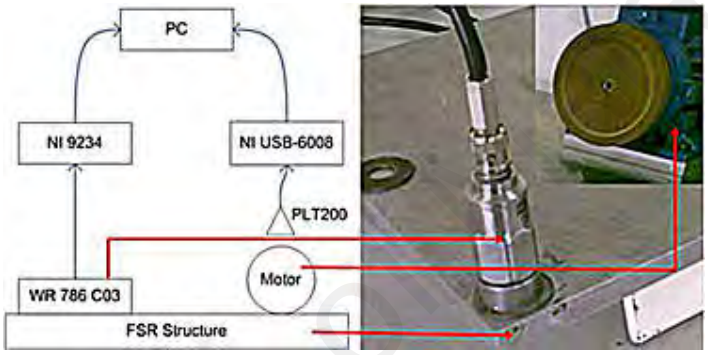

Figure 4.11: Hardware configuration for acquiring actual vibration and harmonic data

In this setup, an accelerometer was mounted on FSR structure to continuously obtain the signal from the structure which contains the harmonics from the operating motor. The tachometer was tasked to obtain the actual motor rotating frequency which was later used to determine the actual triggering frequency that satisfied the predetermined r_{HTT}.

In brief, additional modules for conducting real time averaging process are given in Figure 4.12 and are further described as follows: module *AI-Tacho* acquires signal from tachometer and module *PulseAnal00* translates the period between two successive high signals into frequency of the disk.

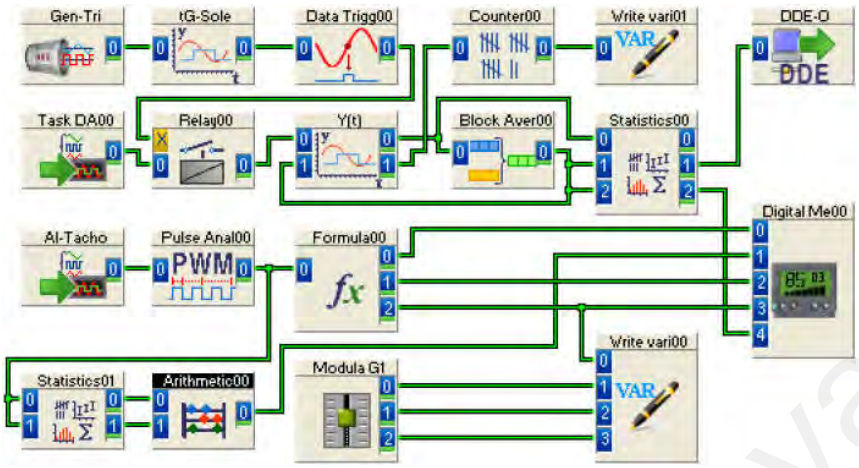

Figure 4.12: Worksheet for performing averaging process with real harmonic experimental data

This frequency served as input to module *Formula00* in which the actual triggering frequency was calculated from Equation (4.3) and automatically transferred into module *Gen-Tri* in real time. Signal from module *PulseAnal00* also flows into module *Statistic01* that evaluates the maximum and minimum values. Module *Aritmetic00* calculates the difference of the maximum and the minimum values of the signal. Similar to the previous worksheet the triggering signal from module *Gen-Tri* flows through module *tG-Sol* and module data *Trigg00* to trigger the relay that enables the actual vibration signal from module *Task DA00* to pass in predetermined block size. Module *Task DA00* acquires signal directly from the accelerometer. Block signal from module *Relay00* flows into module *Block Aver00* to be processed by Equation (4.1). The post-averaging signal was evaluated by module *Statistic00* to extract the maximum value before being written into excel file through module *DDE-0*. The experiment was performed using similar sets of data from Table 4.1 with real time data input from the operating structure.

Figure 4.13 shows the amplitude decay under the present averaging technique using real time experimental data.

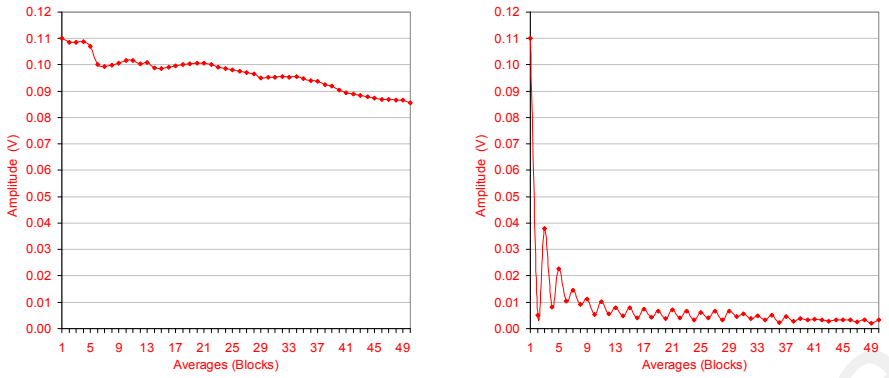

(a) (b)

Figure 4.13: Real time averaging results of the harmonic on the operational structure for a) Set 1 (b) Set 2 configurations

It is interesting to note that the trend of amplitude reduction poses high resemblance to the simulation results (Figure 4.10) which consolidates the effectiveness of the proposed averaging criteria to eliminate harmonic excitation signal. Further, the results also highlight the ability of the worksheet to synchronize with the actual data to achieve the desired elimination. The fact that the signal from the accelerometer contains different levels of noises on top of the harmonics has proven that the existing TSA can be adopted to achieve both noise and harmonic elimination, provided that a periodical triggering signal can be attained. It is evident from Figure 4.13 that the randomness in the output response acquired by the accelerometer contributes to the overall amplitude reduction, particularly where r_{dec} close to 0 and 1. Further, a well selected value of r_{dec} predominantly affects the time taken to achieve the desired elimination.

4.3.2 Validation of Harmonic Amplitude Suppression

A comparative assessment was conducted to gauge the performance of simulation with respect to the experimental results. The error was calculated via equation (4.5). Where, a_s and A_m represent the magnitude of amplitude reduction obtained after 50

blocks under simulation and experimental modes respectively, while A_0 denotes the initial amplitude. The results between the two approaches are summarized in Table 4.2. The above results suggest that both approaches demonstrate similar characteristic in term of reducing the harmonics excitation amplitude. However, it is evident that the averaging provides much closer agreement between the experiment and the simulation for r_{HTT} containing a decimal part in comparison to single natural part value.

$$\varepsilon = \left| \frac{A_s - A_m}{A_0} \right| x100\% \tag{4.5}$$

Table 4.2 Amplitude reduction for simulation and experiment under different set of design criteria

Parameter	**Set1**	**Set 2**
Decimal Part , r_{dec}	0	0.5
Initial Amplitude, A_0 (V)	0.11	0.11
Final amplitude (simulated harmonic data), A_s (V)	0.0774	0.0053
Final amplitude (Actual harmonic data), A_m (V)	0.085	0.0075
Error, ε (%)	9.8%	2%

Further, randomness in harmonic excitation frequency renders insignificant effect on the sensitivity of the averaging process with r_{dec} away from 0 and 1. This also implies that as long as the nominal motor running frequency can be measured, a proper design criterion can be selected to achieve optimum harmonic excitation signal elimination. The results have proven that harmonic excitation signal elimination can be accomplished under simulated environment which could save time and effort for hardware con- figuration. The user can choose r_{dec} that suits the motor running condition which would off-set the effect of fluctuation and noise to yield high performance harmonic excitation signal elimination. Ultimately, this concept would serve as an essential tool for predicting the best combination of design parameter in conducting EMA under operational condition.

4.4 Simulation-Based Study on Varying Input Parameters

4.4.1 Effect of Decimal Part, r_{dec} of the Ratio (r_{HTT})

In this section, the effect of decimal part r_{dec} selection on harmonic excitation signal elimination is systematically addressed. From the previous results, it is obvious that careful selection of this parameter would enable rapid decay of a harmonic amplitude signal. Using worksheet as shown in Figure 4.6, series of simulations were conducted with varying f_{ST} at specific f_{SH} = 20 Hz and the results are shown in Figure 4.14. For each of the simulation, the triggering frequency was adjusted to yield r_{HTT} of 40.1, 40.4, 40.5 and 40.9. The random coefficient for harmonic excitation, U_{SH} and triggering frequency, U_{ST} were set at 0.040 and 0.0015, respectively. Figure 4.14 illustrates the effect of r_{dec} values of r_{HTT} on the performance of harmonic excitation signal elimination. It is evident from the results that rdec equivalent to 0.5 demonstrates the best combination of both final amplitude reduction and rate of decay for the harmonics. The trend is exponentially smooth in comparison to other values of r_{dec}. The averaging is minimally affected by the randomness in both the harmonic excitation frequency and the triggering frequency, suggesting that this value can be used as design criteria in performing harmonic excitation signal elimination. Further, the results from Figure 4.14(a) and (d) indicate that performing the averaging with r_{dec} near 0 and 1 would not be recommended due to the much closer value of r_{dec} towards approaching the natural number. Nevertheless the trend of the results indicates that the signal elimination would ultimately converge for sufficiently large number of averaging blocks given the randomness in the input data is negligible to alter the r_{dec}.

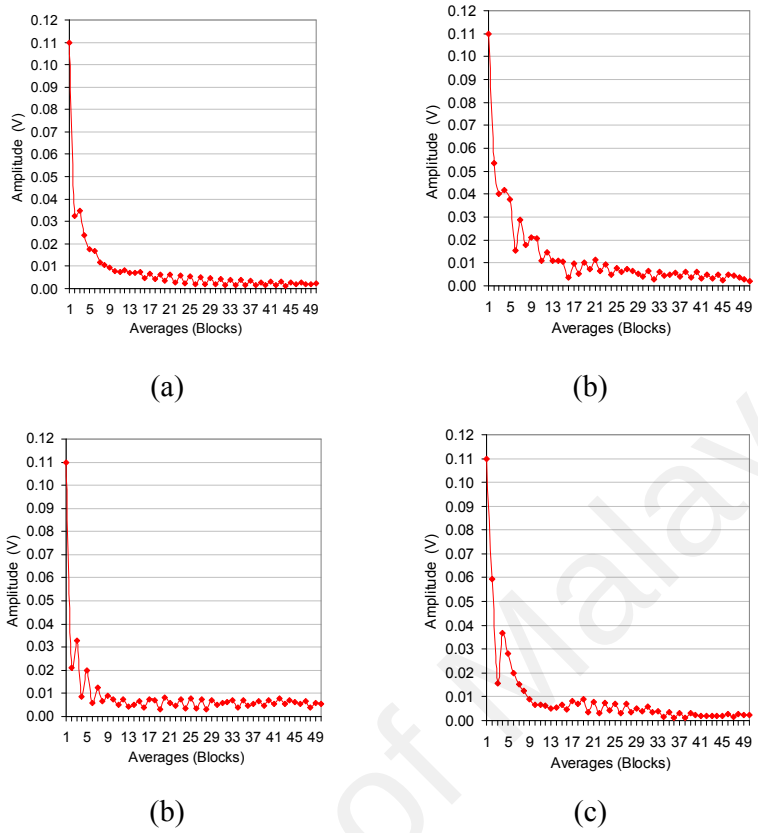

Figure 4.14: Amplitude reduction of the harmonic for different r_{dec} : (a) 0.1, (b) 0.4, (c) 0.5 and (d) 0.9

4.4.2 Effect of Natural Part, rnat of the Ratio, r_{HTT}

The investigation was extended by evaluating the effect of natural part r_{nat} within the designed r_{HTT}. Figure 4.15 further elucidates the fact that the elimination is not sensitive to change in r_{nat}. As highlighted earlier, the selection of this component is less critical in comparison to r_{dec} due to the fact that the value is predominantly translates into phase synchronization of the harmonic signal for each averaging block. This indicates that more focus can be directed on configuring r_{dec} which reduces the complexity of signal elimination procedure.

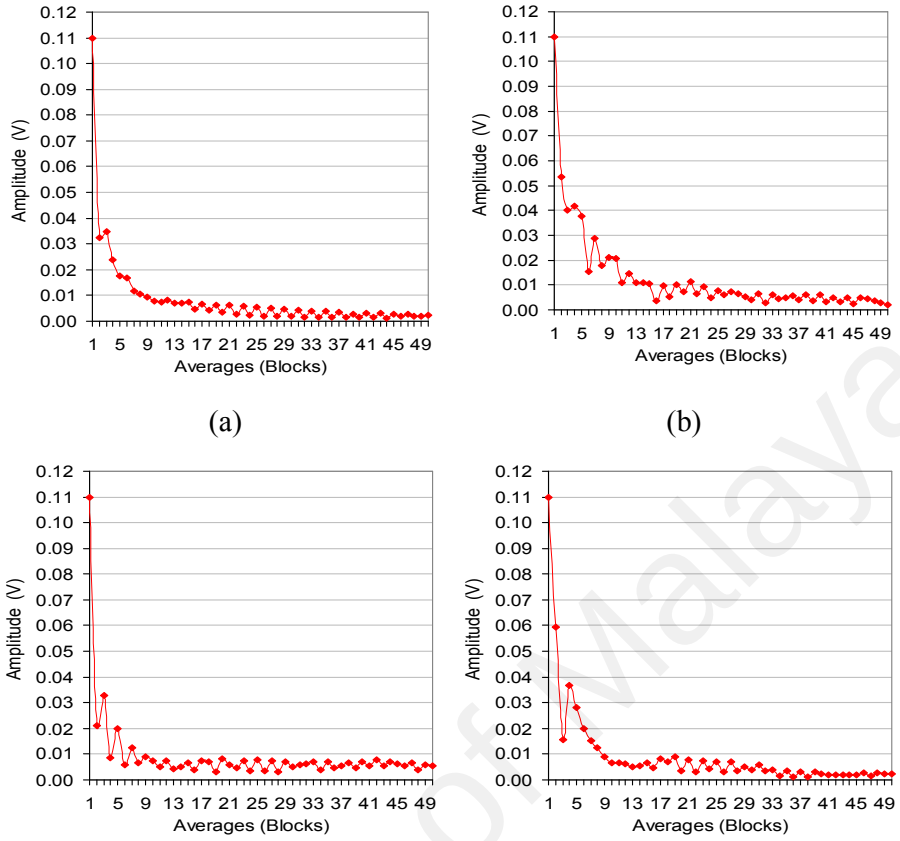

Figure 4.15: Amplitude reduction of the harmonic at different r_{nat} : (a) 40 (b) 50 (c) 70 and (d) 80

4.4.3 Effect of Harmonic Excitation Frequencies (f_{SH})

A specific study was conducted to gain an in-depth under- standing on the effect of different f_{SH} based on optimum level of r_{dec} (i.e. 0.5). The simulation was conducted at f_{SH} of 10 Hz and 100 Hz with identical r_{HTT}. Similar set of random coefficients as to the previous investigation (i.e. Section 4.4.1) were selected for the harmonic and triggering frequencies under the present simulation. Using worksheet as given in Figure 4.6 and designated data input, the results were obtained as shown in Figure 4.16. Figure 4.16 shows simulation results for harmonic excitation signal elimination at two different f_{SH}. Both results showed that the amplitude decreased after 50 averages, with the amplitude for 10 Hz running speed reduced to 0.003 V,

while for 100 Hz, the amplitude diminished to 0.008 V after 50 averages. The results indicate that the averaging produces consistent amplitude reduction for a low running speed while more averaging blocks are required to achieve steady state amplitude reduction at higher running speed.

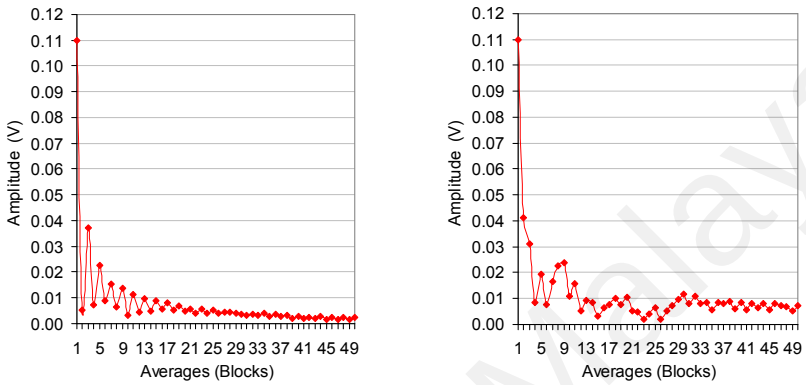

(a) (b)

Figure 4.16: Amplitude reduction of the harmonic at different motor speed. (a) 10 Hz and (d) 100 Hz trial

The above results highlight the importance of randomness to influence the elimination at much higher running speed. Nevertheless the present simulation accentuates the ability of the proposed averaging criteria to perform harmonic elimination at low and high speed condition.

4.4.4 Effect of Triggering Random Coefficient (U_{ST})

In EMA, the triggering input generated by an ICP impact hammer is controlled by human operator subjected to a large variance in term of triggering frequency, f_{FST} generated. In this section, the effect of non-periodic triggering signal was further investigated by varying the random coefficient for the triggering frequency, U_{ST} from 0.0015 to 0.1 and 0.5. Parameters for harmonic frequency and its associated random coefficient were kept constant at 20 Hz and 0.040, respectively during the simulation. Using worksheet as shown in Figure 4.6 and the relevant data input, the results were

obtained as shown in Figure 4.17. Further, the result from Figure 4.17(b) shows that the harmonic excitation amplitude remains high after 50 blocks averaging with U_{ST} = 0.5. Both results underline that the conventional way of manual impact hammer approach for generating input signal in EMA is not compatible to be adopted in performing harmonic elimination, which impede its application under operational condition. This can be further explained by looking into the triggering signal generated under present condition as shown in Figure 4.17(c) and (d).

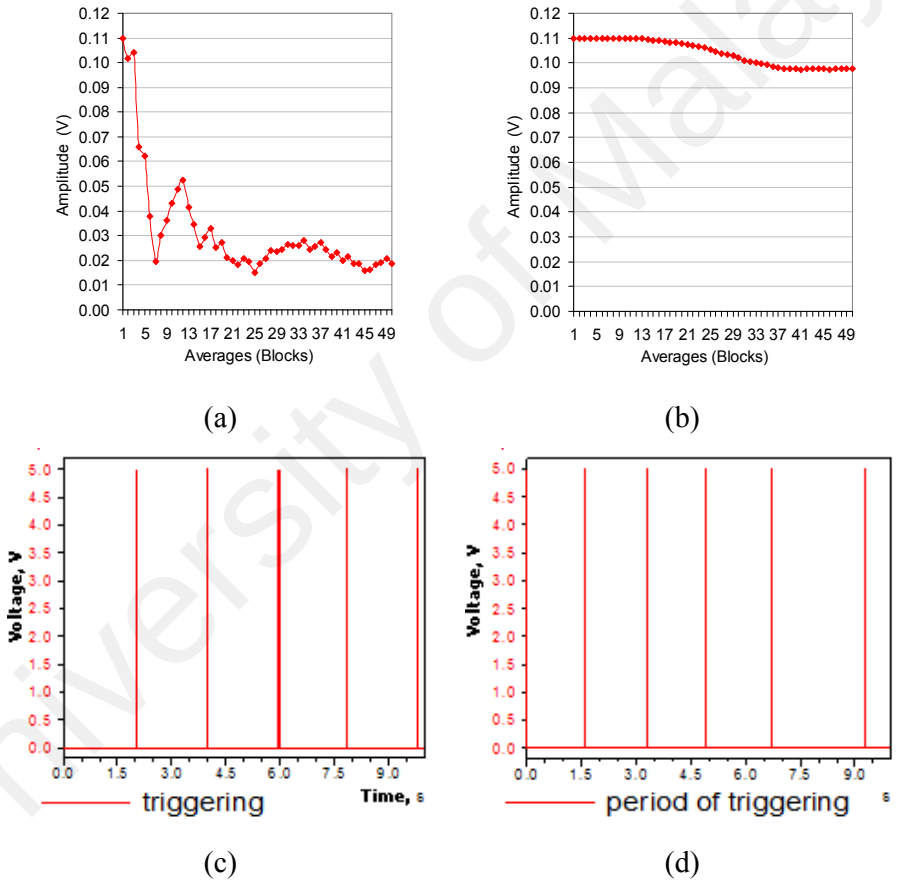

Figure 4.17: Amplitude reduction of the harmonic along with time based triggering signals obtained by non-periodic triggering frequency. Random coefficient was set at 0.1 for (a) and (c) and 0.5 for (b) and (d)

The period between each knocking was non-periodic particularly at high U_{ST} which contributes to the inconsistent phase cancellation between each averaging. This result also suggests that consecutive knocking approach by using ICP impact hammer as

mentioned by Rahman et al. (2011) may not be favorable to eliminate the harmonic excitation as it could provide a misleading impression that amplitude reduction has been achieved in less than 10 knocks as shown in Figure 4.17. Thus, a new set of apparatus is required in order to generate periodic knocking input onto the test structure for conducting harmonic elimination by using TSA.

4.5 Summary

This paper described the development of a simulation plat- form for conducting harmonic excitation signal elimination. A new concept of employing the ratio between harmonic and triggering frequency (r_{HTT}) was explored under block averaging technique with an aim to yield rapid and consistent amplitude elimination of the harmonics signal. The results elucidates that under the new scheme, harmonic excitation signal elimination can be accomplished in much systematic and efficient way. A validation was performed with real time measurement data of the harmonic from actual structure which indicates as close as 2% agreement between the simulation and the experimental approaches. Further, investigation revealed that a value of 0.5 led to an optimum elimination performance with respect to the rate of decay and reduction of the signal amplitude. Further simulation with varying speed showed that the present elimination scheme is highly robust at both the low and high motor speeds. Investigation on the effect of non-periodic triggering frequency unveiled detrimental outcome in terms of both the magnitude reduction as well as the trend of amplitude elimination. This work suggests that by a simple tuning of the frequency ratio between the harmonic and the triggering, harmonic signal originating from the rotating machine can be suppressed. A modification of the existing EMA set-up is required to realize this concept which involves developing an automatic impact device to replace the existing ICP impact hammer to yield periodic input to

the test structure. Several experiments using hardware, software and specified file names involved to eliminate harmonic excitation signal tabulated in Appendix C, under classification, namely harmonic excitation elimination.

CHAPTER 5: SYSTEM INTEGRATION FOR PERFORMING EMA UNDER OPERATIONAL CONDITION

5.1 Introduction

EMA procedure has long been associated with non-operational condition of the tested structure. On the other hand, the present approach takes advantage of the newly developed automatic driving impact system coupled and the well-established TSA technique, prior mentioned in CHAPTER 3: and CHAPTER 4: respectively. This would provide consistent periodic input onto the structure that enables the harmonic signal originating from cyclic devices to be suppressed, thus allowing modal parameters to be efficiently extracted. A combination of an electromechanical linear solenoid (which motion is controlled by a dedicated instrumentation software), and force sensor were employed to deliver periodical input on the structure. A phase cancellation strategy was employed within TSA protocol of the output vibration signals to suppress the harmonic component for a sufficient number of block averages. The results showed that harmonic signal was successfully suppressed which demonstrates high quality coherence and FRF of the dynamic system. Evaluation of the results obtained via the new approach with respect to classical EMA showed high resemblance on the dynamic characteristics (i.e. natural frequency, damping ratio and mode shape). As low as 1.05 Hz shift in natural frequency and 0.07% difference in modal damping were obtained at specific mode of vibration, indicating the reliability of the proposed method to be adopted in getting the modal parameter at operational mode. This work will pave a new route towards conducting EMA with running harmonics, which have direct impact on vibration analysis.

5.2 Structure and Methodology

5.2.1 System Development and Integration

The proposed operational EMA system for the present work is presented in Figure 5.1 along with the schematic. It consists of three major components, namely, automatic knocking device, FSR and PC based data acquisition and control system. The communication between the hardware and software as well as the data processing stage was realized in Dasylab virtual instrumentation platform depicted in Appendix H. Interface to enable interaction between operator and the running application were developed base on the same platform, namely layouts depicted in Appendix I to Appendix GG. The software contains different modules for receiving and sending data as well as performing data processing to generate FRF, which is one of the critical steps for extracting the modal parameters.

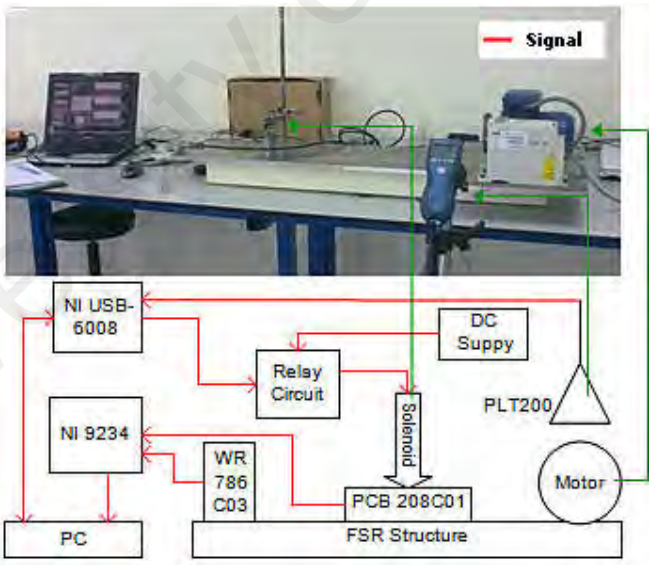

Figure 5.1: Hardware configuration for EMA under operational condition

In principle, as shown in the figure, the source of harmonic excitation is given by the motor mounted on the FSR, which is regulated at specific frequency using an inverter. The PC controlled automatic knocking device provides the necessary input

onto the FSR to excite the structure at predetermined frequency. All the data will then be acquired and further processed to determine the modal parameter which will be compared to the classical EMA. The hardware and software for realizing automatic impact system are given in CHAPTER 3:. The scope of the present work will be narrowed on integrating the system and conducting rigorous analysis from the acquired data in order to demonstrate and validate the proposed concept.

5.2.2 Designed Solenoid Period Time Delay

In complex measurement system, the synchronization between incoming signals during data processing stage is important. Block size, which represents the number of samples per block for different measurement parameters need to be similar in order to proceed in between modules. However, block size is principally constraint by the DAQ hardware specification, computer processing capability and the desired quality of the related signal to avoid loss of information during processing task. Two different DAQs were used to perform series of measurement in the present work, namely NI USB-6008 and NI 9234. As shown in Figure 5.2, the solenoid output and tachometer input signal flows through NI USB-6008 while the force sensor and accelerometer input measurements were acquired using NI 9234. The time setting of DAQ for designated transducers is given in Table 5.1.

Table 5.1: Time base for operational condition

Specification	SR, Hz	BS, n	BR, Hz
Tachometer	10000	2000	5
Accelerometer & Force Sensor	2048	4086	0.5
Solenoid	150	1	150

The block size for tachometer measurement was chosen in such a way to sufficiently capture the motor speed. On the other had the much higher block size for

accelerometer measurement is required to give reliable Fast Fourier Transform (FFT) signal.

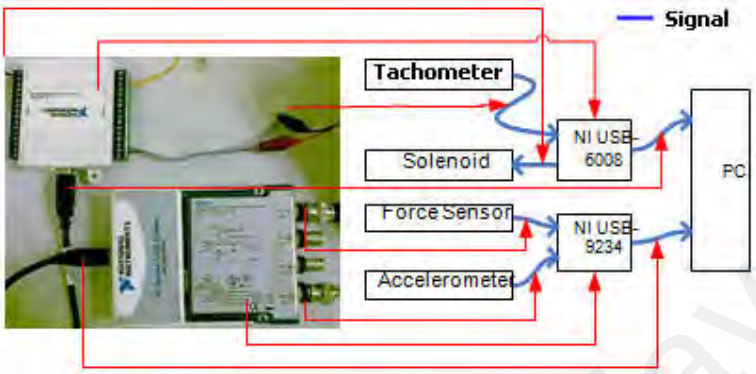

Figure 5.2: Hardware configuration for EMA under operational condition using three time bases

Likewise, the force sensor block size measurement specification was chosen identical to accelerometer to ease in processing of other dynamic parameters which rely on input/response output signal.

The data obtained from the respective DAQ devices flow to Dasylab processing software, which is composed of different modules. In order to ensure only the data related to the specific input are considered for further processing, a relay module as shown in Figure 5.3 was appended which allow the force signal generated by the solenoid impact to act as triggering function, enabling all the data to flow to the next processing stage.

Data block transferred between two modules were stored in a buffer before undergo further processing by First In First Out, (FIFO) criteria. At this stage, a bottleneck condition may manifest if the triggering signals from force sensor enter the relay module in between the data processing tasks, forcing the worksheet to stop. Therefore, selecting the solenoid knocking period is crucial to address the above issue. In the present work, the output signal that generate the solenoid motion, T_{sole} as designed to be larger than the entire processing period, T_{AD} which was obtained by

incorporating a delay module at the end of the processing stage and run the test rig at single knocking. The total delay time for complete processing was recorded at 2.17 s.

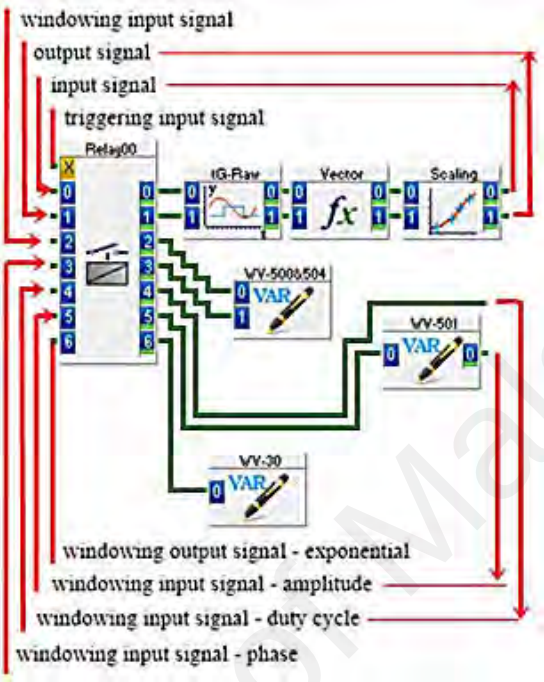

Figure 5.3: Signal synchronizing process by Dasylab relay module

Figure 5.4 demonstrates the output signal to control the solenoid knocking period and the corresponding force signal acquired by the DAQ and further displayed by the module within the worksheet. The figure shows that the acquired force signal was delayed from the moment the control signal was passed to the solenoid to initiate the knocking procedure until it reaches the display module within the software.

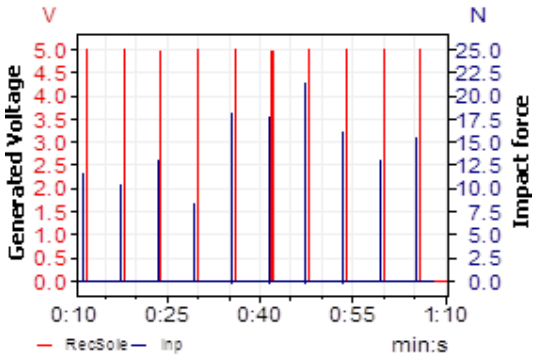

Figure 5.4: Output signal to energize the solenoid (red) and the generated force signal acquired by the force sensor (blue)

Thus, by considering Central Processing Unit (CPU) capability and safety factor, the time delay T_{sole} was chosen to be at least double the value of the recorded delay time.

5.2.3 Generating and Processing Force Input and Response Output Signals

Force input and output response signals flow from the force and accelerometer sensors enter the PC and worksheet as raw data. These data are acquired in time domain that requires further adjustment to convert them into frequency domain for extracting the dynamic characteristics. A well-known approach is to perform a windowing technique that uses a specific signal generated by the software module in order to modulate the raw signals into the desired form prior to transformation. Two windowing techniques were used, namely, exponential and square windows. In order to perform mathematical operation which involves the use of both input and output signal the windowing scheme has to be identical. In this case, the input force signal was transformed via the following expression:

$$F_p = F_r \; x \; y_{EIW} \; x \; y_{SIW} \tag{5.1}$$

Where, F_r is raw input, y_{EIW} is exponential input window and y_{SIW} is square input window. Exponential input window was evaluated by following equation:

$$y_{EIW} = e^{-a_e x_s} \tag{5.2}$$

Where, y is dependent variable, a_e is independent variable that set by observation the graph and x_s is the linear line with a particular gradient. The square wave formula is represented by the following equation (5.3):

$$\begin{aligned} y_{SIW}(t) &= \{1, |t| < T_{sole} \\ y_{SIW}(t + T_{sole}) &= y_{SIW}(t) \end{aligned} \tag{5.3}$$

Where, T_{sole} represents the solenoid knocking period which depends on the block rate of the sample of the input signal. The windowing scheme for the response output signal, X_p is given by equation (5.4) as follows:

$$X_p = X_r \times y_{EIW} \times y_{ST} \tag{5.4}$$

Where, X_r is raw response output signal and y_{EIW} is calculated from Equation (5.2) The saw tooth signal, y_{ST} is given as follow, equation (5.5):

$$y_{ST} = -\left(A \; x \; R_{BT}\right) \tag{5.5}$$

Where, A is the maximum amplitude of the acceleration signal determined by pre-running the experiments and R_{BT} represents the block rate where the data is transferred upon receiving the triggering signal as shown in Figure 5.3.

5.2.4 Harmonic Elimination Process

Under operational condition, natural frequencies of structure shifts from the non-operational condition by some magnitude as highlighted by Gagnol, Le, and Ray (2011). This shift is primarily attributed to the change in boundary condition that later affect overall stiffness of the structure under continuous dynamic load. The key component on realizing harmonic elimination lies on the ability to perform the averaging on the response output signal to naturalize the harmonic contribution. The concept is identical to TSA which implement consecutive data block averaging to eliminate the noise. Due to the ability of the newly developed automatic impact device to deliver consistent periodic knocking, a strategy can be designed to initiate impact at specific interval, which also serves as relay or stamping time for the data to cross the averaging stage, leading to cancellation of the harmonic at each averaging sequence. A specific knocking frequency presented in CHAPTER 4:, was selected to yield the decimal part of the ratio between the knocking frequency and motor

running frequency of 0.5. Further, the knocking period also need to meet the minimum requirement of the processing delay time to avoid bottleneck and sudden termination of the software operation. Each knocking would trigger the data flow for subsequent averaging process to attenuate the harmonic disturbance. It is worth to highlight that in typical EMA procedure, the transfer function module used for generating FRF, which is positioned at the later stage of the process has the capability to average the signal in frequency domain. However, in the present case a block average module was incorporated at the beginning stage of the data processing to perform the elimination procedure in time domain prior to reaching the transfer function module. This step aims to ensure the response output signals that flow to the later module are free of harmonic disturbance. Figure 5.5 shows part of the main worksheet to average the signal. Within this section, the signals leaving the windowing module were directed to module *Block Aver01* which was tasked to average the signal. Module *tG-Aved* was added to display the averaged signal.

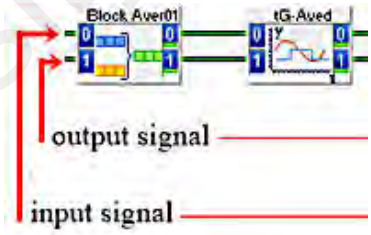

Figure 5.5: Part of main worksheet to average the signals

In order to verify the proposed harmonic elimination a specific worksheet was introduced within the software to monitor the elimination progress. Data from the averaging module (Figure 5.5) were channeled to FFT module where the signal was transformed into frequency domain via FFT numerical algorithm as shown in Figure 5.6. As shown in the figure, the resulting FFT signals from *Module FFT17* were extracted and displayed in module *wG-OutCA*. By using module *SL-X*, the frequency of the running harmonic was selected and later monitored in module *D-wAvRSA*. The

amplitude of the running frequency signal was finally transferred to module *DDE-Amp*, where the elimination can be monitored in real time.

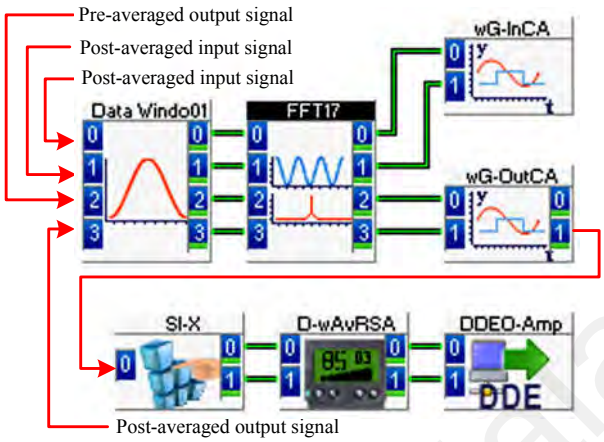

Figure 5.6: Worksheet to monitor elimination of harmonic amplitude

In the present study three different running speeds (i.e. 7 Hz, 10 Hz and 20 Hz) were selected to demonstrate the ability of the newly proposed technique to eliminate the harmonics. The worksheet in Figure 5.6 was used to monitor and record the progress of the harmonic amplitude with increasing data averaging.

5.2.5 Evaluating the FRF and Coherence

The next procedure in performing modal analysis requires the averaged vibration data with suppressed harmonics to be converted into FRF form, which enables further interpretation of the dynamic characteristics. FRF is represented by the following formula,

$$X(\omega) = H(\omega) \cdot F(\omega) \tag{5.6}$$

Where, $H(\omega)$ represents the transfer function, $X(\omega)$ is the response output and $F(\omega)$ is the input. A part of worksheet to compute FRF is shown in the Figure 5.7.

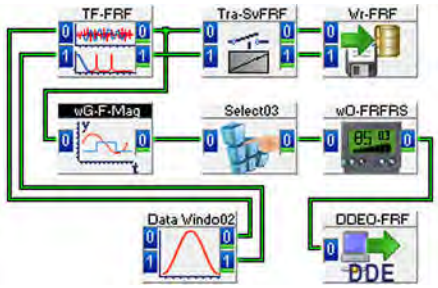

Figure 5.7: Part of worksheet to evaluate FRF

The modules used in the worksheet are explained as follows: The average signals enter module *Data Windo02* which serves to perform windowing using the scheme as described within the previous section. These signals then move to transfer function module *TF-FRF* which serves to convert the signal into FRF. The converted signal travels to *Tra-SvFRF* and *wG-F-Mag* where the magnitude at specific running speed frequency can be monitored inside the module *select03*. Module *Wr-FRF* was appended to record the entire spectrum of the FRF within the specific frequency band in ASC format. The timing of signal flow to module *Wr-FRF* was controlled by the action controlled relay module, *Tra-SvFRF* which initiates data flow upon receiving the action condition. The FRF results were finally exported to MEScope Vers4 software which was used to determine the modal parameters.

The evaluation of coherence was performed in the similar manner by selecting the coherence function within the transfer function module. The coherence is a useful indicator to identify any disturbance that penetrates into both the input and response output signals. It is well documented that coherence value of less than 0.75 signifies low quality FRF spectrum (Inman, 2014). Furthermore, it also implicates the mode shape which is an essential modal parameter to visualize structural deformation under cyclic load. It is well understood that the harmonic excitation will enter the FRF as disturbance which result in low coherence value. Therefore, in the present work, the coherence level at running frequency will be monitored to reach and

acceptable value via the newly proposed technique. The formula to calculating the coherence is described as follows, from Inman (2014):

$$\gamma = \frac{\left|S_{xf}(\omega)\right|^2}{S_{xx}(\omega)S_{ff}(\omega)} \tag{5.7}$$

Where S_{xf} represents the cross-spectral density between two signal, response of the structure to the driving force signal *x(t)* and driving force signal, *f(t)*. S_{xx} represents power spectral density (PSD) of the response signal. S_{ff} represent PSD of driving force signal.

5.3 Result and Discussions

5.3.1 Effect of Harmonics on EMA Results

In order to validate the capability of the newly automatic impact device performance, a test was conducted to compare the FRF results between manually driven impact hammer and solenoid based impact device. The ICP impact hammer model PCB 086C03 was connected to the NI 9234 to acquire the force generated by manual knocking on the FSR structure. The acceleration was measured using an accelerometer model WR 786C. In automatic impact mode, an electromechanical solenoid driven by a square wave was held on a laboratory stand to give desired periodic knocking on a force sensor model PCB 208C01. A bronze disk with number of holes at its peripheral side was mounted on the motor shaft. Series of bolts were slotted on the holes to create mass imbalance, which would translate to amplification of the harmonics amplitude. Both measurements were taken after five consecutive knocking to eliminate noise. Figure 5.8 provides the set-up for performing each of the experiment. Figure 5.9 provides the results of bode plot for EMA under manual and automatic knocking modes on the experimental test rig.

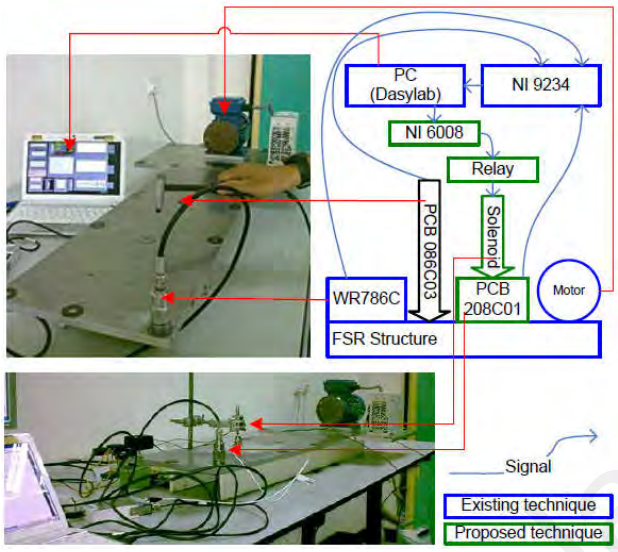

Figure 5.8: Comparison of hardware configuration of EMA at non-operational condition for the existing and proposed techniques

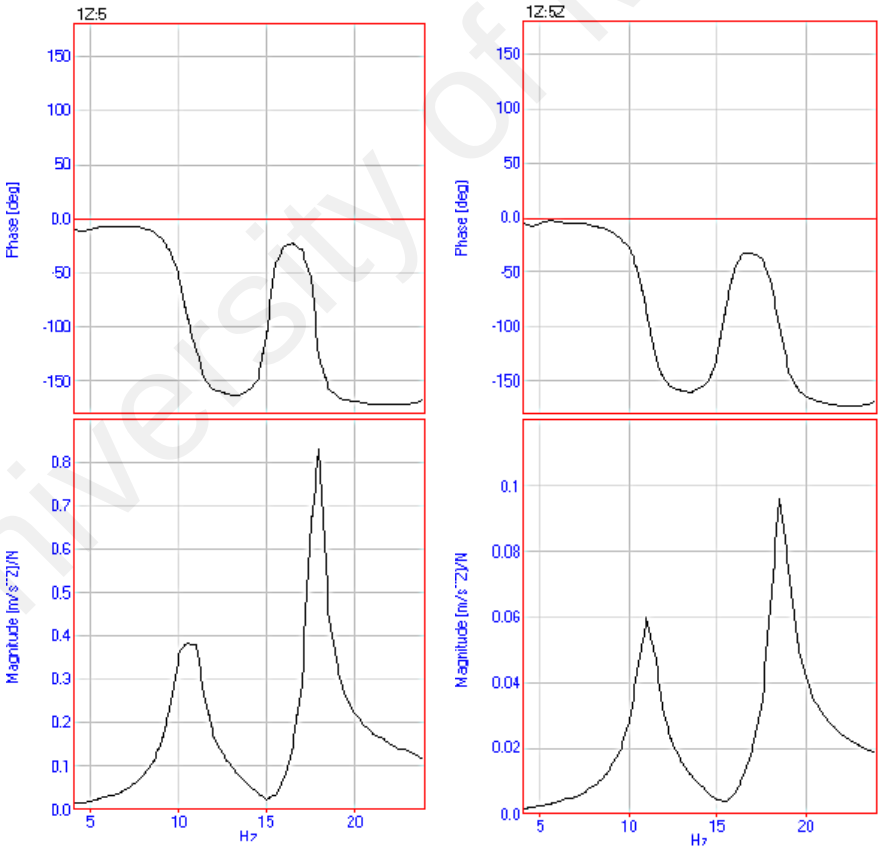

(a) **(b)**

Figure 5.9: Comparative assessment of FRF generated using : (a) Manual and (b) automatically driven impact device

The results show that the frequencies of interest were successfully captured using the newly developed automatic impact device. The first two natural frequencies at different modes are listed in Table 5.2 for both approaches.

Table 5.2: List of resonance frequency with different driving impact system

Parameters	1st mode (Hz)	2nd mode (Hz)
ICP impact hammer	11	18
Solenoid driven impact system	10.9	18.3

In general, two frequencies manifest at 11 and 18 Hz, which represent the damped natural frequency of the system. This is verified by examining the phase at each designated frequencies which indicate ± 90º, signifying the resonance state of the system as indicated by Inman (2014). These frequencies remain in close agreement between the manually and automatically conducted EMA, signifying the ability of the new system to replace the classical approach for conducting modal analysis as well as paving route for harmonic elimination via systematic knocking strategy.

Further investigation was conducted to evaluate the effect of harmonics disturbance from the motor on the FRF result. As highlighted previously, under static condition (Figure 5.10(a)), the FRF revealed two distinctive peaks at 11 and 18 Hz, indicating the natural frequency of the tested structure. On the other hand, EMA procedure conducted under operational condition whereby the motor speed was regulated close to the first natural frequency revealed significant change in amplitude.

It was evident that the peak of resonance frequency was masked by the harmonic excitation signal as shown in (Figure 5.10(a)). Further, it was also suggested that the resonance peak shifted as the measurement was switched from static toward operational condition. This phenomenon underlines the effect of dynamic change in

stiffness at the boundary condition between interconnected parts within the overall structure that implicate the dynamic response of the system as articulated by Gagnol et al. [26].

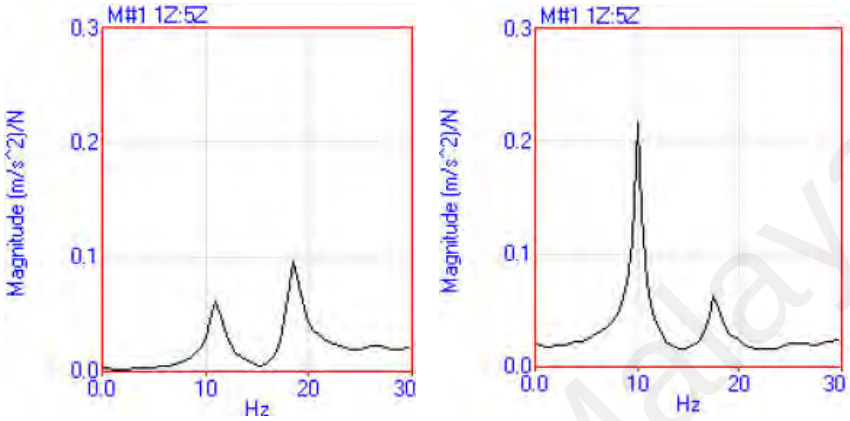

(a) (b)

Figure 5.10: Comparison of FRF by classical EMA for (a) Non-operational condition and (b) Operational condition at running frequency of 10 Hz

The magnitude increase sharply indicating the harmonic and natural frequency coincides. Hardware and software utilized to produce FRF shown in Figure 5.10, is tabulated in experiment under classification, namely background in 0.

5.3.2 Effect of Running Speed on FRF and Coherence

In order to demonstrate the need to perform harmonic elimination using the proposed concept, series of EMA experiments were conducted at different motor running speed. Three motor frequencies were chosen which encompass two conditions:

1. Running speed far from the first natural frequencies, 7 Hz and
1. Running speed close to first and second natural frequencies (i.e. 10 and 20 *Hz*)

These measurements aim to correlate the effect of harmonic disturbance on staining the coherence which is one of the indicative criteria to judge the quality of the

results. Figure 5.11 shows FRF and coherence results while running at the above mentioned speeds. For running speed of 7 Hz (Figure 5.11(a)), despite the presence of harmonic amplitude was not clearly visible due to the applied low speed that generates small unbalance force, the coherence revealed significant drop in magnitude at the speed of interest. This disturbance result in non-correlated force input/response output, which further tainted the natural frequency of the structure particularly if the disturbance is close to the natural frequency.

Another test conducted at 10 Hz running speed as shown in Figure 5.11(b) demonstrates direct overlapping of the harmonic on the first natural frequency under operational mode. The coherence was recorded below the threshold of 0.75, which gives strong indication of harmonic disturbance penetrating into the coherence calculation.

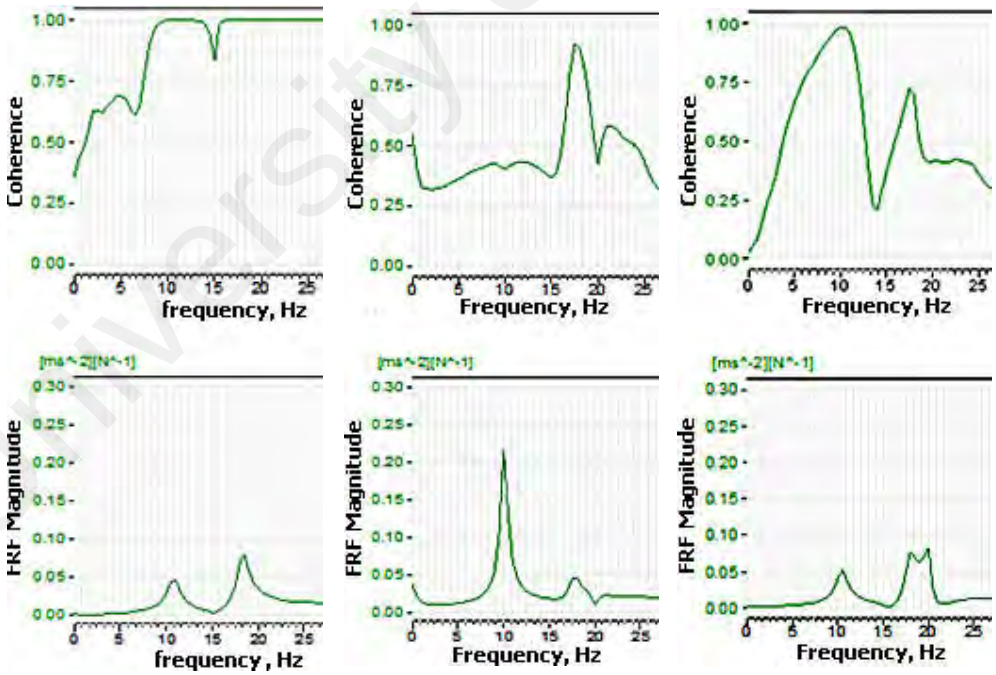

(a) (b) (c)

Figure 5.11: FRF and coherence at different running speed: (a) 7 Hz (b) 10 Hz and (c) 20 Hz

This condition further complicates the attainment of accurate natural frequency at other modes within the frequency band of interest, as evident by the degradation of coherence amplitude at 18 Hz.

The final test was conducted at 20 Hz which is close to the 2nd natural frequency of the FSR system. As evident in Figure 5.11(c), this running frequency was clearly captured which show a distinctive peak adjacent to the resonance frequency. Again, as mentioned previously, the running harmonic adversely affects the nearest natural frequency as evident by the coherence value at 18 Hz which is less than the acceptable threshold value. The above results demonstrate the potential problem that manifest when conducting EMA under operational mode that would complicate fault detection and condition monitoring tasks on the structure.

5.3.3 Harmonic Elimination at Resonance Frequency

Further investigation was directed to evaluate the FRF and coherence parameter at resonance frequency. As mentioned earlier, the solenoid knocking frequency was assigned to give the decimal part of the ratio between the harmonic and knocking frequencies of 0.5. In order to monitor the elimination progress, the worksheet as shown in Figure 5.6, and Figure 5.7 were used to extract the amplitude of acceleration, FRF and coherence at specific running frequency and the results were shown in Figure 5.12. under harmonic elimination scheme, monitored at the first natural frequency of the structure under operational condition (i.e. 10 Hz). The progress of each post-processing parameter was displayed in real time for 100 consecutive averaging. It is worthy to highlight that the elimination of harmonic signal that coincide with the natural frequency of the system has not been feasible under EMA scheme which rely on random knocking on the structure.

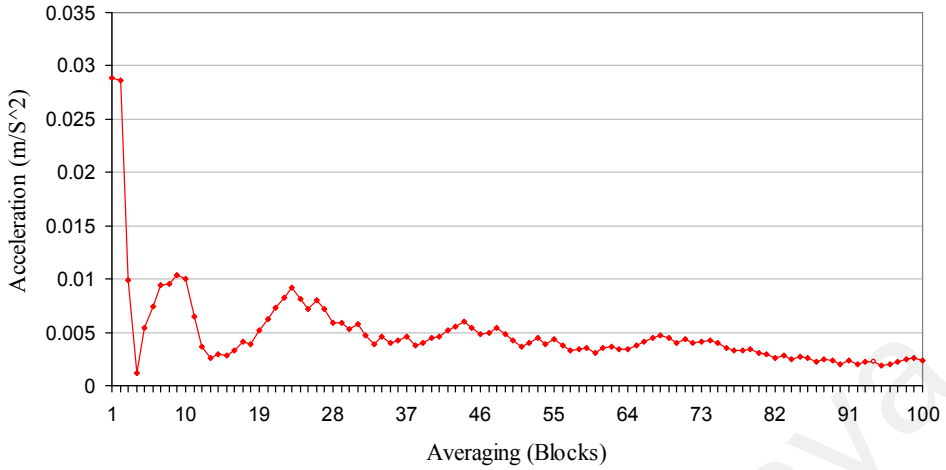

(a)

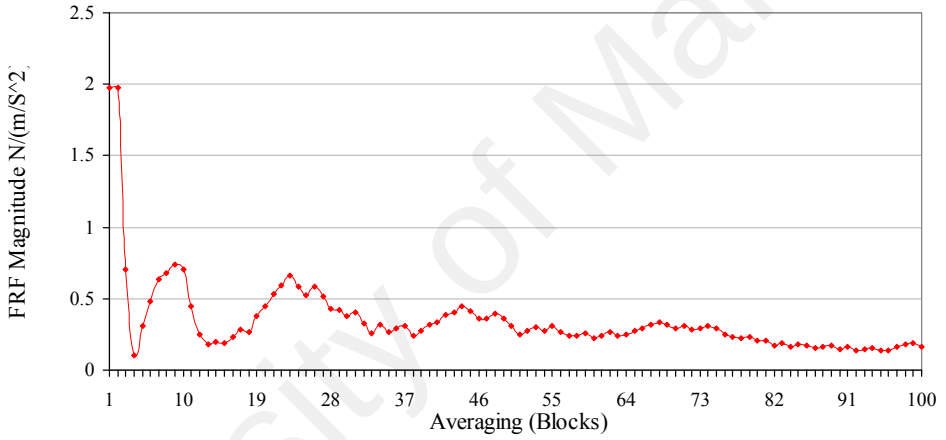

(b)

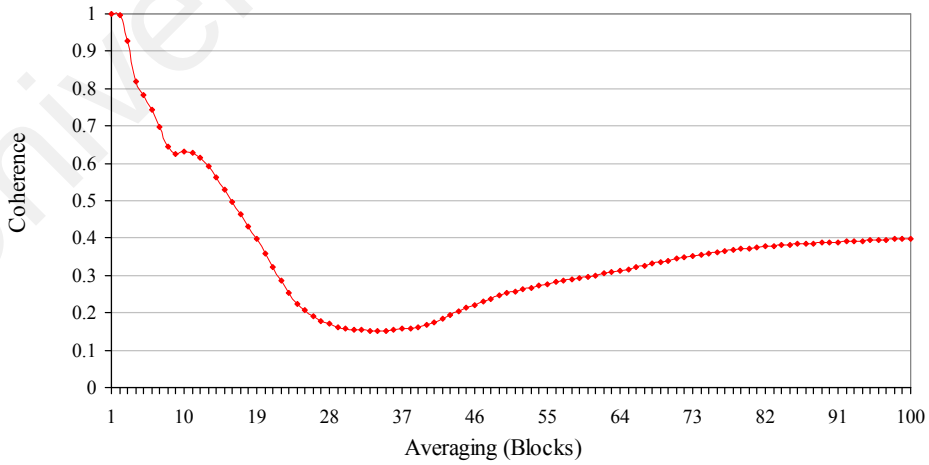

(c)

Figure 5.12: Progress of signal attenuation at motor running speed of 10 Hz. (a). Harmonic amplitude (b) FRF magnitude and (c). Coherence

However, the use of automatically driven solenoid based impact device enables a consistent periodical input force to be generated that also serves as triggering signal for data block to flow. An accurate stamping of the harmonic signal serves as the underlying key to accomplish amplitude suppression via phase cancellation strategy.

Figure 5.12 shows the results of amplitude for acceleration, FRF and coherence. The results show strong evidence of harmonic suppression based on sharp amplitude reduction of both the acceleration and FRF parameters extracted at the tested frequency. The coherence however experiences a dramatic drop in magnitude within the first 30 block averaging. This may be attributed to the fluctuation in the elimination trend as evident by the acceleration and FRF plots. As the coherence is the cross correlation products between the signal and structural driving forces in frequency domain, small changes in these parameters would implicate significant affect to the resultant outcome. However, the coherence showed an increasing trend beyond the 30 blocks averaging which was also well-portrayed by the consistent downtrend of FRF and acceleration. The results show that the newly proposed technique is capable of filtering the harmonic component even at the most extreme case of overlapping between the harmonic and natural frequencies.

5.3.4 Comparison of Dynamic Characteristic between Static and Operational Conditions

In order to ascertain the capability of the proposed technique to extract reliable modal parameters under operational mode, separate tests were conducted without and with the running harmonics using the automatic impact device as the input source. EMA testing under non-operational condition is conducted using prior Dasylab worksheet and its layout developed by Rahman et al. (2011) as depicted in Appendix HH and Appendix II, respectively. In order to obtain the modal parameters (i.e.

natural frequency, modal damping and mode shape), FRF and coherence data generated from Dasylab transfer function module were stored in ASC format. These data will serve as input for MEScope VES4 software to perform further visualization and analysis to determine the modal parameters. It is noteworthy to highlight that in order to demonstrate the mode shape of the structure, three different points within the FSR were selected as shown in . Then, The output signal at each point flows to the Dasylab and to MEScope VES4 which would animate the relative motion between each designated point for each resonance frequency.

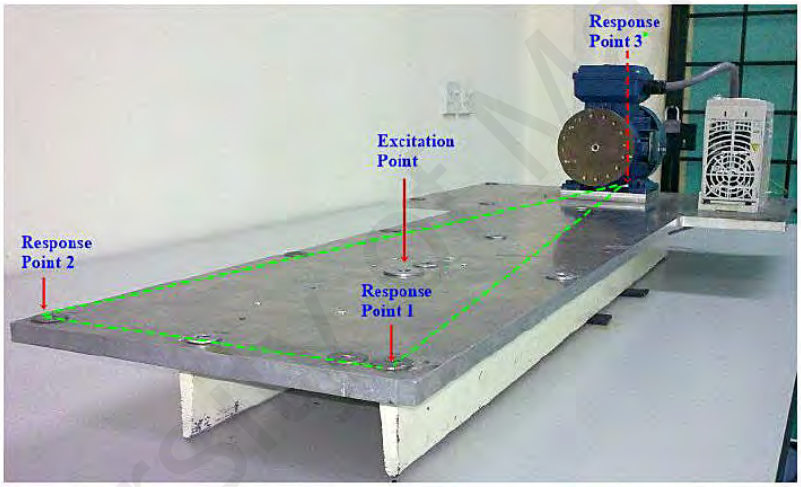

Figure 5.13: Selected point for modal parameter identification

For validation of the natural frequency and modal damping, results obtained from point 1 were adopted for comparative assessment. Using worksheet as shown Appendix H to Appendix U built by parts of worksheet as depicted in Figure 5.6 and Figure 5.7 and layouts shown in Appendix V to Appendix GG, series of data were taken both under shutdown and operational conditions and subsequently transferred into MEScope VES4 software for post-processing. For the operational condition, the running speed was set to overlap the first resonance frequency under running mode (i.e.10 *Hz*). This value was selected to simulate the effectiveness of the present scheme to attain reliable dynamic response in the most extreme dynamic condition.

Figure 5.14 shows the magnitude of FRF and it is corresponding coherence at point 1. As described earlier, under static mode, two natural frequencies (i.e. 11 and 18 *Hz*) were clearly extracted based on the FRF and coherence results as highlighted in (a). Under operational condition, by adopting the proposed harmonic elimination strategy, it was evident that the harmonic component was successfully filtered based on the improved coherence to meet the acceptable condition (Inman, 2014). The original resonance peak was also restored as evident from the FRF result. Further, the 2nd peak remains uninterrupted which give excellent coherence value.

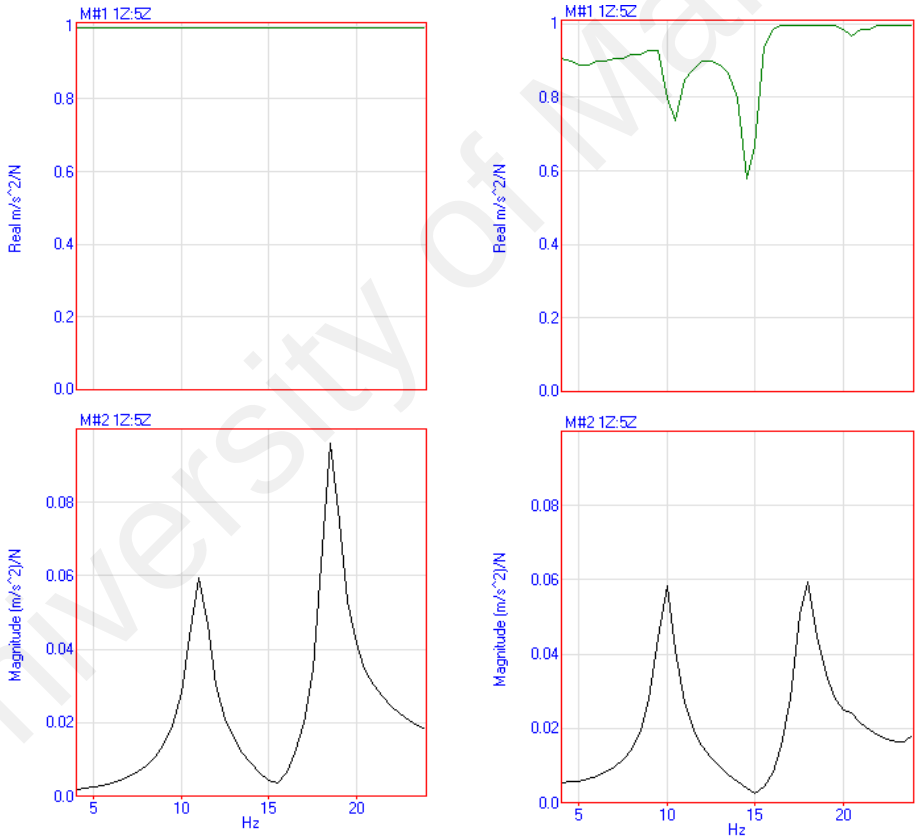

Figure 5.14: FRF and coherence of the FSR structure at point 1 (a) Non-operational condition after 5 averages, and (b) Operational condition at 10 Hz

The results provide strong indication on the ability of the proposed scheme to filter the harmonics signal of the output data for delivering reliable modal parameters.

The frequency and damping ratio for the tested condition are presented in for all the points under consideration. The table highlights a slight shift of resonance frequency between static and operational modes. As mentioned by Gagnol et al. (2011), the gyroscopic moment and centrifugal force originated by the rotating machines induces speed dependent dynamic change which disseminates throughout the structure and affect the modal parameters. The dynamic load also changes the boundary condition which implicates the stiffness in modal identification.

Table 5.3: Frequency and damping constant of FSR structure

Modal Parameter	**Natural frequency, Hz**						**Damping constant, %**					
Mode	1st mode			2nd mode			1st mode			2nd mode		
Measured points	1	2	3	1	2	3	1	2	3	1	2	3
Non-operational	10.9	10.9	10.9	18.4	18.3	18.4	5.22	5.36	5.25	2.88	2.91	2.91
Non-operational (overlaid)	11			18.4			5.25			2.88		
Operational	9.94	9.95	9.90	17.8	17.6	17.6	5.32	5.05	5.95	3.23	3.18	3.28
Operational (overlaid)	9.94			17.6			5.32			3.21		
Deviation	0.96	0.93	1	0.6	0.7	0.8	0.1	0.31	0.70	0.65	0.27	0.37
Deviation (overlaid)	1.06			0.8			0.07			0.33		

The downward shift in resonance frequency was recorded at all the points, consolidating the above theory that the dynamic characteristic is depended on the operational condition of the structure. In average, the difference in resonance frequency for the first and second modes was determined at 1.06 and 0.8 Hz, while the average difference in damping ratio was found at 0.13 and 0.33*%,* respectively.

This relatively low deviation indicates the ability of the proposed technique to capture the dynamic characteristics of integrated structure which is affected by harmonic disturbance. This would pave new route for solving the persistent problem in classical EMA which is known to be performed under static condition that require complete shutdown of the rotating machineries mounted on the structure.

Further comparative assessment was conducted to evaluate the mode shape parameter between the two tested conditions. The points were specifically chosen to demonstrate potentially different modes of excitation that occur during resonance (i.e. heaving, pitching or rolling). For static condition the stop criteria for averaging task was set at 5 while for the operational mode, the block averaging stops after the coherence reaches 0.75. Module *Select*, incorporated after the transfer function module as shown in Figure 5.6 was employed to monitor the coherence progress at predetermined frequency (i.e. 10 Hz).

Figure 5.15 provides simulation results of the structural motion for the first two resonance modes. The result under static measurement exemplifies two distinctive motions, namely pitching and heaving which transpire at the first and second natural modes, respectively. dynamic change during operational conditions (Gagnol et al., 2011) as well as the coherence not reaching unity, which affects the output response. The above results indicate the reliability of the proposed technique to capture the mode shape with running By switching to operational condition, the proposed periodical block averaging using the force input as triggering signal enables the original mode of vibration to be captured, judging by the close agreement of relative displacement between the points of consideration to the classical EMA results. Further, the trajectory of each point was well articulated under the proposed scheme with relatively small deviation as indicated by the color signature. The slight difference may be attributed to the aforementioned structural harmonic.

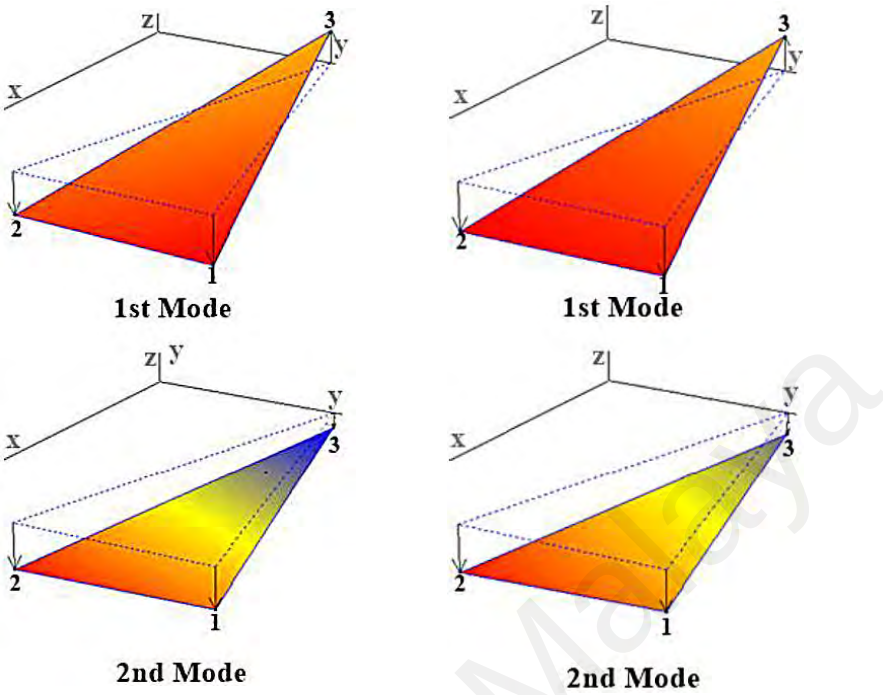

(a) (b)

Figure 5.15: Mode shape comparison using different approach (a) Non-operational condition, (b) Operational condition

This may pave avenues to enrich the usability of the existing EMA as well as serving as alternative to the OMA technique in addressing the harmonic disturbance issue.

5.4 Summary

The present work focused on introducing a new scheme for conducting EMA under operational condition. The process involves developing and a hardware and software to filter the harmonic signal, originating from cyclic devices that infiltrate into the raw vibration data during the measurement and further taint the post-processing results. Major modification of the classical EMA lies on replacing the manually driven impact hamper with automatically driven electromechanical-based solenoid and force sensor unit to generate an impact force required as input for modal parameter identification. A dedicated circuit was built to allow periodical impulse signals generated from virtual instrumentation software to control the

solenoid plunger motion. The motion would bring the end-effector of the plunger onto the force sensor pad to deliver the required input force onto the structure. The data from different sensors were captured via a dedicated hardware interface onto custom-made software specially built to perform the harmonic elimination as well as extracting the modal parameters. The novel feature of the work lies on the establishment of harmonic elimination scheme which involves generation of a periodical force signal from knocking sequence that serves as both input and relay to trigger output data block stamping within the software. An additional block averaging module was incorporated within the initial stage of data processing to perform the harmonic cancellation in time domain. Further, the knocking input and running harmonic within the response output was synchronized to allow attenuation of the harmonic on every block averaging, thus leaving more purified output in response to input. The results showed that, under the static mode the newly developed automatic impact device produced relatively similar response in comparison to classical EMA, further underlying its capability to replace the manually driven ICP impact hammer on generating the required input force. Experiment conducted under operational mode revealed slight shift in the resonance frequency relative to static condition. Further, by activating the harmonic elimination module the results clearly demonstrated the attenuation of the harmonic as evident by the FRF and coherence results. As low as 1.05 Hz deviation in resonance frequency and 0.07% difference in modal damping were attained via the proposed technique. Further, the mode shape was found to mimic the static EMA based on the trajectory of the structure on each resonance mode. This highlights the reliability of the present scheme to restore the original parameters for giving high fidelity results. Within modal analysis perspective, the proposed harmonic elimination technique would

broaden the applicability of the classical EMA towards operational mode, benefiting wide spectrum of engineering fields that require structural modal identification and monitoring. Future work would involve evaluating the harmonic elimination performance with multiple harmonic sources as well as improving the coherence convergence towards achieving unity value indicating pure response output/input.

CHAPTER 6: CONCLUSIONS AND RECOMMENDATION

This research was dedicated to seek an alternative technique in performing modal identification of dynamic structures under harmonic loading, originated from cyclic device mounted on the structure. Typically, this task is conducted using OMA regime. However, in this endeavor, a modification of the classical EMA procedure was implemented to incorporate an automation feature within the impact process along with the synchronization of the force input and the harmonic excitation frequency via TSA platform. This would enable the harmonic signal to be filtered within the raw signal, leading to much 'cleaner' product of modal parameters. The works have been divided into three major sections which are summarized as follows:

6.1 Conclusion

6.1.1 Development of Automatic Impact Device

In order to accomplish the proposed harmonic elimination scheme, a consistent periodical input force is required that would be further integrated into the signal block averaging process. On this note, an automatic impact device has been developed to replace the existing ICP impact hammer device. This new arrangement consists of an electromagnetically driven solenoid and a force sensor. To realize the automation within the system, a dedicated relay circuit was constructed to allow a computer generated signal from Dasylab virtual instrumentation software to govern the solenoid motion on the force sensor pad. The impulse signal generated to drive the solenoid was further correlated to the harmonic source from the motor whose frequency was captured by a tachometer. This information together with the impulse frequency was used to configure the appropriate time interval between each knocking which served as trigger for data flow into the software. Communication between the

hardware and software was synchronized using a block system to ensure smooth transmission of outbound and inbound signals. Calibration of the force sensor was performed systematically to ensure the reliability of the signal generated within the proposed system. Issue of mobile platform vibration transmissibility during knocking operation was successfully alleviated via suitable damping. Interference of signals due to the use of multiple sensors mounted on the same structure was addressed by applying appropriate isolation materials. An optimum clearance between the plunger end-effector and force sensor pad was configured in order to eliminate double knocking, particularly during operational mode, leading to high quality input signal. To ensure linear motion of the plunger, the dynamic response of the solenoid was extracted to obtain the rise time of the system. This led to specific designation of 'ON' and 'OFF' time of the generated square wave signal to allow the impact to be executed within the rise time of the end-effector motion. Comparative assessment on the results attained via the proposed concept and the classical method showed close agreement on the quality and characteristic of the impulse signals generated. Further evaluation on the calculated modal parameters also showed relatively similar resonance frequency between the two approaches. The results suggest that the new system has the capability replicate the result of impact hammer based EMA. Further, the element of automatic impact incorporated within the new scheme serves as additional feature to the existing EMA, paving avenue for resolving the modal parameters of dynamic structure under harmonic loading condition.

6.1.2 Removal of Harmonic Excitation

The second segment of the research work dealt with formulating a strategy to isolate the harmonic signal from the raw response output data acquired by the DAQ. In principle, this concept lies on assigning an appropriate block size, representing

pre-designated amount of sampling of the accelerometer data, as well as the knocking sequence that would serve as the triggering signal to release the block for consecutive averaging. In order to achieve this objective the existing EMA protocol was modified by introducing a time based averaging task at the raw data stage on top of the calculated FRF product which also undergo similar averaging progress. Further, in order to achieve the desired elimination, the triggering signal was executed in periodical form, such that output raw data were segmented in block to synchronize with the desired predetermined attributes of the harmonic component. In this way, the harmonic was suppressed while preserving the transient signal originating from the impact. By properly selecting the block size as well as the triggering interval, elimination of the harmonic was accomplished under progressive block averaging, leaving pure output response signal generated by the impact device. In order to demonstrate this concept, a simulation platform was established to enable artificially generated harmonic excitation, representing the operating motor to be segmented in block by triggering signal, representing impact hammer knocking. By modulating the ratio between the harmonic and triggering signal, r_{HTT}, it was demonstrated that the harmonics signal was efficiently attenuated with minimum number of averaging blocks. Further, it was determined that by assigning the triggering frequency to yield r_{HTT} containing a decimal part, r_{dec} ranging from 0 to 1, different harmonic elimination performance was obtained. Specifically, pre-selecting the triggering frequency to give r_{dec} of 0.5 unveiled the most efficient elimination while any value near 0 or 1 produced unfavorable results. Further investigation was conducted by using a real time response output data from the tested structure under harmonic loading. The results showed that real time harmonic signal was successfully suppressed and the performance was comparable with the simulation

results. The investigation highlighted that non-periodic triggering frequency adversely implicate the elimination progress, particularly due to the effect of inconsistent block averaging which led to superimposing similar phase of harmonic signal in each incoming block. This work underlined the importance of controlling the triggering frequency to yield the desired design criteria for achieving rapid and highly efficient elimination of harmonic excitation signal. This work elucidated a simple but promising technique to isolate the harmonic by tuning of the frequency ratio between the harmonic and the triggering. This further laid a foundation to conduct EMA under operational condition by modifying the EMA impact apparatus to allow much controlled impact sequence onto the structure.

6.1.3 Building-up of EMA under Operational Condition

The final segment of the research involved integrating the hardware and software within the first two tasks to establish fully automated EMA system. All the sensors and actuator were linked to the specific DAQs whose data were collected inside a PC using dedicated instrumentation software interface. A GUI was constructed to enable data taking and processing to be centralized. The knocking period was adjusted to be larger than the processing time of the software to avoid bottleneck of data which prompts sudden termination of the software operation. Within this section, the evaluation of FRF and modal parameters was conducted systematically. Comparative assessment of these parameters under non-operational/stationary condition of the structure revealed close agreement between classical EMA and the proposed automated approach, indicating the ability of the later technique to emulate the performance of the widely adopted manually driven impact hammer based EMA. Further investigation under operational condition showed that the new system was capable of isolating the harmonics, judging by the amplitude reduction of the

harmonic signal as well as the improvement of the coherence value. Investigation on the dynamic parameters between static and operational conditions highlighted slight shift in magnitude for both resonance frequency and damping constant. This phenomenon was primarily due to the external forces generated by the rotating machine which changes the boundary conditions and further implicates the stiffness in modal identification. Nevertheless the mode shape of the structure was well-replicated under operational conditions; with pitching and heaving dominate the first to mode shapes. The similarities of the mode shape has proven that the contribution of the harmonic in modifying modal parameters was much suppressed, leading to reliable results that can be obtained without shutting down the operation of integrated system. In conclusion, the ability to perform harmonic elimination on the structure under EMA platform has charted a new dimension on resolving the dynamic properties which will benefit wide spectrum of engineering disciplines in terms of providing seamless structural monitoring as well as fault and failure detection.

6.2 Recommendations

6.2.1 Potential Application

6.2.1.1 Integrating Resonance as Root Cause in Component Failure

Within the scope of CBM, vibration induced components failure or damage are clustered under specific category depending on the characteristic of the acquired response signal such as phase difference and irregular amplitude and shape. Often resonance is not considered as the root of the above problem due to the inability to resolve the modal parameters during monitoring scheme. This led to misleading or incomplete diagnostic of structure which affects cost and productivity of the machine operation due to frequent shut down and premature recurrence of similar fault. However, the proposed concept highlighted within this research enabled the dynamic

parameters to be obtained, particularly the resonance frequency and mode shape such that the effect of resonance in component failure can be included during diagnostic stage and much accurate and reliable root cause can be resolved. This modal identification process is performed while the machine is in running mode, which further accentuates the advantage of the proposed concept. Continuous monitoring which includes the effect of resonance into the decision making process produces high integrity diagnostic scheme and enable rapid intervention by engineers

6.2.1.2 Dynamic Design Verification

The ability to resolve the modal parameters of the structure during operation paves new horizon on performing 'on-line' structural design modification. Identifying the weak point of the structure can be made based on resonance and mode shape characteristics, which can be attained while the machine is running. Consequently, strengthening of the overall structure can be accomplished via 'on-line' intervention of adding trusses or damping as part of long term counter measures, further avoiding machine shutdown.

6.2.2 Future Work

This research has focused on enhancing the classical EMA technique to broaden its applicability within the scope of resolving modal parameters of structures under running condition of cyclic device. An innovative concept via the combination of automatic impact device and TSA has been adopted to realize the objective, which has shown favorable outcome. However, due to its proof-of-concept stage, the investigation was constraint to basic architecture of vibration scenario to demonstrate the feasibility of the proposed idea. Thus, within the scope of the future works, more

comprehensive issues will be considered to reflect much realistic scenario of structure subjected to vibration. Some of the potential works are given as follows:

6.2.2.1 Development of Solenoid Stand

A more sophisticated solenoid mobile platform will be developed which will reduce the transmission of force onto the structure during measurement. This will include finite element design which will provide the desired stiffness during knocking operation while vibration generated due to inertial motion will be absorbed by the platform base, thus replicating human response to absorb and stabilize motion. Plus, the stand should be able to hold the solenoid in Cartesian axis (X, Y, and Z) to allow more flexibility in input knocking as well as extending the coverage of investigated domain. A linear translational stage will be incorporated to gain high precision position of the solenoid as well as the setting the optimum gap with the force sensor achieve maximum impact while avoiding double knocking.

6.2.2.2 High Resolution and Response Impact Device

It is well known that multi-component rotating devices within the structure induces different level of vibrations within wide spectrum of bandwidth. Thus, in order to ensure that the knocking is executed at the precise time for specific running frequency, the impact device response time has to be at the lowest level such that the impact is synchronized with the desired phase of the harmonic. A delay in impact would result in miss segmentation of the block which renders the averaging inefficient or worse, it could lead to failure in harmonic elimination. Within the scope of the future work, a high speed translational actuator such as voice coil or piezo resistive linear actuator will be explored as the literatures have shown that these two devices are capable of generating large force and exceptional response in

comparison to conventional solenoid. In addition, the relay circuit would be upgraded to support high frequency operation which will deliver wide spectrum of knocking frequencies. This would in turn fortify the capability of the impact device in order to formulate different strategy on eliminating large bandwidth of harmonic sources.

6.2.2.3 Block Averaging for Multi-Machine Running

In actual industrially related scenario, an integrated structure would consist of more than a single cyclic device, working in either identical or different speed. Thus, the resultant harmonic excitation would be a composite of individual excitation which can be extracted in frequency domain. In this light, eliminating these harmonic requires a radical modification of the current algorithm to allow much selective averaging process which meet the phase cancellation strategy. This is to ensure that blocks that contain similar phase of the designated harmonic can be excluded to render successful signal isolation. The challenge is to formulate an asynchronous knocking in contrast to much fixed interval periodic knocking implemented within the present research. A prospectively viable strategy is to extract the harmonics in real time and analyses the data to identify the point where the phase closely match each other in maximum and minimum. The determination of the interval between these two apexes would be crucial to ensure successful elimination of all the individual harmonics. This interval however might not be periodic which will complicate the effort the resolve the time in between consecutive knocking.

REFERENCES

Agneni, A., Coppotelli, G., & Grappasonni, C. (2012). A method for the harmonic removal in operational modal analysis of rotating blades. *Mechanical Systems and Signal Processing, 27*(0), 604-618.

Ameri, N., Grappasonni, C., Coppotelli, G., & Ewins, D. J. (2013). Ground vibration tests of a helicopter structure using OMA techniques. *Mechanical Systems and Signal Processing, 35*(1-2), 35-51.

Assaad, B., Eltabach, M., & Antoni, J. (2014). Vibration based condition monitoring of a multistage epicyclic gearbox in lifting cranes. *Mechanical Systems and Signal Processing, 42*(1), 351-367.

Batel, M. (2002). Operational modal analysis - Another way of doing modal testing. *Sound and Vibration, 36*(8), 22-27.

Beyen, K., & Kutanis, M. (2011). *Comparison of the Results Inferred from OMA and IEMA.* Paper presented at the 4th international operational modal analysis conference.

Braun, S. (2011). The synchronous (time domain) average revisited. *Mechanical Systems and Signal Processing, 25*(4), 1087-1102.

Brincker, R., & Kirkegaard, P. H. (2010). Special issue on Operational Modal Analysis. *Mechanical Systems and Signal Processing, 24*(5), 1209-1212.

Cakir, F., Uysal, H., & Acar, V. (2016). Experimental modal analysis of masonry arches strengthened with graphene nanoplatelets reinforced prepreg composites. *Measurement, 90*, 233-241.

Capoluongo, P., Ambrosino, C., Campopiano, S., Cutolo, A., Giordano, M., Bovio, I., . . . Cusano, A. (2007). Modal analysis and damage detection by Fiber Bragg grating sensors. *Sensors and Actuators A: Physical, 133*(2), 415-424.

Cheung, Y. L., Wong, W. O., & Cheng, L. (2013). Optimization of a hybrid vibration absorber for vibration control of structures under random force excitation. *Journal of Sound and Vibration, 332*(3), 494-509.

Choi, F. C., Li, J., Samali, B., & Crews, K. (2007). An experimental study on damage detection of structures using a timber beam. *Journal of mechanical science and technology, 21*(6), 903-907.

Combet, F., & Gelman, L. (2007). An automated methodology for performing time synchronous averaging of a gearbox signal without speed sensor. *Mechanical Systems and Signal Processing, 21*(6), 2590-2606.

Cumunel, G., Delepine-Lesoille, S., & Argoul, P. (2012). Long-gage optical fiber extensometers for dynamic evaluation of structures. *Sensors and Actuators A: Physical, 184*, 1-15.

. DASYLab Help. (2007): National Instruments Ireland Resources Limited.

DATASHEET NI 9234. (2015). http://www.ni.com/pdf/manuals/374238a_02.pdf

De Vivo, A., Brutti, C., & Leofanti, J. (2013). Modal shape identification of large structure exposed to wind excitation by operational modal analysis technique. *Mechanical Systems and Signal Processing, 39*(1), 195-206.

Debonnel, C. S., Yu, S. S., & Peterson, P. F. (2005). Progress towards thick liquid fusion chambers for assisted-pinch and solenoid focusings. *Nuclear Instruments & Methods in Physics Research Section a-Accelerators Spectrometers Detectors and Associated Equipment, 544*(1-2), 342-346.

Devriendt, C. (2010). *On the use of transmissibility functions in operational modal analysis.* PhD thesis, Vrije Universiteit Brussel.

Devriendt, C., De Sitter, G., Vanlanduit, S., & Guillaume, P. (2009). Operational modal analysis in the presence of harmonic excitations by the use of transmissibility measurements. *Mechanical Systems and Signal Processing, 23*(3), 621-635.

Devriendt, C., & Guillaume, P. (2008). Identification of modal parameters from transmissibility measurements. *Journal of Sound and Vibration, 314*(1-2), 343-356.

Dion, J. L., Tawfiq, I., & Chevallier, G. (2012). Harmonic component detection: Optimized Spectral Kurtosis for operational modal analysis. *Mechanical Systems and Signal Processing, 26*(0), 24-33.

Ebrahimi, R., Esfahanian, M., & Ziaei-Rad, S. (2013). Vibration modeling and modification of cutting platform in a harvest combine by means of operational modal analysis (OMA). *Measurement, 46*(10), 3959-3967.

Eissa, M., & Amer, Y. A. (2004). Vibration control of a cantilever beam subject to both external and parametric excitation. *Applied Mathematics and Computation, 152*(3), 611-619.

Farshidi, R., Trieu, D., Park, S. S., & Freiheit, T. (2010). Non-contact experimental modal analysis using air excitation and a microphone array. *Measurement, 43*(6), 755-765.

Gagnol, V., Le, T.-P., & Ray, P. (2011). Modal identification of spindle-tool unit in high-speed machining. *Mechanical Systems and Signal Processing, 25*(7), 2388-2398.

General operating guide for use with piezoelectric ICP Accelerometer. (2015). www.pcb.com

General purpose accelerometer 786C. (2017). from https://buy.wilcoxon.com/786c.html

Gevers, M. (2005). Identification for control: From the early achievements to the revival of experiment design. *European Journal of Control, 11*(4-5), 335-352.

Hanson, D., Randall, R. B., Antoni, J., Waters, T. P., Thompson, D. J., & Ford, R. A. J. (2007). Cyclostationarity and the cepstrum for operational modal analysis of MIMO systems—Part II: Obtaining scaled mode shapes through finite element model updating. *Mechanical Systems and Signal Processing, 21*(6), 2459-2473.

Inman, D. J. (2014). *Engineering vibration* (4th ed.). Upper Saddle River,

New Jersey: Pearson Education Inc.

Islam, M. Z., McMullin, J. N., & Tsui, Y. Y. (2011). Rapid and cheap prototyping of a microfluidic cell sorter. *Cytometry A, 79*(5), 361-367.

Jaffey, A. H., & Khoe, T. (1974). Application of solenoid focusing in a superconducting heavy-ion linear accelerator. *Nuclear Instruments and Methods, 121*(3), 413-419.

Jalali, H., & Parvizi, F. (2012). Experimental and numerical investigation of modal properties for liquid-containing structures. *Journal of mechanical science and technology, 26*(5), 1449-1454.

Jamil, N., & Yusoff, A. R. (2016). Electromagnetic actuator for determining frequency response functions of dynamic modal testing on milling tool. *Measurement, 82*, 355-366.

Leber, C., & Evanski, P. M. (1986). A comparison of shoe insole materials in plantar pressure relief. *Prosthetics and Orthotics International, 10*(3), 135-138.

Lee, C.-W., & Kim, S.-K. (2001). Complex modal testing of asymmetric rotors using magnetic exciter equipped with hall sensors. *Journal of mechanical science and technology, 15*(7), 866-875.

Li, B., Luo, B., Mao, X., Cai, H., Peng, F., & Liu, H. (2013). A new approach to identifying the dynamic behavior of CNC machine tools with respect to different worktable feed speeds. *International Journal of Machine Tools and Manufacture, 72*, 73-84.

Li, Q., & Wu, F. X. (2004). Control performance improvement of a parallel robot via the design for control approach. *Mechatronics, 14*(8), 947-964.

Li, Q., Zhang, W. J., & Chen, L. (2001). Design for control-a concurrent engineering approach for mechatronic systems design. *IEEE/ASME Transactions on Mechatronics, 6*(2), 161-169.

Li, Y., Chen, X., Zhang, P., & Zhou, J. (2017). Dynamics modeling and modal experimental study of high speed motorized spindle. *Journal of mechanical science and technology, 31*(3), 1049-1056.

Low-Cost, Bus-Powered Multifunction DAQ for USB – 12- or 14-Bit, up to 48 kS/s, 8 Analog Inputs. (2008). http://www.ni.com/pdf/products/us/20043762301101dlr.pdf

Luk, B. L., Liu, K. P., Jiang, Z. D., & Tong, F. (2009). Robotic impact-acoustics system for tile-wall bonding integrity inspection. *Mechatronics, 19*(8), 1251-1260.

Magalhães, F., Cunha, Á., Caetano, E., & Brincker, R. (2010). Damping estimation using free decays and ambient vibration tests. *Mechanical Systems and Signal Processing, 24*(5), 1274-1290.

Mao, X., Luo, B., Li, B., Cai, H., Liu, H., & Pen, F. (2014). An approach for measuring the FRF of machine tool structure without knowing any input force. *International Journal of Machine Tools and Manufacture, 86*, 62-67.

Mark, W. D. (2015). Time-synchronous-averaging of gear-meshing-vibration transducer responses for elimination of harmonic contributions from the mating gear and the gear pair. *Mechanical Systems and Signal Processing, 62*, 21-29.

McFadden, P. (1989). Interpolation techniques for time domain averaging of gear vibration. *Mechanical Systems and Signal Processing, 3*(1), 87-97.

Mendrok, K., & Kurowski, P. (2013). Operational modal filter and its applications. *Archive of Applied Mechanics*, 1-11.

Miki, N., & Yamamoto, H. (1999). Linear solenoid valve: Google Patents.

Modak, S. V., Rawal, C., & Kundra, T. K. (2010). Harmonics elimination algorithm for operational modal analysis using random decrement technique. *Mechanical Systems and Signal Processing, 24*(4), 922-944.

Model: 086C03. (2017). from http://www.pcb.com/Products/model/086c03

Model: 208C01. (2017). from http://www.pcb.com/Products/model/208C01

Mohanty, P., & Rixen, D. J. (2004). Operational modal analysis in the presence of harmonic excitation. *Journal of Sound and Vibration, 270*(1), 93-109.

Najafi, N., Schmidt Paulsen, U., Belloni, F., Bedon, G., & Mann, J. (2014). *Dynamic behaviour studies of a vertical axis wind turbine blade using Operational Modal Analysis (OMA) and Experimental Modal Analysis (EMA)*. Paper presented at the European Wind Energy Conference & Exhibition 2014.

Nguyen, V. D., & Woo, K. C. (2008). Nonlinear dynamic responses of new electro-vibroimpact system. *Journal of Sound and Vibration, 310*(4-5), 769-775.

P.C.B. Piezotronics, Impact Hammers Model: 086C03. (2013). www.pcb.com.

Pocket Laser Tach 200. (2017). from https://monarchinstrument.com/collections/best-selling-products/products/pocket-laser-tach-200

Principle of Operation, Why use solenoids? (2017). *2017*(August 16). http://www.johnsonelectric.com/en/resources-for-engineers/solenoids/principle-of-operation

Rahman, A. G. A., Ong, Z. C., & Ismail, Z. (2011). Effectiveness of Impact-Synchronous Time Averaging in determination of dynamic characteristics of a rotor dynamic system. *Measurement, 44*(1), 34-45.

Rashedin, R., & Meydan, T. (2006). Solenoid actuator for loudspeaker application. *Sensors and Actuators A: Physical, 129*(1), 220-223.

Riemann, B., Perini, E. A., Cavalca, K. L., de Castro, H. F., & Rinderknecht, S. (2013). Oil whip instability control using mu-synthesis technique on a magnetic actuator. *Journal of Sound and Vibration, 332*(4), 654-673.

Ristivojevic, M., Mitrovic, R., & Lazovic, T. (2010). Investigation of causes of fan shaft failure. *Engineering Failure Analysis, 17*(5), 1188-1194.

Rogers, W. W., & Wang, C. C. (1987). Linear suction control system: Google Patents.

Salim, M., Aljibori, H. S. S., Salim, D., Khir, M. H. M., & Kherbeet, A. S. (2015). A review of vibration-based MEMS hybrid energy harvesters. *Journal of mechanical science and technology, 29*(11), 5021-5034.

Schwarz, B. J., & Richardson, M. H. (1999). *Experimental Modal Analysis*. Paper presented at the CSI Reliability week, Orlando, FL.

Scott, M. (2009). Understanding Key Accelerometer Specs. http://www.evaluationengineering.com/articles/200906/understanding-key-accelerometer-specs.php.

Shang, J., Tian, Y., Li, Z., Wang, F., & Cai, K. (2015). A novel voice coil motor-driven compliant micropositioning stage based on flexure mechanism. *Review of Scientific Instruments, 86*(9), 095001.

Sharma, V., & Parey, A. (2017). Frequency domain averaging based experimental evaluation of gear fault without tachometer for fluctuating speed conditions. *Mechanical Systems and Signal Processing, 85*, 278-295.

Song, S. H., & Jhung, M. J. (1999). Experimental modal analysis on the core support barrel of reactor internals using a scale model. *Journal of mechanical science and technology, 13*(8), 585-594.

Szczepanik, A. (1989). Time synchronous averaging of ball mill vibrations. *Mechanical Systems and Signal Processing, 3*(1), 99-107.

Taghizadeh-Alisaraei, A., Ghobadian, B., Tavakoli-Hashjin, T., & Mohtasebi, S. S. (2012). Vibration analysis of a diesel engine using biodiesel and petrodiesel fuel blends. *Fuel, 102*(0), 414-422.

Tian, J., Tian, Y., Guo, Z., Wang, F., Zhang, D., Liu, X., & Shirinzadeh, B. (2016). Development of a novel 3-DOF suspension mechanism for multi-function stylus profiling systems. *International Journal of Precision Engineering and Manufacturing, 17*(11), 1415-1423.

Tian, Z. G., & Liao, H. T. (2011). Condition based maintenance optimization for multi-component systems using proportional hazards model. *Reliability Engineering & System Safety, 96*(5), 581-589.

Trebuňa, F., & Hagara, M. (2014). Experimental modal analysis performed by high-speed digital image correlation system. *Measurement, 50*, 78-85.

Van Horenbeek, A., Van Ostaeyen, J., Duflou, J. R., & Pintelon, L. (2013). Quantifying the added value of an imperfectly performing condition monitoring system—Application to a wind turbine gearbox. *Reliability Engineering & System Safety, 111*(0), 45-57.

Xiong, X., & Oyadiji, S. O. (2017). Design and experimental study of a multi-modal piezoelectric energy harvester. *Journal of mechanical science and technology, 31*(1), 5-15.

Xu, Y. F., & Zhu, W. D. (2013). Operational modal analysis of a rectangular plate using non-contact excitation and measurement. *Journal of Sound and Vibration, 332*(20), 4927-4939.

Yao, J., Di, D., & Han, J. (2012). Adaptive notch filter applied to acceleration harmonic cancellation of electro-hydraulic servo system. *Journal of Vibration and Control, 18*(5), 641-650.

Zhao, J. F., & Seethaler, R. J. (2010). Compensating combustion forces for automotive electromagnetic valves. *Mechatronics, 20*(4), 433-441.

Zio, E., & Compare, M. (2013). Evaluating maintenance policies by quantitative modeling and analysis. *Reliability Engineering & System Safety, 109*(0), 53-65.

LIST OF PUBLICATIONS AND PAPERS PRESENTED

Jannifar, A., Zubir, M. N. M., & Kazi, S. N. (2017). Development of a new driving impact system to be used in experimental modal analysis (EMA) under operational condition. *Sensors and Actuators A: Physical*.